NASA-CR-72713
WANL-PR-(RRR)-001

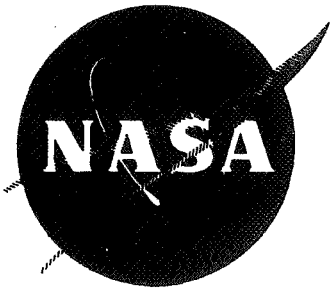

EVALUATION OF MECHANICAL PROPERTIES, OXIDATION RESISTANCE, AND STRUCTURE OF SLURRY SILICIDE COATED T-222

by
A. M. FILIPPI

Westinghouse Astronuclear Laboratory

Prepared for

NATIONAL AERONAUTICS AND SPACE ADMINISTRATION
NASA Lewis Research Center
Contract NAS 3-12410

Robert E. Oldrieve, Project Manager
Robert H. Titran, Research Advisor
Salvatore J. Grisaffe Research Advisor

Astronuclear Laboratory

FINAL REPORT

EVALUATION OF MECHANICAL PROPERTIES, OXIDATION RESISTANCE AND STRUCTURE OF SLURRY SILICIDE COATED T-222

by

A. M. Filippi

WESTINGHOUSE ASTRONUCLEAR LABORATORY
P. O. Box 10864
Pittsburgh, Pennsylvania 15236

prepared for

NATIONAL AERONAUTICS AND SPACE ADMINISTRATION

December 19, 1969

CONTRACT NAS 3-12410

NASA-Lewis Research Center
Cleveland, Ohio
Robert E. Oldrieve, Project Manager
Robert H. Titran, Research Advisor, Mechanical Testing
Salvatore J. Grisaffe, Research Advisor, Coatings

FOREWORD

The work described herein was done at the Astronuclear Laboratory, Westinghouse Electric Corporation, under NASA Contract NAS 3-12410. Messrs. Robert E. Oldrieve, Robert H. Titran and Salvatore J. Grisaffe, Materials and Structures Division, NASA-Lewis Research Center, functioned as Project Manager and Research Advisors, respectively.

The author wishes to acknowledge several people for outstanding assistance on the program. These are: Messrs R. W. Conlin and A. W. Danko for x-ray diffraction and microprobe analyses, Messrs J. J. Lesczynski, G. O. Yatsko, and E. F. Vandergrift for mechanical property testing, Mr. R. L. Berrier for oxidation testing, and Messrs K. J. Galbraith and J. M. Lott for metallography.

ABSTRACT

Slurry silicide coated T-222 sheet was studied to define oxidation behavior, mechanical properties, and microstructural features. The as-applied coating displayed erratic oxidation behavior, surviving continuous oxidation on creep tests performed at 2400° F for over 400 hours, but failing in 21 to 304 hours on cyclic oxidation tests at this temperature. Failure of the as-applied coating occurred in 2 to 4 hours at 1400° F, but oxidation at higher temperatures prior to exposure at 1400° F eliminated this behavior.

Bend, tensile and creep evaluation of coated material produced data consistent with that inherent in the T-222 alloy. Creep extension of 9 percent was sustained without failure in an air environment test of over 400 hours duration at 2400°F.

Some increase in oxygen, nitrogen and carbon levels, primarily oxygen, was noted for the as-coated substrate, but little additional change was found after various oxidation tests. Interstitial element levels of coated samples were below that which would impair mechanical properties, but changes in precipitation from that characteristic of T-222 were noted.

A primary oxide surface barrier of TiO_2 particles in a SiO_2 matrix formed during oxidation of the study coating. Oxidation also occurred within fissures and pores traversing the coating.

Substrate recession due to reaction with the coating was measured for temperatures in the range 1000° F to 2400° F. An increase in coating-substrate reaction rate occurs at approximately 1600° F. Penetration of coating elements into the substrate beyond the obvious interaction boundary did not occur for any condition where coating-substrate reaction was promoted.

TABLE OF CONTENTS

LIST OF FIGURES

LIST OF FIGURES (CONTINUED)

LIST OF FIGURES (CONTINUED)

LIST OF FIGURES (CONTINUED)

LIST OF TABLES

SUMMARY

Oxidation behavior, coating and substrate changes and interaction, and mechanical properties, were studied for the tantalum-base alloy T-222*, coated with an oxidation resistant silicide layer**. Well characterized 0.030" thick T-222 sheet was employed in the study.

Oxidation behavior was examined in slowly moving air primarily at 1400° F and 2400° F, employing repeated 2, 2 and 16 hour time-at-temperature periods, and air cooling to room temperature between periods. The as-applied coating proved entirely unsuited for protection of the substrate at 1400° F, with coating failure developed on seven of seven samples tested during 2 to 4 hours time-at-temperature. Samples first oxidized at 1600° F and 2400° F, however, were tested at 1400° F for 600 hours without coating failure occurring.

Oxidation behavior at 2400° F was erratic with four of twelve samples surviving 304 hours of testing, the others exhibiting coating failure at times between 21 and 304 hours at temperature. Coating cracks developed on many samples oxidized at 2400° F during the first two hour exposure period, but were observed to fill with oxidation product upon further exposure, forestalling coating failure for some time.

A positive answer to the many coating failures experienced during oxidation testing at 1400° F and 2400° F was not achieved. Coating failure occurred at the same general region on a majority of samples, indicating a possible connection with preparation; on others, failure occurred at obviously vulnerable edge locations. Some evidence suggesting that the "pest" mechanism might be linked to the abrupt failure of the as-applied coating at 1400° F was uncovered.

---

* Ta-10 w/o W-2.5 w/o Hf-0.01 w/o C

** 32 w/o W-13 w/o Mo-9 w/o V-9 w/o Ti-37 w/o Si

An averaged oxidation rate measured at 2400° F followed the equation:

$$M = 0.69 \ln t + 0.85$$

M: mgs/square cm

t: hours at 2400° F

A much higher oxidation rate than given by this relationship, which is biased by long oxidation periods, was observed over the repeated back-to-back two hour oxidation periods. Oxidation is thought to be accelerated until coating cracks induced from the thermal stress of cyclic testing are repaired by oxide build up. Measurement of a high oxidation rate over the short 2 hour exposure periods compared to those of longer duration is assumed a consequence of this, since the time taken in repairing coating cracks would occupy a greater percentage of the short period.

Bend test results on as-coated material, on samples surviving oxidation for 600 hours at 1400° F following higher temperature treatment, and on samples surviving 10 hours and 304 hours oxidation at 2400° F, reflected substrate ductility comparable to uncontaminated T-222. Tensile ductility determined from tests of as-coated material was similarly consistent with that inherent in the substrate alloy.

Creep behavior was examined on six samples, two after oxidation at 2400° F for 304 hours, the others in the as-coated condition. Data was gathered in air environment at 2400° F employing test stresses from 4 ksi to 12 ksi.

Both samples oxidized prior to creep testing ruptured in less than 25 hours, when coating failure, occurring at an edge location in the gauge sections, led to gross substrate oxidation. Two of the four as-coated samples creep tested at 2400° F also ruptured as a result of substrate oxidation, but failure occurred well outside the gauge section at test times beyond 400 hours. From the closeness of creep strains measured near the time of failure and elongation measured directly from the gauge sections, and an analysis of the manner by which oxidation was likely to have propagated at the failure sites, it was concluded that creep rates determined on these tests were unaffected by the eventual failure process. The other two as-coated samples were creep tested for 500 hours without sample failure occurring.

Depending upon test stress employed, elongation of 2 percent to 9 percent was obtained from creep strain measurement, and confirmed by direct measurement of gauge length after testing. Measured creep rates compared well with behavior of T-222 tested under the inert condition of vacuum. Because of this, and the results of bend and tensile testing, it was concluded that when the coating did not fail leading to gross substrate oxidation, its protectiveness was sufficient to maintain mechanical properties of the substrate comparable to uncontaminated material.

Chemical analysis of the substrate on coated samples representing various conditions confirmed that interstitial element levels were below that necessary to cause obvious mechanical property impairment. Also revealed by chemical analysis was little change in interstitial element content caused by oxidation from that characteristic of the as-coated condition. Roughly 0.025 to 0.037w/o oxygen, 0.014 to 0.017w/o carbon, and 0.0039 to 0.0090w/o nitrogen were detected in coated samples. By comparison, 0.0030w/o oxygen, 0.0120w/o carbon and 0.0015w/o nitrogen were present in the T-222 sheet before coating.*

Study of the primary oxide barrier formed during oxidation at 2400° F revealed development of a two phase, particle-in-matrix, structure. The particle phase increased in amount present with time at 2400° F. This structure was identified as TiO_2 particles in a matrix of SiO_2. The coating constituents, tungsten, molybdenum and vanadium, are apparently lost from the surface during oxidation at 2400° F, probably by formation of their volatile oxides, leaving TiO_2 and SiO_2 as the oxidation products. Study of conditions representing 500 hours time-at-temperatures between about 1000° F and 2100° F revealed development of a similar primary oxide barrier structure. A layer of particles rich in titanium, presumed to be TiO_2, was also found below the primary oxide barrier on a sample oxidized 437 hours at 2400° F. This layer did not develop for oxidation conditions involving 500 hours at 2100° F and below.

*0.0001 w/o = 1 PPM

Where oxidation conditions were sufficient for a primary oxide surface barrier to develop, the product of coating oxidation also formed inside pores and fissures in the metallic-intermetallic reservoir. Oxidation plugging of fissures opened in the metallic diffusion zone during 2400° F creep testing was also observed.

Diffusion of coating elements into the substrate beyond the obvious interface between the regions, was not observed for any condition examined where growth of the metallic diffusion zone had occurred. Measurement of substrate recessions due to interaction with the coating at 2400° F, revealed roughly 0.004" to 0.005" decrease in thickness will occur in 500 hours time-at-temperature. Substrate recession was also examined as a function of temperature in the range 1000° F to 2100° F. A major increase in the rate of recession with increased temperature, was observed to occur at approximately 1600° F.

Structure change in the T-222 substrate was examined on samples exposed for various times in air at 2400° F, and compared to material similarly treated under ultrahigh vacuum. Overall precipitation was somewhat greater in air tested material reflecting the higher interstitial element level but, for the most part, precipitate morphology and location in the structure were similar to that in vacuum tested material. The most striking structural feature distinguishing air and vacuum treated materials, was formation of some large individual precipitates at grain boundary triple points in the former. The results of chemical analysis, and some indirect microprobe data, indicated the particles were probably HfO_2.

I. INTRODUCTION

Refractory and reactive metal silicides are compounds which, with few exceptions, display good oxidation resistance and compatibility with refractory metals, two necessary prerequisites for use as protective coatings on advanced air breathing engine components. This coating potential has led to extensive study of the simple monometal silicide compounds, with the work extended to alloy systems consisting of the silicided product of several metals. A review of current work in this area has been reported by Metcalfe and Stetson[1].

One promising silicide coating system consists of the metals tungsten, molybdenum, vanadium, and titanium, sintered and diffusion bonded to tantalum or columbium alloys and silicided to a silicon-to-metal atom ratio of 2-to-1[2, 3]. Optimum performance of this coating is approached at the metal composition, 50 w/o W-20 w/o Mo-15 w/o Ti-15 w/o V. A noteworthy achievement of the coating is demonstrated protection of the tantalum-base alloy T-222, Ta-10 w/o W-2.5 w/o Hf-0.01 w/o C, from oxidation in air at both 1600°F and 2400°F, in tests of greater than 218 hours duration[2].

In the principal effort undertaken on this program, mechanical property samples of 0.030 inch* thick T-222 sheet were coated with the optimized (W, Mo, V, Ti)Si_2 composition, then tested in the as-coated condition, and after elevated temperature exposure in air. The substrate alloy, T-222, displays one of the finest combinations of strength, ductility and fabricability available in a refractory metal alloy[4-6] and, as a consequence, is a potential candidate for advanced air breathing engine nozzle vane application. Evaluation of the mechanical properties of this coating-substrate combination, therefore, represented a logical extension of current refractory metal and oxidation protection technology.

Mechanical property tests were preformed to characterize tensile, bend and creep behavior of as-coated and coated plus elevated temperature air exposed samples. Tensile

* Throughout the text dimensions are referred to in inches, stress in kilopounds per square inch, ksi, and temperature in Fahrenheit Degrees, ° F. Common and international system units are used to describe data in tables and figures.

properties were determined at room temperature and 2400° F, and creep behavior was studied at 2400° F. Bend data was gathered to define the ductile-to-brittle transition temperature*, which was typically at cryogenic temperatures. All testing of coated material was performed in an air environment.

Comparison of tensile, bend and creep data gathered on coated samples, was made to properties displayed by the T-222 sheet used for the substrate of these samples in inert environment tests - air at low temperatures, vacuum at elevated temperatures. Creep test data were also compared with properties reported from vacuum tests on other lots of the substrate alloy. Commercially produced 48 inch wide T-222 sheet, extensively characterized under contract from the Naval Air System Command and observed to display properties entirely consistent with those reported for the alloy during its development[6], was used for substrate material.

A flow sheet outlining the original mechanical property test program is displayed in Figure 1. Note that included in the project was evaluation of what affect air exposure at 1400° F and 2400° F would have on material properties. Severe oxidation tests accumulating 600 hours at these temperatures, by repeating time-at-temperature periods of 2, 2 and 16 hours, were planned. The as-applied coating, however, proved unsuited for even a few hours of substrate protection at 1400° F, and related experiments were substituted. Examination was made of whether coating failure at 1400° F was linked to the technique used to hold the specimens, or to sample configuration. Experiments into what affect higher temperature oxidation prior to oxidation at 1400° F would have on coating life were also performed.

Oxidation for 600 hours at 2400° F prior to mechanical property examination also proved too severe a test, and it was terminated after accumulation of 304 hours time-at-temperature, with but a few samples surviving to this time. Thorough examination of samples oxidized at 2400° F was substituted in place of further testing at this temperature.

---

*Referred in later text as DBTT.

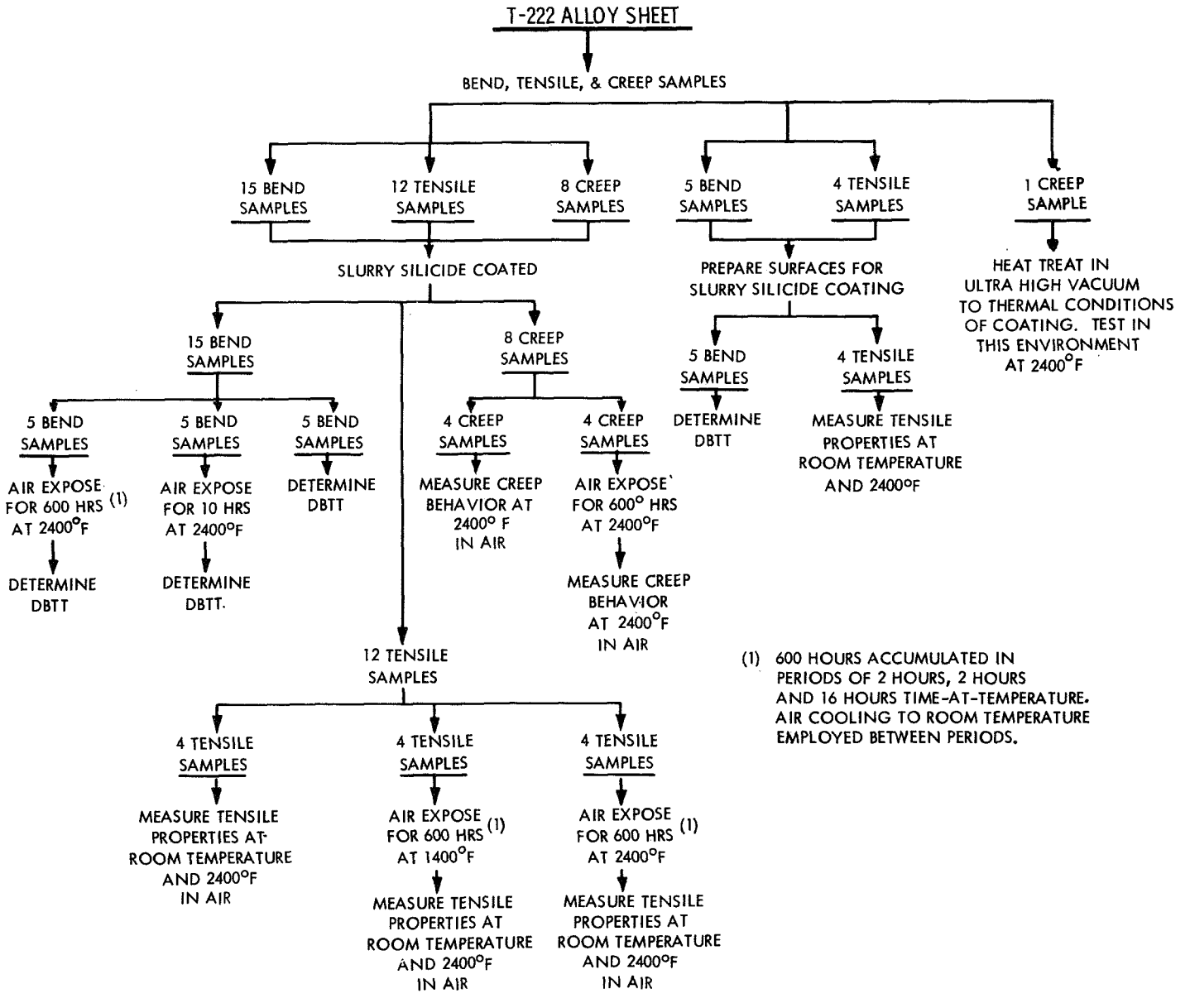

FIGURE 1 - Original Test Program

In addition to mechanical property evaluation, oxidation behavior, and coating-substrate interaction caused by elevated temperature exposure, were studied. Weight gain of samples exposed in air at elevated temperatures was recorded to define oxidation rates. X-ray diffraction, electron microprobe analysis, and metallographic inspection, were employed on the coating in situ, and on coating-substrate cross sections, to assist definition of high temperature behavior. Chemical analysis for interstitial element content in the substrate was also employed to characterize the contamination level of selected test samples.

II. MATERIALS AND EXPERIMENTAL PROCEDURES

Substrate Material

Substrate material was removed from one commercially produced 0.030" thick sheet of T-222 alloy provided for the program by the Naval Air Systems Command. The sheet had received extensive characterization at the Westinghouse Astronuclear Laboratory under contract from this agency, and was shown to display properties typical of those reported during development of the alloy[6]. It had received a final vacuum anneal of one hour at 3000° F after 80 percent cold reduction to gauge, causing solutioning of carbon and development of a fine, 0.0004 inch, grain size. (Grain size finer than ASTM No. 8)

Tensile, stress rupture, and bend properties reported for the sheet are given in Table 1. Major alloy element and impurity analyses are also shown in this table.

Coating

Mechanical property samples were coated at the Solar Division of the International Harvester Company. Processing included surface and edge preparation by barrel finishing, pickling, and sand blasting. Following this, a 50 w/o W-20 w/o Mo - 15 w/o V - 15 w/o TiH_2 powder slurry was sprayed on the samples to approximately 0.005" thickness, and sintered for 15 hours at 2760° F to 2800° F at a pressure of 10^{-5} to 10^{-6} torr. Conversion of the metallic coating to the silicide was accomplished by heat treatment for 16 hours at 2150° F in a silicon pack. An outline of the coating process is shown in Table 2.

TABLE 1 - Mechanical Properties and Composition of the Substrate Material[1]

Tensile Properties at Room Temperature									
0.2% Y.S.		Upper Y. Pt.		Lower Y. Pt.		U.T.S.		% Elongation	
ksi	$N/m^2 \times 10^{-7}$	ksi	$N/m^2 \times 10^{-7}$	ksi	$N/m^2 \times 10^{-7}$	ksi	$N/m^2 \times 10^{-7}$	Uniform	Total
111.1	76.5	112.7	77.8	107.3	73.9	120.4	85.7	14.5	28
108.8	75.1	110.9	76.4	108.2	74.6	120.8	83.4	14.2	25

Stress Rupture Properties				Bend Ductility	Major Alloy Element and Impurity Analysis				
33ksi /2400°F		25ksi /2400°F		-320°F & 1T Punch	w/o		PPM		
Creep Rate	Life	Creep Rate	Life						
%/Hr.	Hrs.	%/Hr.	Hrs.	>95°	W	Hf	C	O	N
.488	8.4	.090	59.7	Bend	10.5	2.2	140	17	22

1. Data reported in ref. 6 for sheet 10B

   33 ksi = 22.7×10^7 N/m^2
   25 ksi = 17.2×10^7 N/m^2
   -320°F = 77°K
   2400°F = 1589°K

TABLE 2 - Silicide Coating Sequence

Step.	Process
1.	Barrel finish to produce a 0.015" radius on the sample edges.
2.	Pickle and sand blast.
3.	Spray a powder slurry containing 50%W, 20%Mo, 15%V and 15%TiH_2, producing a 0.005" thick coating.
4.	Oven dry.
5.	Rack samples on tungsten wires and heat treat at 2760 to 2800°F for 15 hours in vacuum of 10^{-5} to 10^{-6} torr.
6.	Pack in silicon and heat treat at 2150°F for 16 hours under argon at 800 torr.

0.015": 0.381mm

0.005": 0.127mm

2800°F: 1811°K

2150°F: 1450°K

Coating thickness and weight gain were recorded for each sample, both after application and sintering of the metallic coating components, and after siliciding. This information is displayed in Tables 3 and 4. Coating thicknesses of 0.006" to 0.007" at edge locations, and 0.007" to 0.008" at flat areas, were produced. Weight changes of between 58 and 68 mgs/square cm. resulted from application of the metallic coating components, while siliciding added another 36 to 39 mgs/square cm. Using 63 mgs/square cm. and 37.5 mgs/square cm. as typical metallic and silicon coating component weights, and assuming none of the metallic constituents are lost during the heat treatments, a coating composition of 31.4 w/o W-12.5 w/o Mo-9.4 w/oV - 9.4 w/o Ti - 37.3 w/o Si (8.6 a/o W - 6.6 a/o Mo-9.3 a/oV-9.8 a/o Ti-65.7 a/o Si) is calculated. This composition yields a metal-to-silicon atom ratio of 1-to-1.94.

Photographs of mechanical property samples as prepared for coating, and after coating, are displayed in Figure 2. The coating surface can be characterized as grey, and of matte texture.

Microstructure through the cross section of the as-applied coating is displayed in Figure 3. The terminology used in the figure to describe the structurally differing regions, metallic diffusion zone (ternary barrier*), metallic-intermetallic reservoir (secondary barrier*), are those used by Metcalfe and Stetson[1].

X-ray diffraction analysis of these coating zones is presented in Table 5, and compared to ASTM compound standards. Similar results were obtained from diffractometer analysis of the as-applied surface, and from a Debye pattern of removed and crushed metallic-intermetallic reservoir. These results compared most favorably to the ASTM standards for $(Ti_{0.6}W_{0.4})Si_2$, $(Ti_{0.8}Mo_{0.2})Si_2$, $MoSi_2$, and WSi_2. Similarity of diffraction patterns for $(Ti_{0.6}W_{0.4})Si_2$ and $(Ti_{0.8}Mo_{0.2})Si_2$, and for $MoSi_2$ and WSi_2, as well as the overall isomorphous behavior of the metallic constituents, prevents an absolute determination of the exact compounds present in the metallic-intermetallic reservoir. Wimber and Stetson[3] came to a similar conclusion concerning x-ray diffraction analysis of a coating close to the study composition.

---

*The term primary barrier is used to distinguish the layer of oxidation product formed on the coating during elevated temperature air exposure.

Table 3 - Tensile Sample Coating Data

Sample[1] Number	Changes Resulting from 50W-20Mo-15Ti-15V Application			Changes Resulting from Silicide Coating		
	Thickness Increase. (Mils/surface)[2]		Weight Gain	Thickness Increase. (Mils/surface)		Weight Gain
	Edge	Flat	(Mgs/Cm^2)	Edge	Flat	(Mgs/Cm^2)
1-10						
11	3.30	4.55	66.06	2.60	2.80	38.59
12	3.30	4.25	63.41	2.60	2.90	38.52
13	3.55	4.50	66.03	2.75	2.85	38.26
14	3.75	4.20	62.73	2.85	2.80	37.72
15	3.40	3.95	56.75	2.75	2.75	36.68
16	3.40	3.85	57.65	2.75	2.75	36.91
17	3.40	4.00	59.21	2.75	2.90	37.43
18	3.55	4.40	67.82	2.70	3.00	39.47
19	3.35	4.25	65.96	2.75	2.80	38.73
20	3.50	4.35	68.24	2.75	2.80	38.76
21	3.45	4.35	67.31	2.65	2.95	38.62
22	3.75	4.35	65.90	2.80	2.95	39.11
23	3.40	4.05	60.92	2.60	2.75	37.17
24	3.00	4.00	59.86	2.55	2.80	36.80
25	3.00	4.10	59.58	2.65	2.70	36.65
26	3.10	3.80	58.18	2.75	2.80	36.94
27	3.08	4.05	59.05	2.55	2.75	36.08
28	3.20	4.25	64.89	2.60	2.75	37.53
29	3.35	4.20	62.21	2.60	2.80	36.97
30	3.15	4.15	64.25	2.50	2.75	37.15
31	3.20	4.20	64.51	2.55	2.75	37.23
32	3.35	4.00	58.08	2.65	2.70	37.10
33	3.10	4.00	58.63	2.60	2.80	37.36
34	3.20	4.10	58.73	2.55	2.80	37.57
35	3.20	4.10	58.17	2.55	2.75	37.01
36	3.45	4.25	60.14	2.70	2.80	37.41
37	3.25	4.15	58.18	2.60	2.90	36.84
38	3.30	4.20	59.44	2.65	2.90	37.68
39	3.25	4.15	58.14	2.70	2.80	37.33

1. Samples 1 through 10 were not coated. The surface and edges of these samples, however, were prepared for coating.
2. Total thickness or width increase divided by two. 1 Mil = .0025Cm.

TABLE 4 - Bend Sample Coating Data

Sample[1] Number	Changes Resulting from 50W-20Mo-15V-15Ti Application			Changes Resulting from Silicide Coating		
	Thickness Increase (Mils/Surface)[2]		Weight Gain	Thickness Increase (Mils/Surface)		Weight Gain
	Edge	Flat	(Mgs/Cm^2)	Edge	Flat	(Mgs/Cm^2)
1-5						
6	4.10	4.65	65.11	3.05	3.10	39.65
7	3.75	4.50	59.69	2.70	3.00	37.92
8	4.20	4.45	61.72	3.05	3.00	38.87
9	3.95	4.85	64.01	2.85	3.15	39.34
10	3.95	4.45	60.37	2.95	2.95	38.34
11	3.75	4.80	62.10	2.80	3.05	38.38
12	3.95	4.80	64.26	2.85	2.95	38.41
13	3.85	4.65	61.72	2.85	2.95	37.71
14	3.95	4.90	62.07	2.75	2.95	37.53
15	3.85	4.95	65.17	2.90	2.95	38.81
16	3.80	4.85	62.36	2.90	3.10	38.30
17	3.90	4.75	62.05	2.90	2.85	37.36
18	3.85	4.75	62.21	2.85	2.80	37.22
19	3.80	4.75	63.40	2.80	2.95	37.89
20	3.85	5.10	66.25	2.75	2.90	38.59
21	4.05	5.05	67.33	2.80	2.95	38.77
22	4.00	4.80	63.48	2.90	3.00	38.31

1. Samples 1 through 5 were not coated. The surface and edges of these samples, however, were prepared for coating.
2. Total thickness or width increase divided by two. 1 Mil = .0025 Cm.

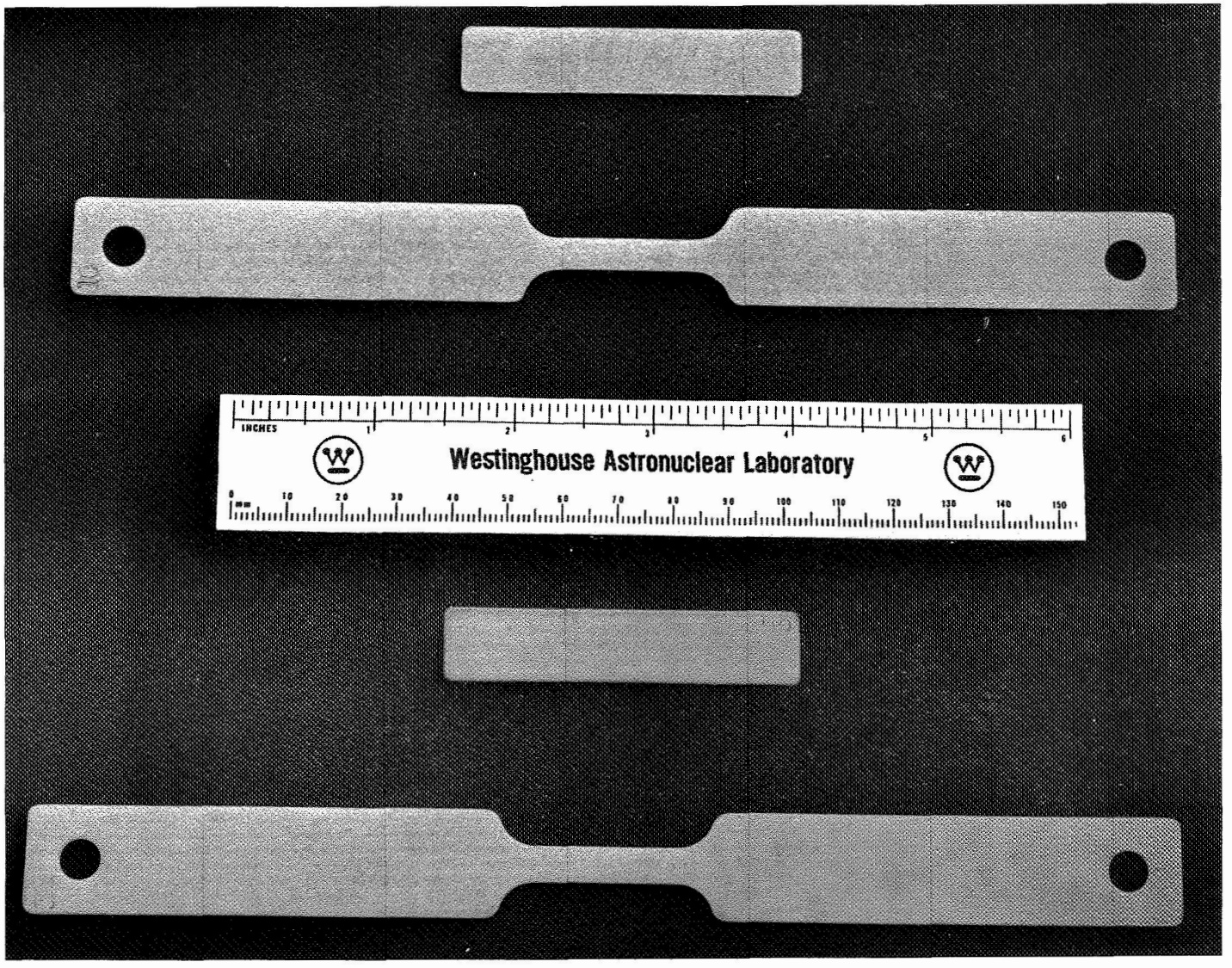

FIGURE 2 - Mechanial Property Specimens. Top: As Prepared for Coating. Bottom: As-Coated.

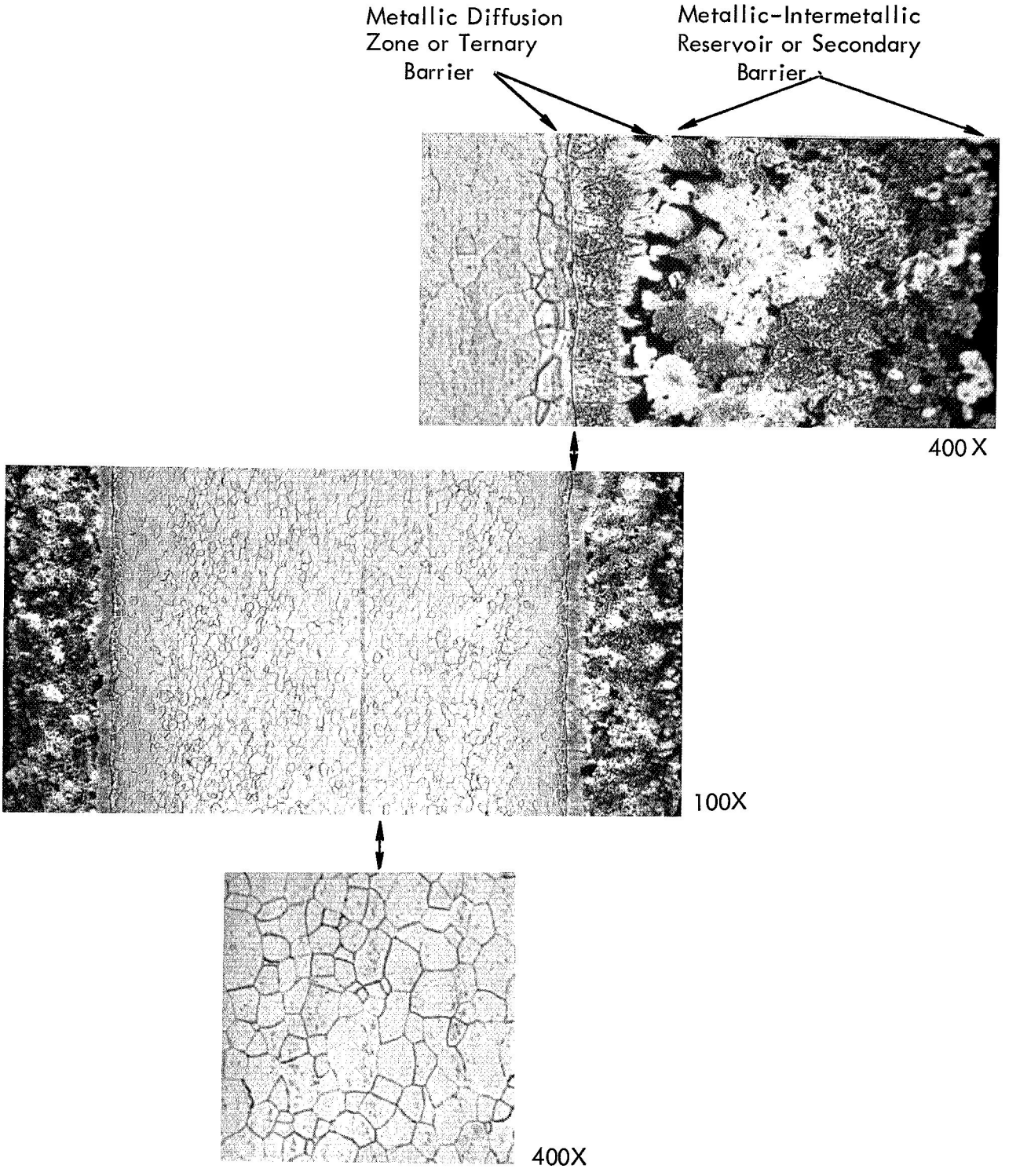

FIGURE 3 - Microstructure of Coating-Substrate Cross Section

TABLE 5 - X-Ray Diffraction Analysis of the As-Applied Coating

Metallic-Intermetallic Reservoir												Metallic Diffusion Zone					
Diffractometer Trace		Debye Pattern		ASTM Standards								Diffractometer Trace		Debye Pattern		ASTM Standard	
				$(Ti_{.6}W_{.4})Si_2$		$(Ti_{.8}Mo_{.2})Si_2$		$MoSi_2$		WSi_2						$TaSi_2$	
d	I*	d	I	d	I	d	I	d	I	d	I	d	I	d	I	d	I
4.02	W	4.03	W			4.02	30					4.10	W	4.10	VW	4.13	22
				4.00	10							3.48	S	3.48	S	3.50	100
3.91	M	3.90	W					3.92	46	3.91	50			2.96	VW		
3.42	S	3.40	M	3.42	80	3.42	50					2.56	M	2.56	W	2.57	58
2.96	M	2.95	M					2.96	96	2.77	100	2.42	W				
2.52	M	2.52	M	2.52	50	2.52	30					2.37	W	2.37	VW	2.389	17
2.32	W	2.32	W	2.33	10	2.33	30					2.29	VW				
2.26	W	2.26	W					2.26	70	2.27	70	2.23	S	2.23	M	2.246	94
				2.20	100							2.18	W	2.18	W	2.187	32
2.19	S	2.19	S			2.19	100					2.05	M	2.05	W	2.070	36
2.16	M	2.15	W			2.17	50							2.03	W		
2.02	M	2.03	M	2.02	30	2.02	20	2.02	100	2.02	85	1.92	M	1.92	M	1.932	63
1.96	W	1.96	W					1.96	70	1.96	50						
1.89	S	1.88	S	1.89	100	1.894	90										
		1.60	W					1.66		1.60	25						
						1.588											
		1.58	W	1.58													

*Intensity Estimates - S: Strong
M: Moderate
W: Weak
VW: Very Weak

Diffractometer analysis of the surface presented after removal of the metallic-intermetallic reservoir, and a Debye pattern of material scraped from that surface, also yielded similar data. The results show the metallic diffusion zone to be principally $TaSi_2$.

Results of electron microprobe analysis taken at several positions in the as-applied coating are summarized in Figure 4. All major coating and substrate elements were analyzed for at five structurally distinct locations encompassing the metallic-intermetallic reservoir and the metallic diffusion zone. Concentration data is presented as a ratio of detected element intensity to that characteristic of a pure standard, uncorrected for effect of other elements.

Single phase regions rich in molybdenum and silicon, A, and tungsten and silicon, B, appear, by analogy to the results of x-ray diffraction analysis, to be particles of $MoSi_2$ and WSi_2 containing some titanium and vanadium. Similarly, the results from area E confirm the ternary barrier to be basically $TaSi_2$, containing a small amount of tungsten, titanium and vanadium. The overall isomorphous behavior of these elements is clearly evident from this information.

Tensile and Creep Tests

Elevated temperature tensile and creep testing of coated material was performed in an air environment employing a platinum wire wound tubular furnace. The furnace was mounted vertically and opened at the ends to permit external gripping and air movement. A protective vacuum environment was used for high temperature tensile and creep tests of uncoated material; 10^{-5} to 10^{-6} torr for tensile tests and $<10^{-8}$ torr for creep testing. Samples were held one hour at temperature before application of load.

Precious metal thermocouples placed at the specimen gauge section were used for temperature control on air and vacuum tests. Temperature was monitored on air tensile tests

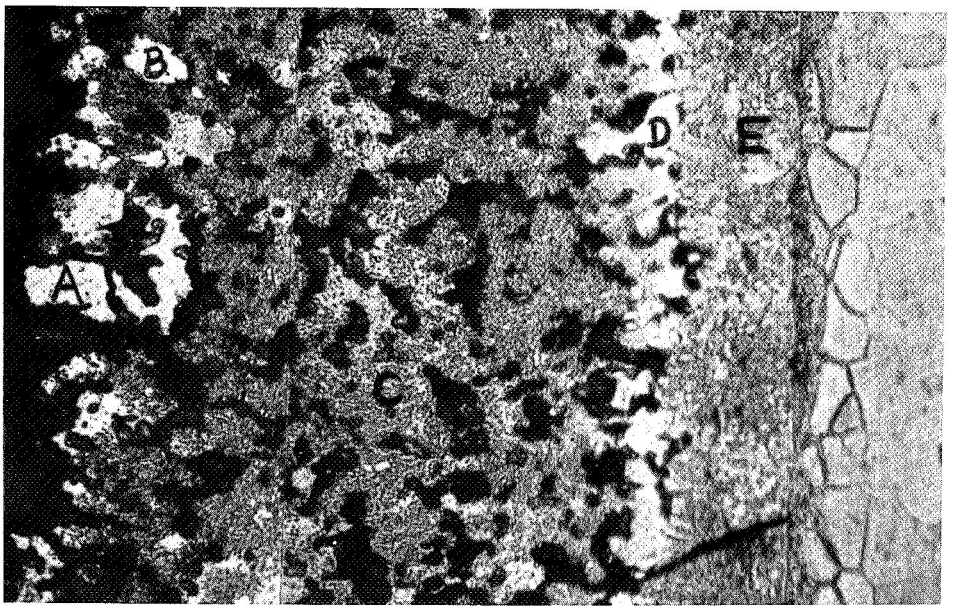

500X

RESULTS

Location	No. of Phases	Ratio of Characteristic X-Radiation $\frac{I\ element}{I\ pure\ std.} \times 100$						
		Si	Mo	W	Ti	V	Ta	Hf
A	1	17.0	28.5	0	5.6	4.9	0	0
B	1	15.2	0	49.8	2.4	3.2	0	0
C	>1	16.1	5.8	31.2	2.3	5.6	0	0
D	>1	13.8	0	28.6	2.3	2.5	38.5	0
E	1	13.9	0	5.6	2.0	1.6	51.0	0

FIGURE 4 - Microprobe Analysis of Phases in the As-Applied Coating

from three precious metal thermocouples wired directly to the specimen, one at the center and one at each end of the gauge section. Furnace power was regulated to maintain the center thermocouple at test temperature. Temperature at the ends of the gauge section deviated by no greater than ± 2°F from that of the center position.

Temperature measurement from thermocouples directly attached to the specimen proved unsuited for the air creep tests due to eventual interaction with the silicide coating. Because of this, a single thermocouple, with its bead shielded inside alumina insulation and positioned centrally in the gauge section, was employed to monitor and control temperature on these tests. Reaction was not observed between the alumina insulation and silicide coating. Temperature determined in this manner proved on a "dummy test" to be within ± 2°F of that measured from a thermocouple directly attached to the sample.

Coated samples were creep tested in a lever-arm unit calibrated against a load cell to compensate for any weight error due to linkage friction. Strain measurement on these tests were taken from a dial gauge attached across the grip positions. Creep strain was determined on the ultrahigh vacuum test of substrate material by cathetometer observation of fiducial marks scribed at each end of the gauge section.

Tensile tests were run at a 0.05/min. strain rate.

An eight inch long pin loaded test sample containing a 1" x 1/4" reduced section was employed to gather tensile and creep properties. The sample, a photograph of which is shown in Figure 2, permitted gripping on elevated temperature air tests to be accomplished external to the furnace, eliminating any problems associated with use of hot grips.

Bend Tests

Bend tests were conducted using a 1/2" wide x 2-1/2" long sample supported across a 1" span. A 0.125" radius punch was employed, and testing was performed at a deflection

rate of 1 ipm. Curves of load against deflection were autographically recorded. Bending was conducted until substrate failure occurred, or a ductile bend of greater than 90 degrees was achieved. Substrate failure, when it occurred during bending, was denoted by a second sudden drop in test load, the first load drop occurring after a few degrees deflection due to coating failure.

Bend tests were performed in the temperature range -150° F to -320° F, achieved by regulating the flow of liquid nitrogen around the specimen. Temperature was read from a thermocouple attached at the tip of the test punch, the signal from which controlled a solenoid valve to regulate coolant flow.

Oxidation Tests

Oxidation of coated samples was conducted in air at 1400° F, 1600° F and 2400° F. A silicon carbide globar furnace of 6" x 15" hearth area was employed on the 2400° F tests; lower temperatures were achieved in a nichrome wire wound resistance furnace of similar dimensions. Construction of the furnaces was such that a gentle movement of air occurred through them.

Tensile samples exposed at 1400° F were supported through their pin holes on an inconel rack, as shown in Figure 5. Bend samples exposed on the program at both 1400° F and 1600° F, were supported inside zirconia boats on wedges of Dynaquartz*, a high purity quartz felt. Samples were held for exposure at 2400° F on edge in 0.050" wide x 0.050" deep slots cut into a silicon carbide brick, as shown in Figure 6.

Time-at-temperature was not accumulated in one continuous heat treatment, but, instead, was principally achieved by repeating exposure periods of 2, 2, and 16 hours duration, with rapid air cooling to room temperature employed between periods. Deviation from the 2, 2, and 16 hour exposure schedule occurred when weekend and holiday periods intervened.

---

* A Johns Mansville trade designation.

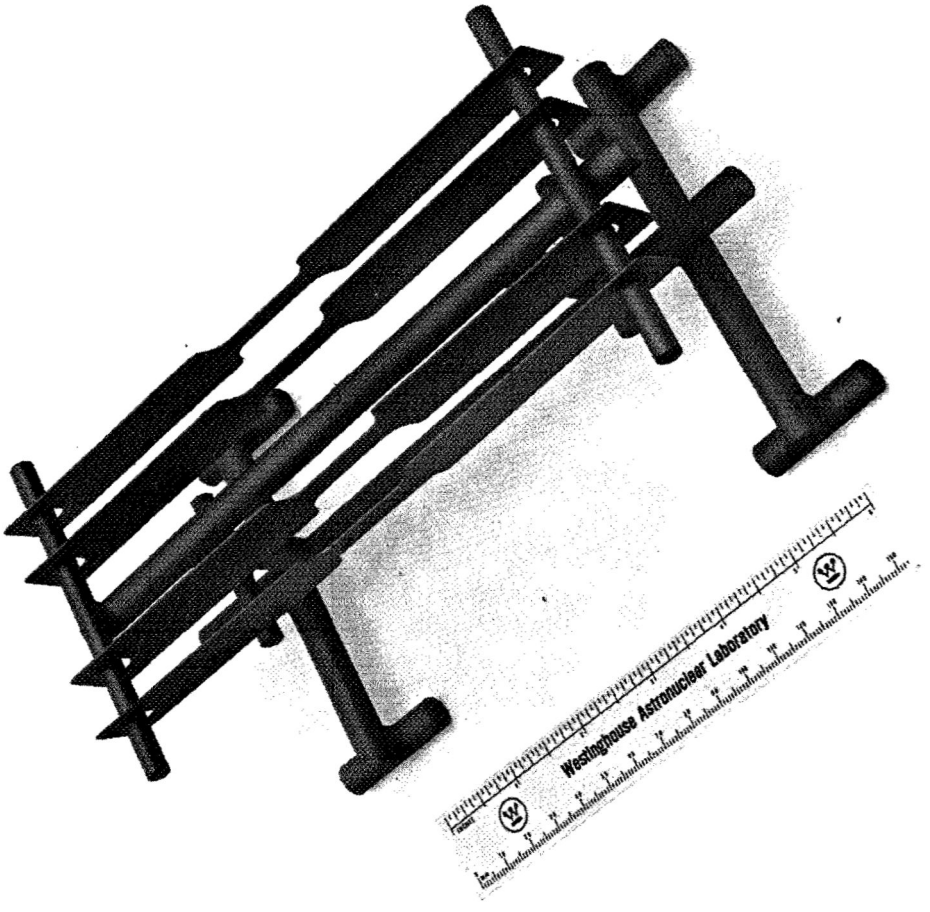

FIGURE 5 - Tensile Specimens Racked on an Inconel Fixture for Oxidation at 1400°F

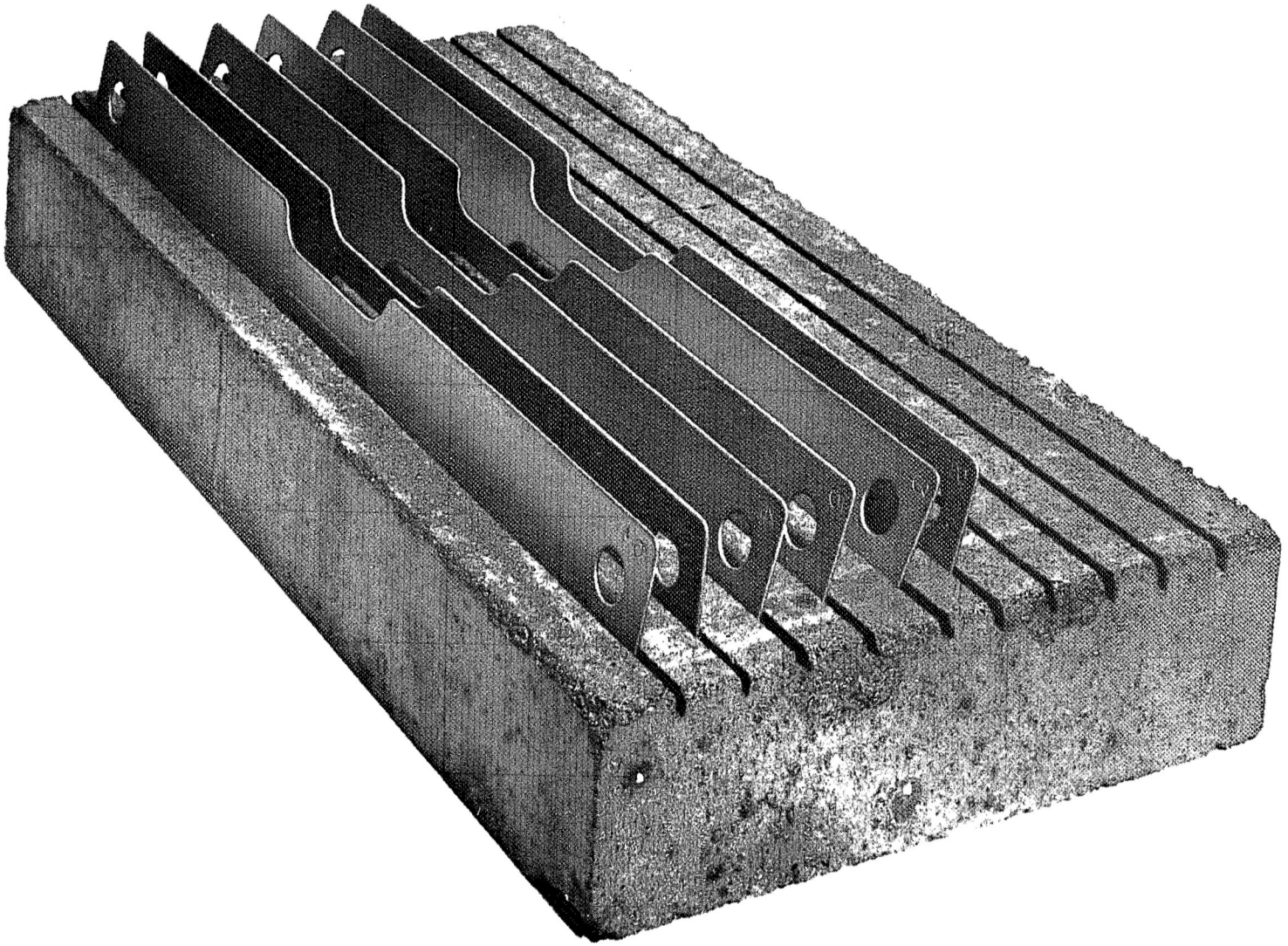

FIGURE 6 - Specimens Supported on a Silicon Carbide Brick for Oxidation at 2400°F

The oxidation rate of all elevated temperature air exposed samples was recorded by determining weight gain after each exposure period. Samples were also visually inspected after each oxidation period, and a photographic record of coating changes kept as dictated by appearance.

Metallography

Samples were ground on 120 through 600 grit emery paper, then rough polished on metcloth using 30, 15, and 6 micron diamond abrasive paste. Final polishing was performed on microcloth employing Linde B abrasive suspended in a solution containing 35 ml. H_3PO_4-50 gms. CrO_3-2.5 ml. H_2SO_4 - 400 ml H_2O. An etch of equal parts glycerin, nitric acid, and hydrofluoric acid, was used to develop structure.

X-ray Diffraction and Electron Microprobe Analyses

A Siemens diffractometer and 114 mm Debye camera were used for x-ray diffraction analysis. Electron microprobe analysis was performed on an Applied Research Laboratory Model AMX unit. Samples were examined on the microprobe in the metallographically polished and etched condition.

III. EXPERIMENTAL PROGRAM AND DISCUSSION

The results of tests performed on the program, and analysis of the data, are presented in this section. Data are reported in three categories: Oxidation Behavior, Mechanical Properties and Chemical Analysis, Structure Studies. An attempt was made to study specimens in numbered sequence to simplify reporting, but this was upset somewhat when sample substitution and repeated tests had to be made due to observation of coating defects on some samples, and unexpected oxidation behavior of others. Several samples described in Tables 3 and 4 are not mentioned in the text. These were either set aside for evaluation at NASA, or were employed to check test procedures.

Oxidation Behavior

Tests at 2400° F. Exposure of four creep, four tensile, and eight bend samples at 2400° F prior to testing formed a part of the test program - Figure 1. Accumulation of 600 hours time-at-temperature in repeated 2, 2, and 16 hour exposure periods was planned for the creep and tensile samples, and four bend samples. The other bend samples were to be oxidized for a total of 10 hours at 2400° F, accumulated in five 2 hour periods. Bend samples 12 through 19, and tensile samples 16 - 19 and 28 - 31* were chosen for these tests.

Oxidation testing at 2400° F was approached cautiously due to an anticipated problem of sample handling, and only one sample, arbitrarily chosen to be tensile 28, was used in an initial two hour test. Unaided visual inspection of this sample after 2 hour exposure at 2400° F revealed a coating crack located approximately 1/2 inch below a pin hole. Oxidation of the substrate at the defective site, however, was not evident.

A photograph showing the crack is presented in Figure 7A. As a consequence of this, close examination was made of the coating on the other samples scheduled for oxidation revealing, with assistance of 5X magnification, fine hairline cracks on tensile samples 29, 30 and 31, at a location similar to that observed cracked on tensile 28. Photographs of two of these samples displaying the defects are presented in Figure 8. Three tensile samples, numbers 12, 13 and 33, inspected and found to be free of any macroscopically obvious coating cracks, were substituted for specimens 29, 30 and 31. Oxidation was continued, however, on tensile 28. Sample handling did not pose any problem on the initial two hour test using tensile 28, and subsequent tests were performed simultaneously on all samples.

Coating cracks were observed after the initial 2 hour exposure at 2400°F on four of the seven tensile samples established free of obvious defects in the as-coated condition. Cracking occurred about 1/2 inch below a pin hole on three samples, and about 1/8 inch

*To simplify discussion, both tensile and creep samples will be referred to as tensile samples where distinction of intended test category need not be made.

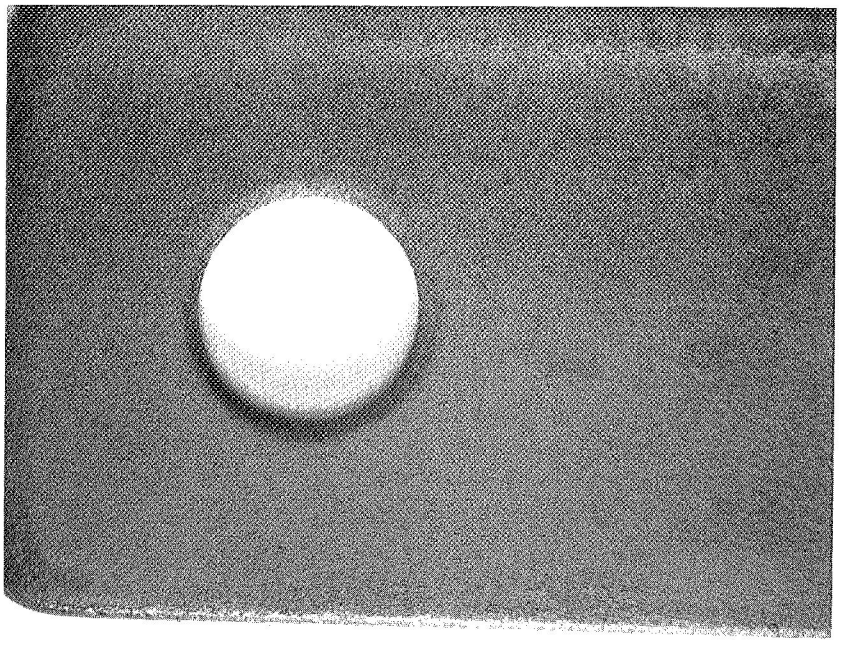

(A)

2 Hrs/2400°F (1589°K)

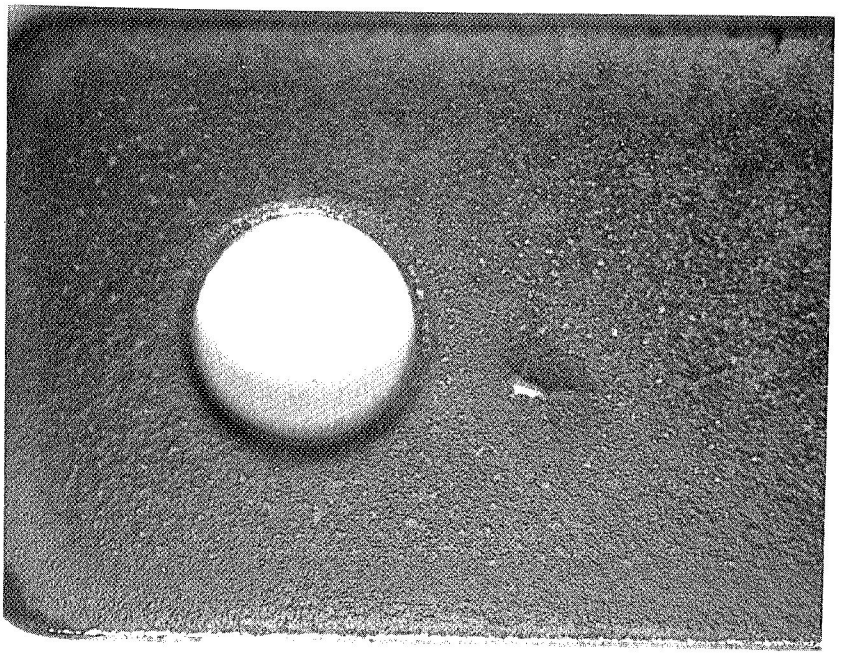

(B)

21 Hrs/2400°F

FIGURE 7 - Progress of Coating Failure on Tensile Sample 28

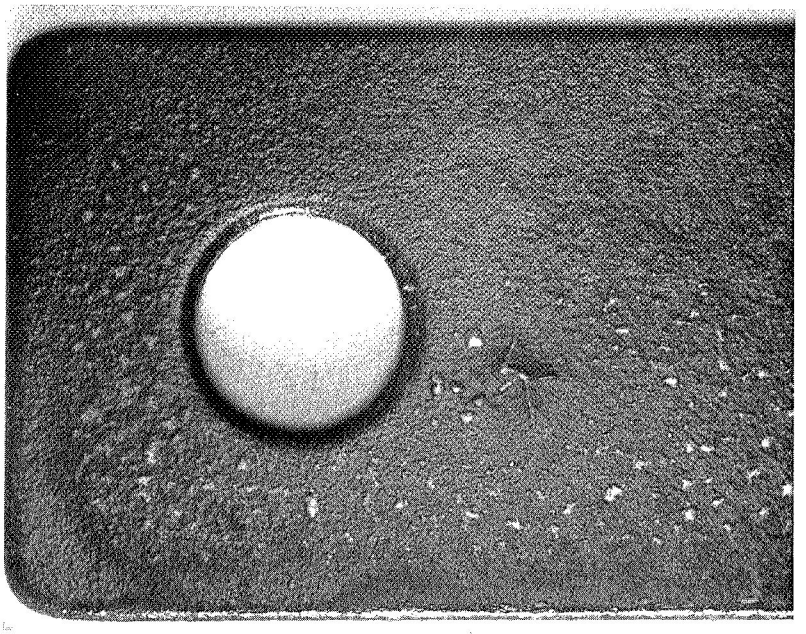

(C)

130 Hrs/2400°F

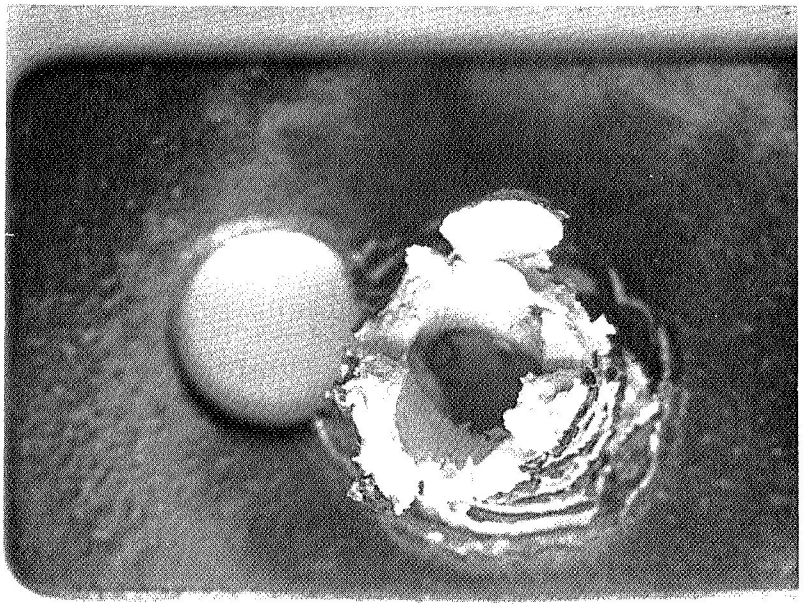

(D)

191 Hrs/2400°F

FIGURE 7 (Continued) - Progress of Coating Failure on Tensile Sample 28

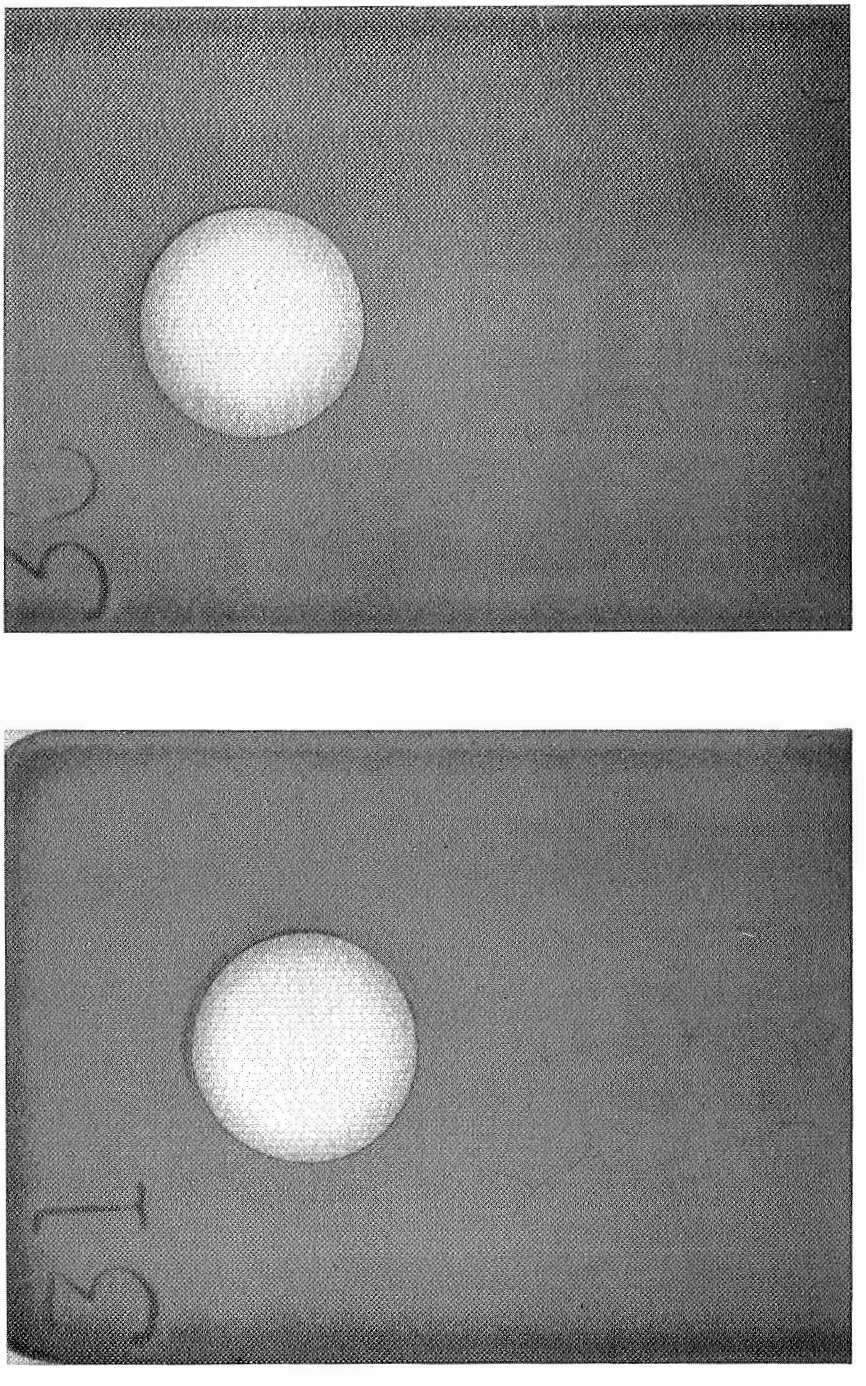

FIGURE 8 - Typical Cracking Found on As-Coated Tensile Samples

above this feature on the other. Because of this, whether the crack found on tensile 28 was present in the as-coated condition or occurred during exposure, cannot be established. Substrate oxidation was not evident at the defective sites on any of these samples, as was observed on tensile 28.

The progress of oxidation testing at 2400° F in terms of sample condition and weight gain is given in Table 6. After 21 hours total time-at-temperature, substrate oxidation started on two of the five samples which revealed coating defects after the initial two hour exposure period - Tensiles 13 and 18. Coating failure occurred at the defective sites. The samples were exposed for three more hours at 2400° F, whereupon gross substrate oxidation became apparent. Photographs showing coating failure on tensiles 13 and 18 are presented in Figure 9. By contrast, the cracks on the other three samples appeared to "heal" by filling with oxidation product during this exposure time. Figure 7B and Figure 10A reveal this development on tensiles 28 and 12.

After 62 hours at 2400°F, tensile 12 developed a second coating crack, this one located approximately 1/2" below a pin hole. Figure 10B shows this defect. Note that the area found cracked after 62 hours was included in the photograph showing coating condition after 21 hours exposure, and appears sound. Both coating cracks on tensile 12 began to open after 153 hours at temperature, and widened further after 155 hours exposure, whereupon testing was terminated. Photographs revealing coating failure on tensile 12 and the "healed" condition documented at 130 hours exposure time are displayed in Figure 10, parts C, D and E.

Coating failure and pronounced substrate oxidation occurred at the defective coating site on tensile 28 after 191 hours at 2400° F. Photographs showing the failure and the "healed" defect condition after 130 hours time-at-temperature are presented in Figure 7, parts C and D.

Oxidation at 2400° F resulted in coating failure on the remaining sample which developed an obvious defect during the initial 2 hour exposure period, tensile 33, after 195 hours time-at-temperature was accumulated. Failure, however, did not occur at the defective

TABLE 6 - Data for Samples Oxidized at 2400°F (1589°K)

Cycle Number	Cycle Time	Accumulated Time	Total Bend Sample Weight Changes; Milligrams[1]									Total Tensile Sample Weight Changes; Milligrams[1]								
	Hrs.	Hrs.	12	13	14	15	16	17	18	19	Ave.	12	13	15	16	17	18	28	33	Ave.
1	2	2	27.0	25.5	26.4	26.9	26.1	25.2	27.3	26.2	26.4	108.8(B)	109.6(A)	90.6	96.4	97.0	109.4(A)	98.1(A)	107.1(A)	102.1
2	2	4	34.5	32.8	33.4	33.7	35.6	33.1	35.3	34.0	34.1	134.4	134.9	120.9	124.0	124.0	117.0	126.1	135.4	127.1
3	2	6	39.1	37.1	37.9	38.0					38.0									
4	2	8	43.0	41.1	41.9	42.0					42.0									
5	2	10	46.3	44.2	44.9	45.2					45.2									
3	17	21					49.2	47.1	49.5	48.4	48.6	184.6	200.4(F)	178.6	177.3	181.8	211.1(F)	191.7	189.5	189.4
4	3	24					53.6	51.5	54.1	53.0	53.1	195.0		195.7	192.1	192.4		205.9	202.4	197.2
5	18	42					59.8	57.9	59.8	59.0	59.1	216.3		215.9	212.5	216.4		226.1	221.8	218.2
6	2	44					61.4	59.9	61.3	60.6	60.8	223.7		223.3	217.9	225.1		232.2	231.1	225.6
7	2	46					63.6	61.5	62.9	62.0	62.5	229.6		227.6	223.4	228.8		240.6	237.6	231.3
8	16	62					66.9	65.5	66.4	65.4	66.1	243.1(A)		238.7	234.3	240.3		252.2	250.3	243.2
9	2	64					70.0	67.1	67.7	66.7	67.9	251.9		243.6	240.4	247.0		257.8	256.3	249.4
10	66	130					76.7	72.4	73.4	73.1	73.9	272.6		265.0	261.6	267.1		281.4	276.7	270.7
11	2	132					77.7	73.6	74.9	74.9	75.3	277.5		268.6	265.8	271.1		285.1	281.7	275.0
12	2	134					N.D.	(F.E.)	75.9	76.0	76.0	282.7		270.6	269.8	274.3		288.6	285.9	278.7
13	17	151					78.3		77.5	76.8	77.5	295.3		276.6	274.5	280.8		297.0	293.2	286.2
14	2	153					78.6		78.9	78.0	78.5	302.7		278.9	279.3	285.0		302.0	297.3	290.9
15	2	155					79.6		79.5	79.0	79.4	318(F)		281.6	282.9	289.0		305.9	300.6	296.3
16	16	171					80.7		80.9	80.4	80.7			287.2	288.7	294.9		312.4	304.0	297.4
17	2	173					81.3		81.7	81.2	81.4			289.6	292.0	298.3		315.9	306.6	300.5
18	2	175					82.3		82.6	82.1	82.3			293.0	294.9	301.3		318.6	308.9	303.3
19	16	191					83.7		83.9	83.5	83.7			297.7	300.3	307.4		(F)	313.0	304.6
20	2	193					N.D.		N.D.	N.D.				N.D.	N.D.	N.D.			N.D.	
21	2	195					85.4		85.9	85.3	85.5			304.6	306.6	314.4			(FE)	308.5
22	89	284					90.6		92.4	90.4	91.3			317.2	322.9	(G)				320.5
23	2	286					N.D.		N.D.	N.D.				N.D.	N.D.					
24	2	288					N.D.		N.D.	N.D.				N.D.	N.D.					
25	16	304					91.8		93.2	91.7	92.2			324.2	330.9(FE)					327.6

1. Starting Sample Weights: gms

Bend		Tensile	
12	12.3887	12	49.7020
13	12.4546	13	49.6031
14	11.7368	15	49.8908
15	12.2841	16	50.0230
16	12.0665	17	50.2605
17	12.1528	18	50.6610
18	12.4755	28	50.1836
19	12.5350	33	50.4470

N.D.: Not Determined
(A) Coating cracks noted 1/4" - 1/2" below a pin hole
(B) Coating crack noted 1/8" above a pin hole
(F) Coating failed at noted defective site
(FE) Coating failed at an edge location
(G) Gross oxidation preventing detection of coating failure origin

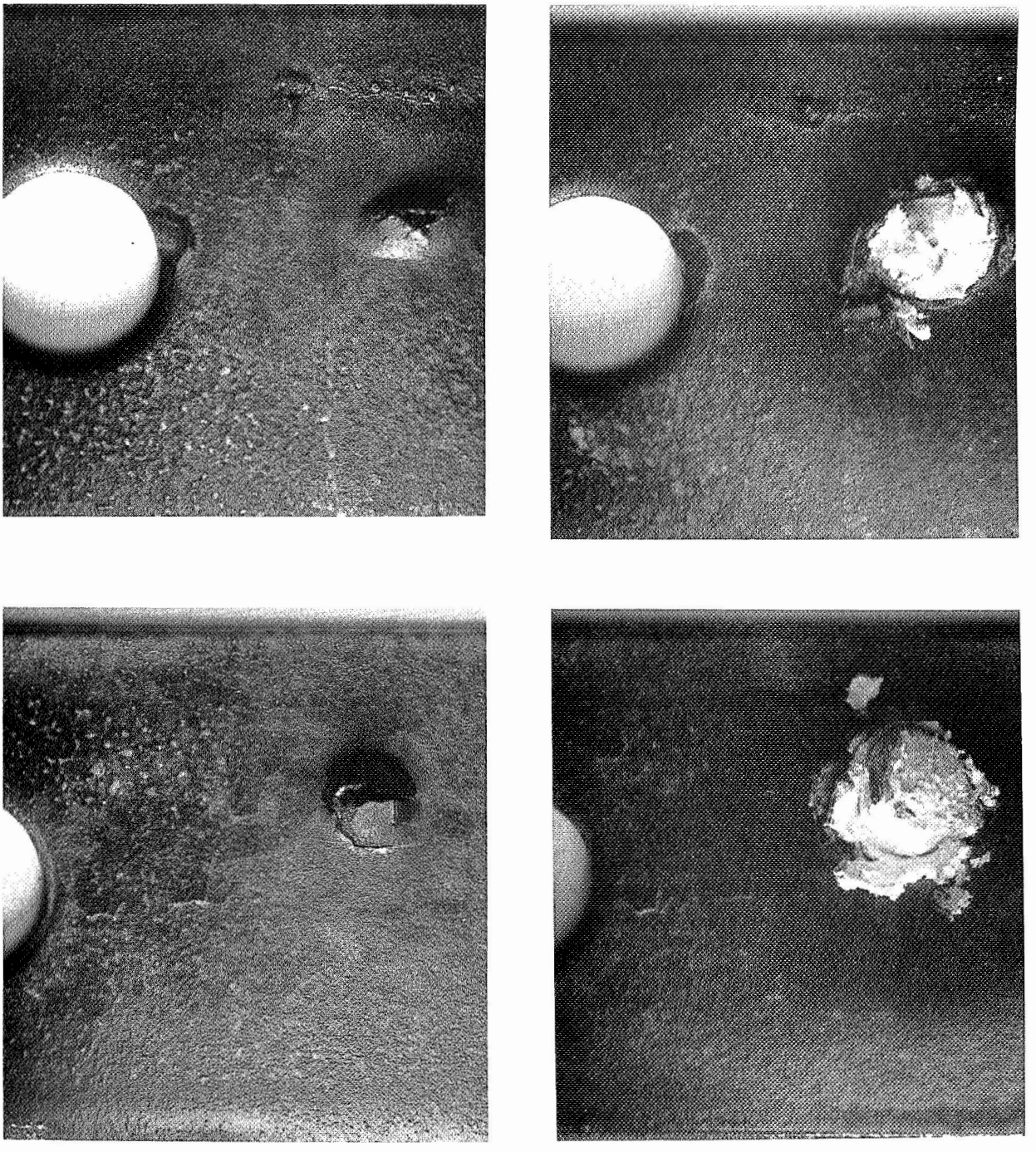

FIGURE 9 - Coating Failure on Tensile Samples 13 and 18
Top: 21 and 24 Hrs. at 2400°F (1589°K); Sample 13
Bottom: 21 and 24 Hrs. at 2400°F; Sample 18

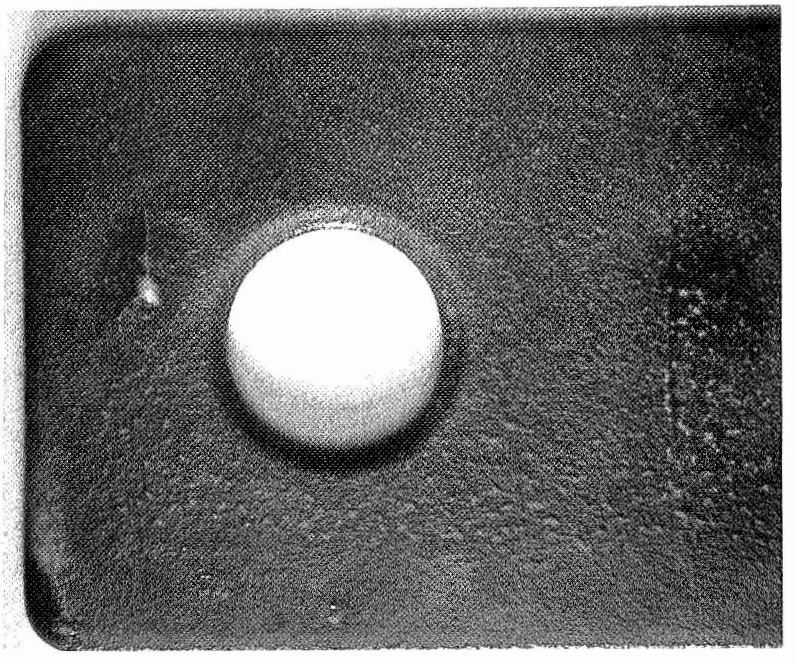

(A)

21 Hrs/2400°F (1589°K)

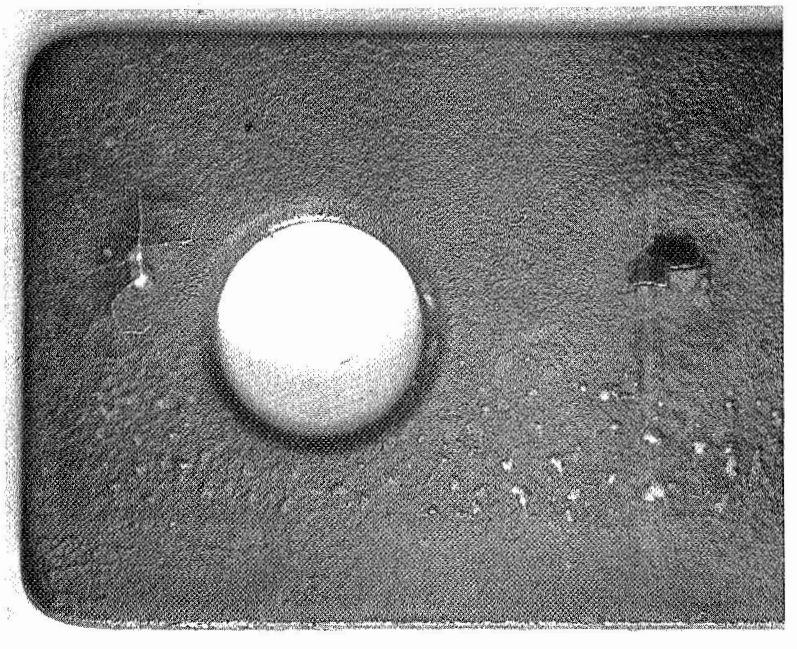

(B)

62 Hrs/2400°F

FIGURE 10 - Progress of Coating Failure on Tensile Sample 12

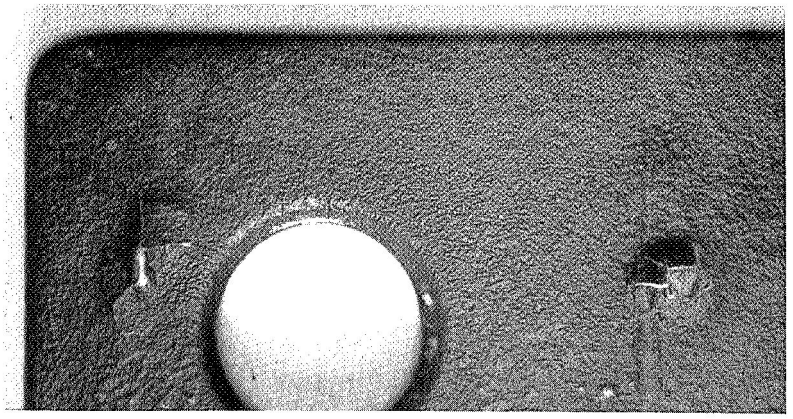

(C)

130 Hrs/2400°F

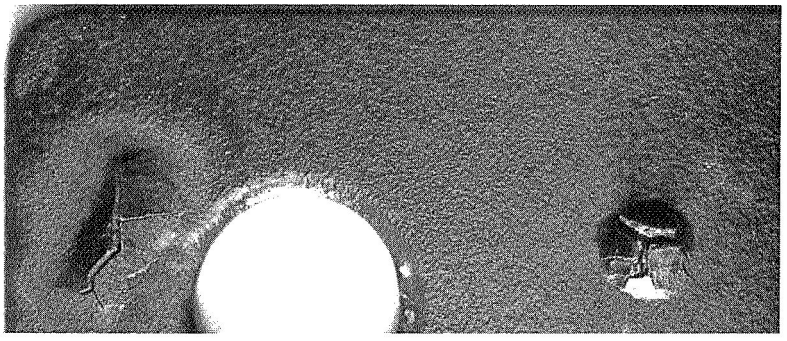

(D)

153 Hrs/2400°F

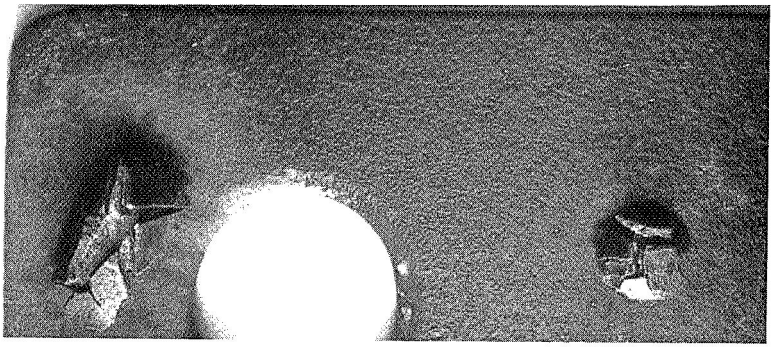

(E)

155 Hrs/2400°F

FIGURE 10 (Continued) - Progress of Coating Failure on Tensile Sample 12

surface location, but, instead, at an edge site within a gauge section radius. A photograph of this coating failure is shown in Figure 11C.

Substrate oxidation was also observed after 284 hours time-at-temperature on tensile 17, one of the three samples which did not reveal development of any obvious coating defect up to that time. Failure occurred during a weekend exposure period and, as a consequence, when noted, substrate oxidation had progressed to where the failure origin was beyond detection. A photograph of the sample is shown in Figure 11A.

Testing was terminated with only two of the original eight tensile samples remaining at 304 hours time-at-temperature, to insure some mechanical property evaluation of material exposed at 2400° F would be made. Inspection of the two surviving tensile samples (tensiles 15 and 16), however, did reveal evidence of oxidation beginning on tensile 16 at an edge site within a gauge section radius. A photograph showing this is given in Figure 11D.

Air exposure of the four bend samples at 2400° F was also terminated after accumulation of 304 hours time-at-temperature. By contrast, these samples fared better than the tensile specimens, with coating failure occurring on only one. Furthermore, none of the bend samples developed any obvious coating defects during oxidation, such as were noted on several tensile samples.

Coating failure occurred on bend 17 after 134 hours at 2400° F, the site being located on a long edge. A photograph showing the failure is displayed in Figure 11B.

Coating failure on bend 17 could not be attributed to any defect caused by contact with the silicon carbide brick used to hold the specimen, since it occurred on the edge opposite that held in the support slot. In this regard, none of the oxidation failures observed on tensile samples could be related to contact with the SiC brick, since those developed at edge positions were located within a gauge section radius (Nos. 16 and 33), while the four flat surface failures occurred well above the brickline (Nos. 12, 13, 18, 28).

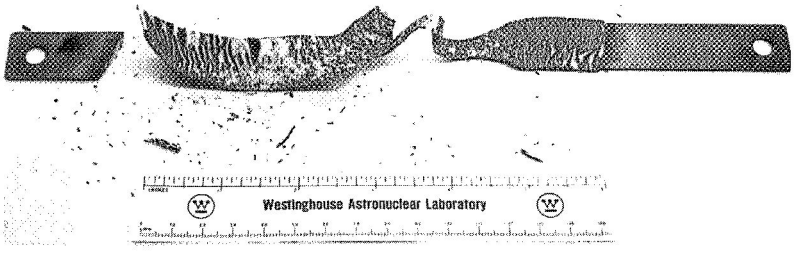

(A)

Tensile 17
284 Hrs/2400°F
(1589°K)

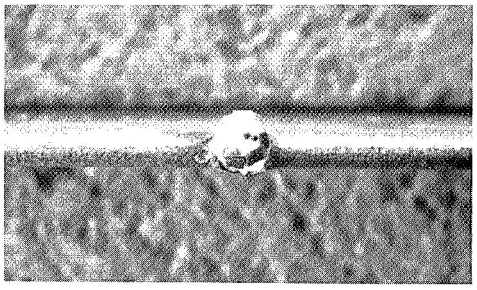

(B)

Bend 17
134 Hrs/2400°F

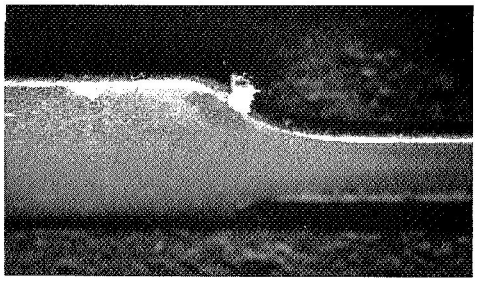

(C)

Tensile 33
195 Hrs/2400°F

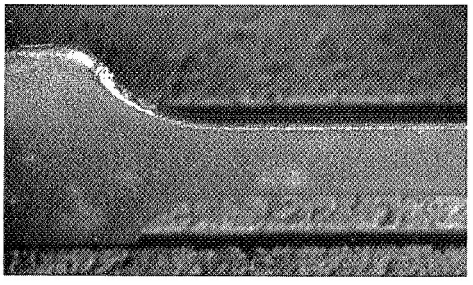

(D)

Tensile 16
304 Hrs/2400°F

FIGURE 11 - Coating Failure on Tensile Samples 16, 17 and 33, and Bend Sample 17

A possible cause for substrate oxidation on tensiles 16 and 33 might be a thin coating at the failure sites. Both samples developed failures at edge sites within a gauge section radius, at a position close to the corner formed by the head section and the radius — Figures 11C & D. The failures, therefore, occurred on an edge nearly perpendicular to the specimen axis. If the metallic coating constituents applied prior to pack siliciding were sprayed on with the jet kept reasonably perpendicular to the axis of the sample, these regions on each gauge section radius would be least covered, and sites vulnerable to failure. The grip pin holes in the tensile sample would likewise be areas susceptible to application of a thin silicide coat. Coating failure, however, was not experienced within even one pin hole on any tensile sample. Perhaps, because the holes are obviously vulnerable in this respect, greater attention was paid them, to insure they were adequately coated. Whether or not the suggestion offered as a possible explanation for oxidation failure on tensiles 16 and 33 is correct, any edge site, because of its shape, is intuitively a region of high defect probability.

Observation of oxidation failures and defects on as-coated samples at a similar location on tensiles 12, 13, 18, 28-31, suggests a possible relationship with sample preparation. Examination of the samples uncovered slight marks on some developed from use of a tungsten wire support to hold them during sintering of the metallic coating constituents. Coating failures were detected at these marks on tensile samples 12 and 13 — Figures 9 and 10. Failure of the other samples, however, developed on the side opposite that displaying wire marks. It appears these marks only present sites of slightly greater coating failure probability. Other coating features which might provide some connection between preparation and coating failure at the similar region on these samples were not uncovered.

A photograph showing the appearance of a tensile and a bend sample after 304 hours exposure in air at 2400° F is given in Figure 12. A line of slightly raised surface spots is obvious on the head section of the tensile sample, running parallel to its axis and concentrated roughly 3/16" from the edge. Some similar spots can be seen on the bend sample shown in the figure, and in the photographs presented for tensiles 28 and 12 in Figures 7 and 10. These spots developed randomly on the bend samples, and principally near the edge of the tensile samples held in the silicon carbide brick, but above the brickline. Although raised from the surface, the spots visually appeared to be dense, and no association could be found to relate their formation with sites of coating failure.

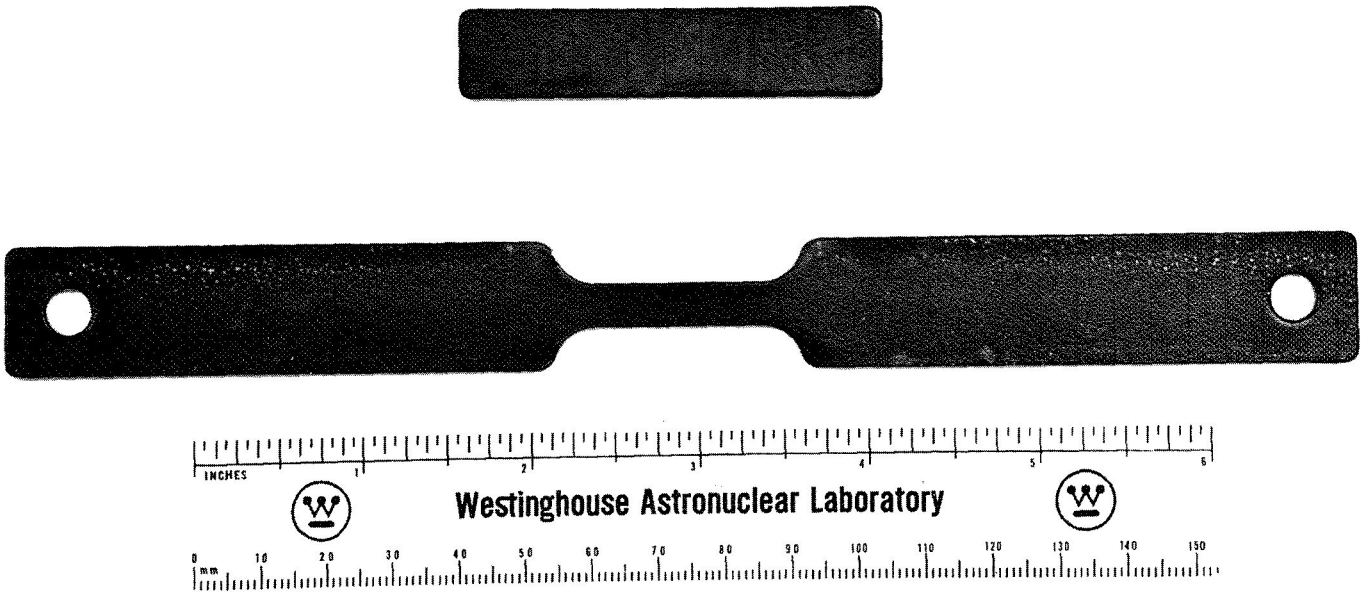

FIGURE 12 - Sample Appearance After 304 Hours Oxidation at 2400°F (1589°K)

Weight gain for the individual samples air exposed at 2400° F, recorded in Table 6, was observed until termination of testing, or until coating failure, signified by obvious substrate oxidation, occurred. As can be seen from the data, extremely consistent oxidation behavior was observed for samples of similar configuration. This information converted to weight gain per unit sample area is plotted against time-at-temperature in Figure 13. A total surface area of 70.8 square cm. determined from the nominal dimensions, was used to normalize the tensile sample data. An averaged area obtained from the actual dimensions of the specimen set defining a single data point, was used to normalize the bend sample results. Values of averaged bend sample area did not vary markedly and, depending upon the set involved, were between 17.00 and 17.36 square centimeters.

Although the overall oxidation rate at 2400° F is similar for both tensile and bend samples, a difference of roughly 10 percent in absolute weight gain is obvious between the data for each specimen type; weight gain for tensile samples being consistently lower than for bend samples. This difference is too large to attribute to error in calculated sample surface areas. Instead, it is believed a result of difference in thermal inertia between the small bend samples and the comparatively larger tensile samples, causing the smaller samples to effectively receive a longer time-at-temperature exposure during a given oxidation period.

A straight line drawn through the data roughly defines an average oxidation rate given by the relationship:

$$M = 0.69 \ln t + 0.85$$

M: mgs/square cm.

t: hours at 2400° F

The rate of weight gain observed over the back-to-back two hour oxidation periods, however, deviates significantly from the average behavior indicated by the above equation, which is biased by the oxidation rate measured over the longer 16 hour and weekend periods. This is believed due to thermal cycling to-and-from 2400° F and room temperature which causes cracks to develop in the coating barriers, resulting in accelerated oxidation until

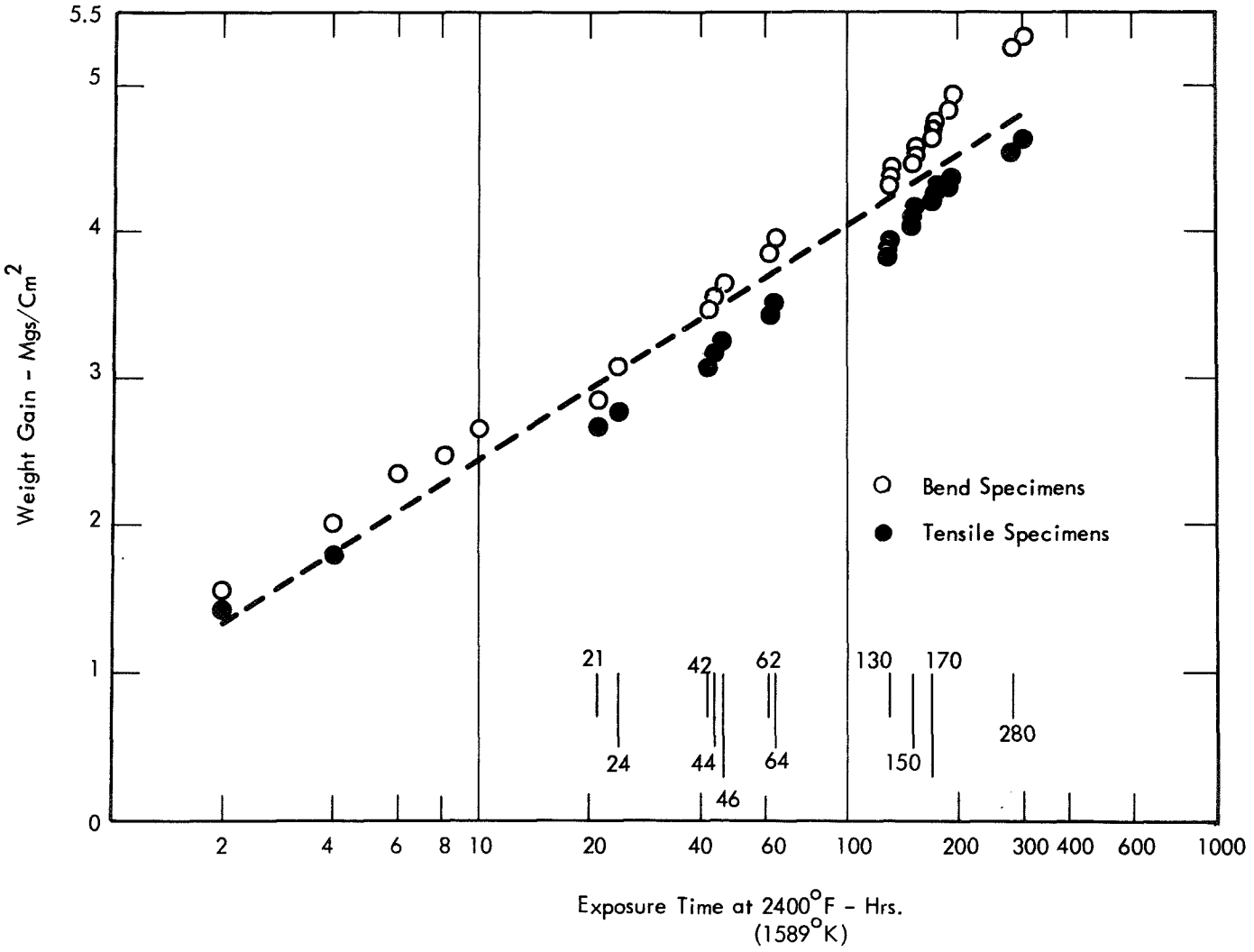

FIGURE 13 - Oxidation Behavior at 2400°F

these defects are repaired by protective oxide formation. Time occupied by oxidation to repair the thermal shock induced defects would be a greater percentage of the two hour exposure periods compared to those of longer duration, and be reflected in observation of a higher oxidation rate. Cracking was a general condition observed metallographically in the primary oxide barrier, metallic-intermetallic reservoir, and metallic diffusion zone, on samples air exposed at 2400° F. Discussion of this condition will be covered in a later section.

Tests at 1400° F. Air exposure of four tensile samples at 1400° F was scheduled in the program — Figure 1. Accumulation of 600 hours time-at-temperature by repeating 2, 2, and 16 hour exposure periods was planned. Tensile samples 19 through 22 were chosen for this test — Table 3.

Pronounced coating failure occurred on all four tensile samples during the initial two hour exposure period at 1400° F. Cracking and lifting of the coating over one or several large flat regions within the head sections characterized the failures. Although the general vicinity of coating failure was similar to that noted on several samples exposed at 2400° F, failure at 1400° F developed over much larger areas, and appeared to be progressing rapidly along the coating-substrate interface toward the gauge sections. A photograph displaying one of the smaller coating failure areas on a tensile sample is shown in Figure 14.

The samples were racked on an inconel fixture and supported through the grip pin holes — Figure 5. Because of this, it was thought perhaps expansion of the fixture might have imposed a stress on the samples, inducing coating failure. To examine the possibility, another sample, tensile 23, was placed unrestricted across the inconel support rods with only its weight holding it in place, and exposed for 2 hours at 1400° F. Coating failure, similar to that noted on tensile samples 19 through 22, occurred on this sample. None of these five samples developed coating failures at locations in direct contact with the fixture.

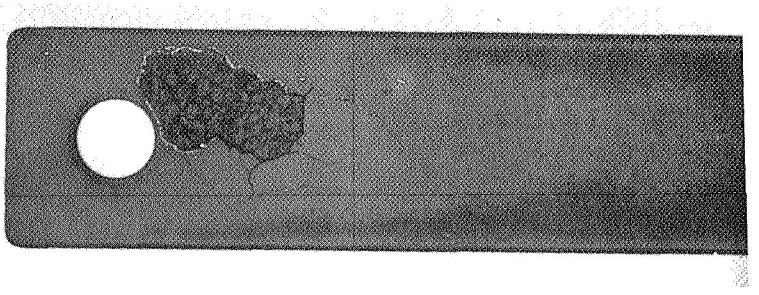

Tensile

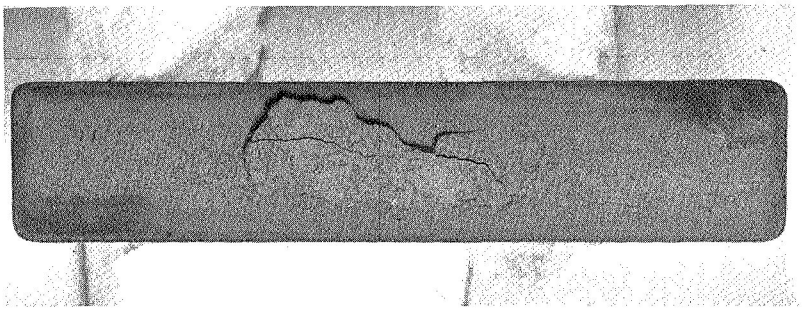

Bend

FIGURE 14 - Coating Failures on Samples Oxidized at 1400°F (1033°K)
Top: 2 Hrs/1400°F
Bottom: 2 Hrs/1400°F + Air Cool + 2 Hrs/1400°F

An answer to the unexpected problem of rapid coating failure at 1400° F was pursued further by exposing two bend samples at this temperature, to explore whether it might be related to sample configuration. The samples, numbers 20 and 21, were supported for this test inside a zirconia boat on wedges of Dynaquartz,* a high purity quartz felt. Coating failure occurred on both samples, on one during an initial two hour exposure period, and on the other during a second two hour period. A photograph showing failure on one of the bend samples is shown in Figure 14.

X-ray diffractometer analysis was performed on the coating surface of one bend sample exhibiting coating failure at 1400° F. The presence of tungstic oxide, WO_3, was detected along with the phases characteristic of the as-applied coating. Samples oxidized at 1400° F developed a yellowish coating appearance which is also consistent with the color of the WO_3 compound. The x-ray information is reported in Table 7.

Perhaps, at 1400° F, the coating exhibits the type of low temperature disintegration characteristic of many silicides, commonly referred to as "pest." Berkowitz-Mattuck et al[7], suggest "pest" may occur in silicides which form metal oxides of low sublimation temperature, egs., $MoSi_2$, WSi_2, VSi_2, through crack propagation caused by oxide build-up at crack tips, when temperature is too low for complete oxide removal by vaporization.

Regardless of the mechanism of coating failure at 1400° F, it is likely not similar to that which resulted in failures at 2400° F. Size of the failed sites, exposure time required to induce failure, and failure frequency with respect to sample type, differed significantly at these temperatures. Comparing 1400° F and 2400° F coating failures: failure sites were much larger at 1400° F, developed during the first 2 to 4 hours exposure at this temperature — at 2400° F the coating was protective for 21 to 304 hours, and occurred indiscriminately on tensile or bend samples at 1400° F while at 2400°F coating failure was more common on tensile samples and frequently occurred within 1/2 inch of the grip pin hole at a site noted to be defective after 2 hours furnace exposure.

*A Johns Mansville trade designation.

TABLE 7 - X-Ray Diffraction Analysis of the Coating After Two Hours Oxidation at 1400°F

Diffractometer Trace		ASTM Standards									
		$(Ti_{.6}W_{.4})Si_2$		$(Ti_{.8}Mo_{.2})Si_2$		WSi_2		$MoSi_2$		WO_3	
d	I	d	I	d	I	d	I	d	I	d	I
4.03	VW	4.00	10	4.02	30						
3.91	W					3.91	50	3.92	46		
3.84	M									3.835	100
3.76	M									3.762	95
3.66	M									3.642	100
3.42	S	3.42	80	3.42	50						
										3.411	5
3.34	VW									3.342	50
3.23	VW									3.109	50
3.10	VW									3.076	50
2.96	M					2.97	100	2.96	96		
2.69	W									2.684	75
2.66	W									2.661	60
2.63	W									2.617	90
2.52	M	2.52	50	2.52	30					2.528	35
										2.509	40
2.32	W	2.33	10	2.33	30						
2.26	W					2.27	70	2.26	70		
2.18	S	2.20	100	2.19	100						
										2.172	50
2.15	M									2.149	60
2.10	VW									2.098	10
										2.038	40
2.02	M	2.02	30	2.02	20	2.02	85	2.02	100	2.020	30
										2.011	25
1.96	VW					1.96	50	1.96	70	1.966	30
1.92	VW									1.917	50
1.89	S	1.89	100	1.894	90					1.879	50

Tests at 1600° F. To examine whether the coating might be suitable for substrate protection at a temperature slightly above 1400° F, one bend sample was exposed at 1600° F. The sample, number 22, was placed on Dynaquartz inside a zirconia boat, and exposed in repeated 2, 2, and 16 hour time-at-temperature cycles. Progress of this test in terms of sample appearance and weight gain, is reported in Table 8, and weight increase per unit area is plotted against square root of test time in Figure 15.

The coating surface developed a yellow color after the initial two hour oxidation period at 1600° F indicating tungstic oxide formation, but coating failure did not occur. This yellow color disappeared during the third, 16 hour, exposure cycle, and an evenly dark and dense surface developed, presumably a sign of primary oxide barrier formation. A major decrease in oxidation rate occurred in the vicinity of 20 hours total exposure time, reflecting the change of coating appearance.

Exposure was continued at 1600° F until 108.5 hours time-at-temperature was accumulated, then the sample was exposed for five 2 hour cycles at 1400° F. The coating survived this 1400° F treatment without change in oxidation rate from that developed during 1600° F exposure. Testing was returned to 1600° F and continued until a total exposure of 364 hours was accumulated, with weight gain progressing at the same retarded rate established after 20 hours at temperature. Oxidation rate observed at 1600° F can be approximated by the following relationships:

$$M = 0.27\, t_1^{1/2} + 0.45 \qquad 2 \leq t_1 \leq \sim 20$$

$$M = 0.19\, t_2^{1/2} + 1.76 \qquad \sim 20 \leq t_2 \leq 364$$

M: mgs./square cm.

t: hours at 1600° F

TABLE 8 - Oxidation Behavior of Bend Sample 22 at 1600°F (1144°K)

Cycle Number	Cycle Time	Accumulated Time	Total Weight Increase 1.	Remarks
	Hrs.	Hrs.	gms.	
1	2	2	0.0138	► The coating developed a yellow hue
2	2	4	0.0167	► The coating retained its yellow appearance
3	16	20	0.0283	► The coating turned dark brown and dense,
4	2	22	0.0294	and remained so throughout the entire 36
5	2	24	0.0304	cycle exposure program.
6	16	40	0.0320	
7	2	42	0.0325	
8	2	44	0.0326	
9	64.5	108.5	0.0327	
10	1.8	110.3	0.0336	► Air exposure was performed at 1400°F
11	2	112.3	0.0337	(1033°K) for cycles 10 through 15
12	2	114.3	0.0336	
14	2	116.3	0.0340	
15	2	118.3	0.0337	
16	2	120.3	0.0339	
17	17.2	137.5	0.0340	
18	2	139.5	0.0341	
19	2	141.5	0.0342	
20	2	143.5	0.0343	
21	64.5	208	0.0344	
22	2	210	0.0347	
23	2	212	0.0348	
24	27	229	0.0349	
25	2	231	0.0350	
26	2	233	0.0351	
27	18	251	0.0351	
28	2	253	0.0353	
29	2	255	0.0353	
30	18	273	0.0354	
31	2	275	0.0357	
32	2	277	0.0354	
33	65	342	0.0354	
34	2	344	0.0359	
35	2	346	0.0359	
36	18	364	0.0360	

1. Starting sample weight: 12.4486 gms.

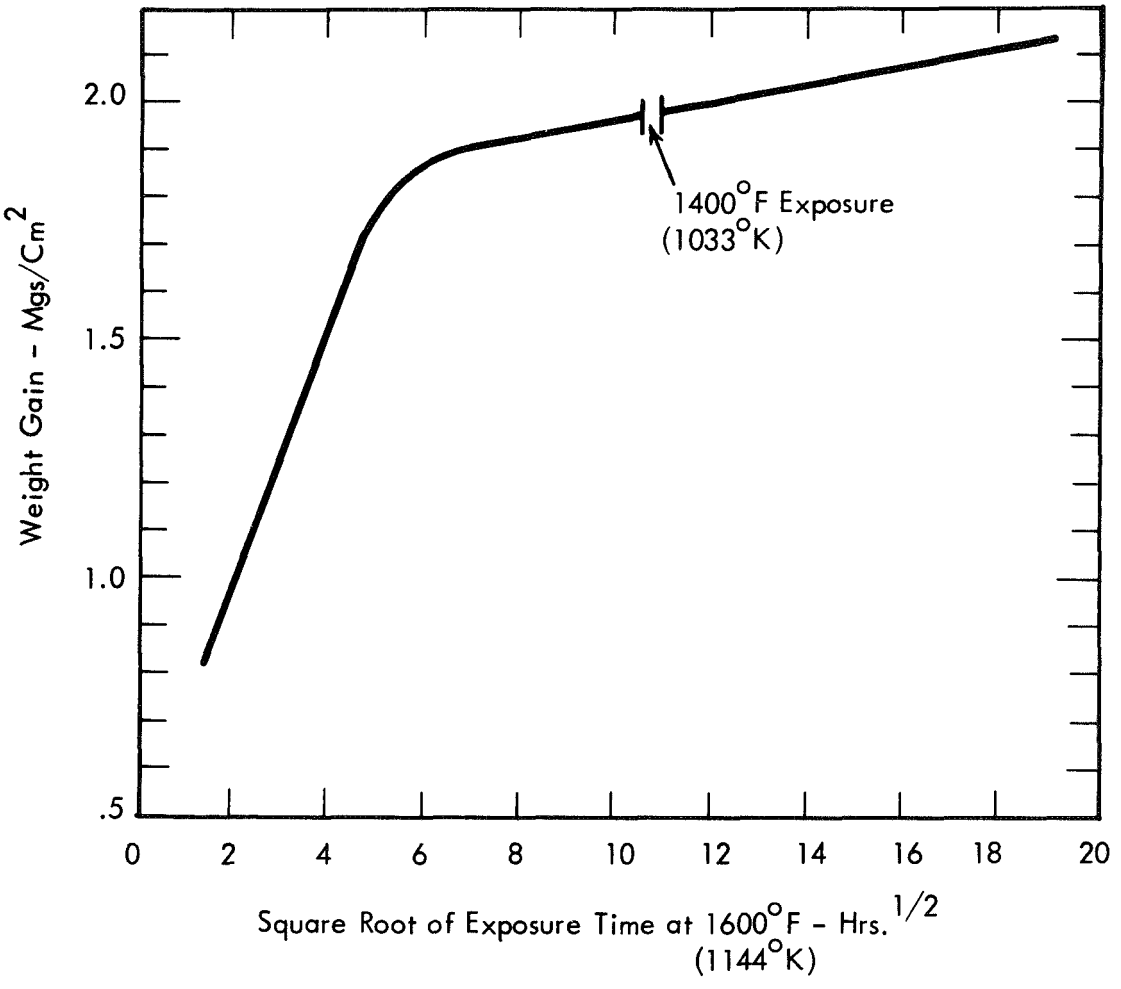

FIGURE 15 - Oxidation Behavior of Bend Sample 22 at 1600°F

Oxidation at 1400° F After Higher Temperature Exposure. These tests were run to determine whether elimination of coating failure at 1400° F by prior 1600° F oxidation, observed on bend sample 22, reflected characteristic rather than unusual behavior, and might be a general effect of higher temperature pre-treatment. Bend sample 22, pre-exposed as discussed in the previous section, and bend samples 14 and 15 which were oxidized for 10 hours at 2400° F (Table 6), were chosen for the study. Testing involved exposure of these three samples in the manner used on other tests, repeated 2, 2, and 16 hour oxidation periods, air cooling to room temperature employed between periods.

Test progress in terms of weight gain is reported in Table 9. A total of 600 hours was accumulated at 1400° F employing 52 test periods, without any major change in sample weight or coating failure occurring. Apparently, avoidance of short time coating failure at 1400° F by higher temperature pre-oxidation reflects real and somewhat general behavior.

Mechanical Properties and Chemical Analysis

Bend Tests. Bend tests were performed on samples of the T-222 alloy substrate as surface prepared for coating, on as-coated samples, and on coated samples which survived the various oxidation treatments discussed under Oxidation Behavior. The results are entered in Table 10.

Tests on base material reflected the excellent ductility characteristic of T-222, i.e., DBTT below the temperature of liquid nitrogen, $<$-320° F. As-coated samples also displayed excellent ductility, the results indicating substrate DBTT between -320° F and -250° F. Similar results were obtained for samples oxidized 10 and 304 hours at 2400° F, indicating the coating certainly prevented major atmospheric contamination from occurring during exposure.

Results from the two samples treated 10 hours at 2400° F then 600 hours at 1400° F indicate a somewhat higher DBTT for this condition, with substrate failure occurring prior to

TABLE 9 - Oxidation Behavior at 1400°F of Samples Previously Oxidized at Higher Temperatures[1]

Cycle Number	Cycle Time	Accumulated Time	Total Weight Increase[2] gms.		
	Hrs.	Hrs.	Bend 14	Bend 15	Bend 22
1	2	2	N.D. 3.	N.D.	N.D.
2	2	4	N.D.	N.D.	N.D.
3	18	22	0.0067	0.0068	0.0003
4	3.3	25.3	0.0067	0.0068	0.0003
5	64	89.3	0.0064	0.0067	0.0002
6	2	91.3	0.0068	0.0071	0.0003
7	2	93.3	N.D.	N.D.	N.D.
8	18	111.3	0.0068	0.0071	0.0004
9	2	113.3	0.0068	0.0071	0.0004
10	2	115.3	N.D.	N.D.	N.D.
11	17	132.2	↓	↓	↓
12	3	135.3			
13	18	153.3			
14	2	155.3			
15	2	157.3			
16	16	173.3			
17	2	175.3	N.D.	N.D.	N.D.
18	66	241.3	0.0075	0.0077	0.0008
19	2	243.3	N.D.	N.D.	N.D.
20	2	245.3	↓	↓	↓
21	17	262.3			
22	2	264.3			
23	2	266.3			
24	16	282.3			
25	2	284.3			
26	2	286.3			
27	16	302.3			
28	2	304.3			
29	2	306.3	N.D.	N.D.	N.D.
30	88.5	394.8	0.0079	0.0081	0.0011
31	2	396.8	N.D.	N.D.	N.D.
32	2	398.8	↓	↓	↓
33	16	414.8			
34	2	416.8			
35	2	418.8			
36	16	434.8			
37	2	436.8			
38	2	438.8			
39	19	457.8			
40	2	459.8			
41	2	461.8			
42	19	480.8			
43	2.2	483.0			
44	2	485.0	N.D.	N.D.	N.D.
45	66	551.0	0.0080	0.0081	0.0010
46	2.3	553.3	N.D.	N.D.	N.D.
47	2	555.3	↓	↓	↓
48	2	559.3			
49	18	577.3			
50	2	579.3			
51	2	581.3	N.D.	N.D.	N.D.
52	19	600.3	0.0086	0.0086	0.0013

1. Pre-1400°F treatments
   Samples 14 & 15: 10hrs/2400°F in five 2hr. cycles
   Sample 22: 109hrs/1600°F + 10hrs/1400°F + 245hrs/1600°F

2. Starting Sample weights
   No. 14 11.7816gms.
   No. 15 12.3292gms.
   No. 22 12.4846gms

3. N.D.: Not determined.

TABLE 10 - Bend Ductility Data[1]

Sample No.	Sample Condition[3]	Test Temp.		Bend Angle Sustained[2]	
		°F	°K	Coating	Substrate
1	1 Hr/3000°F	-320	77	---	>90°
2	(Starting material)	-320	77	---	>90°
6	15 Hrs/2760-2800°F	-320	77	0°	50°
7	+ 16 Hrs/2150°F	-320	77	0°	27°
8	(Coating process)	-250	116	1°	>90°
9		-125	196	3°	>90°
10		75	297	4°	>90°
12	10 Hrs/2400°F	-250	116	2°	>90°
13	(Air exposure)	-320	77	0°	75°
16	304 Hrs/2400°F	-250	116	7°	>90°
18	(Air exposure)	-320	77	4°	>90°
19		-320	77	2°	52°
14	10 Hrs/2400°F	-250	116	3°	32°
15	+600 Hrs/1400°F (Air exposure)	-150	172	2°	80°
22	109 Hrs/1600°F +10 Hrs/1400°F + 245 Hrs/1600°F + 600 Hrs/1400°F (Air exposure)	-150	172	2°	>90°

1. Specimen: .5" x 2.5"
   Punch: .125" radius
   Support Span: 1"
   Test Rate: 1"/Min.

2. >90 indicates a ductile bend; lower figures indicate angles where cracking occurred.

3. 1400°F: 1033°K, 1600°F: 1144°K, 2150°F: 1450°K, 2400°F: 1589°K, 2780°F: 1800°K, and 3000°F: 1922°K

attainment of a 90 degree bend at both -250° F and -150° F. Failure at -150° F after sustaining an 80 degree bend angle, however, suggests the DBTT is in the near vicinity of this temperature. A ductile bend obtained at -150° F on sample 22 lends some support to this conclusion, although the treatments prior to 600 hour/1400° F exposure of this sample differed from that of samples 14 and 15.

These test results definitely show that contamination, to the point where substrate ductility was seriously impaired, did not occur during coating or any oxidation condition examined. The very minor increase in DBTT noted for as-coated, and coated and oxidized material, probably reflects, in part, structural changes induced in the substrate by the treatments. The substrate was in the solution treated, 1 hour/3000° F, condition prior to coating. Coating, and all exposure conditions, were performed at temperatures where carbide precipitation would occur in the substrate[4,5]. The presence of precipitates in the substrate can be seen in the photomicrographs of Figure 3 representing the as-coated condition.

Tensile Tests. Tensile properties were determined on substrate material (surface prepared for coatings), and on as-coated samples, both at room temperature and 2400°F. Room temperature tests, and those at 2400°F on as-coated samples, were performed in air; the 2400°F uncoated substrate material tests were done in vacuum. Test results are presented in Table 11, and photographs of representative tested samples in Figure 16. Values of strength for coated material are based on the substrate area.

Comparison of properties for room temperature tests performed on uncoated and coated samples reveals the latter to be slightly weaker and lower in ductility. Aging resulting from the thermal conditions of coating is probably the cause for the small loss in these properties.

The coated samples displayed considerably higher strength at 2400° F compared to the base material, the difference in this respect being especially pronounced for yield strength. This is believed due to a significant contribution by the coating to load support area for strains up to that of yielding. Comparison of the photographs showing tested samples, Figure 16,

TABLE 11 - Tensile Properties of Base and As-Coated Material[3]

Sample Number	Sample[1.] Condition	Test Temperature		0.2% Yield Strength[2.]		Ultimate Strength		Uniform Elongation	Total Elongation
		°F	°K	ksi	$N/m^2 \times 10^7$	ksi	$N/m^2 \times 10^7$	%	%
7	Base Mat'l.	75	297	103.1	71.1	119.0	82.1	14.2	25.8
8	Base Mat'l.	75	297	98.0	67.2	119.1	82.2	14.9	26.2
11	As coated	75	297	83.4	57.3	107.0	74.0	14.4	22.4
20	As coated	75	297	93.8	64.4	106.4	73.8	14.4	22.0
9	Base Mat'l.	2400	1589	34.7	24.8	48.7	33.5	11.9	34.0
10	Base Mat'l.	2400	1589	33.1	22.7	48.8	33.5	11.7	35.0
14	As coated	2400	1589	40.6	27.9	51.0	35.1	9.4	16.0
32	As coated	2400	1589	40.9	28.1	52.3	36.0	11.9	12.4

1. Base material: 1Hr/3000°F (1589°K) anneal + surface prepared for coating.
   As coated material: 16Hrs/2760 - 2800°F (1811°K) + 16Hrs/2150°F (1450°K)
2. Results for coated material are based on the cross-sectional area of the substrate measured prior to coating.
3. Stain rate: 0.05/Min.

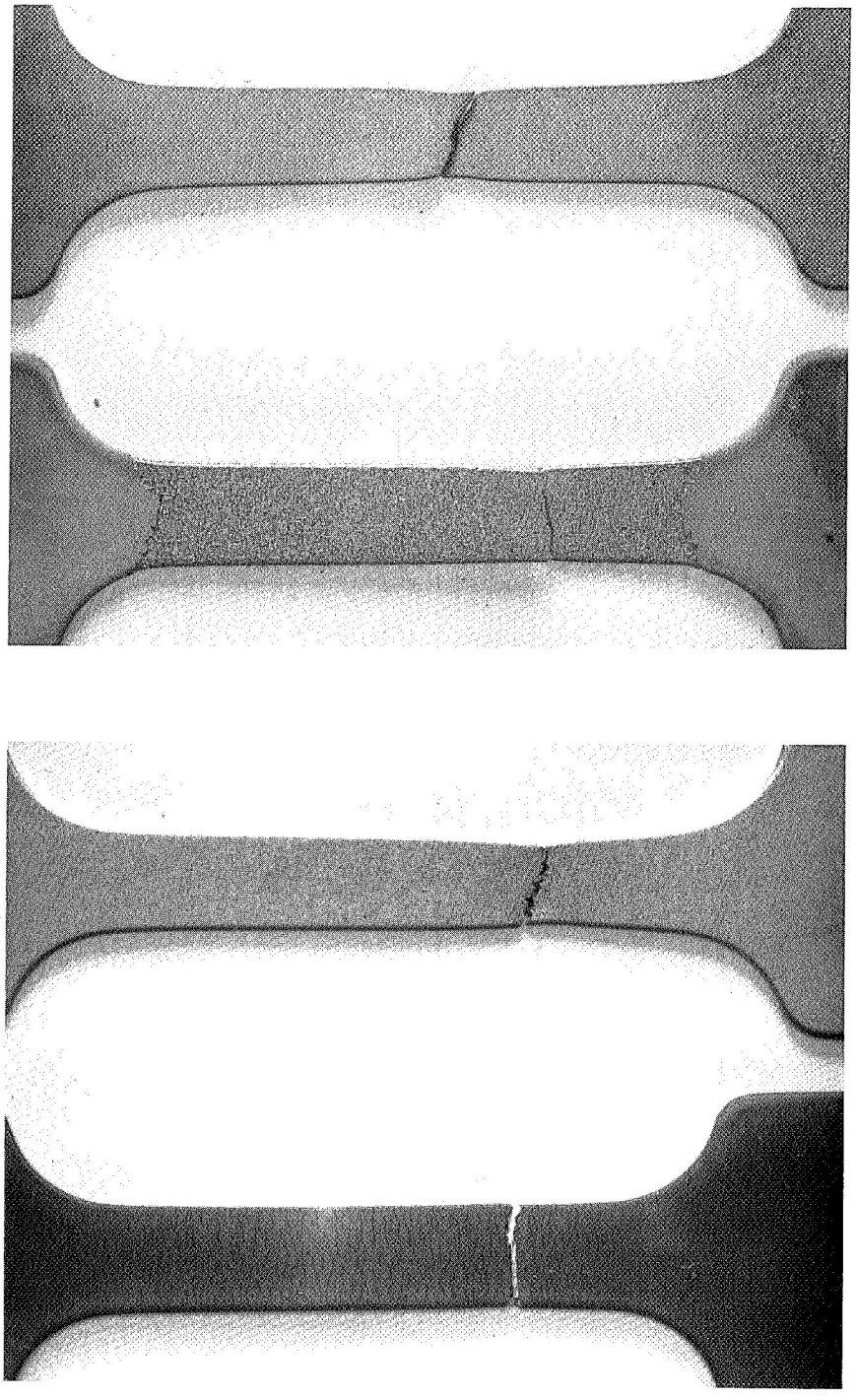

Sample No. 8
(Base)

Sample No. 11
(Coated)

Sample No. 9
(Base)

Sample No. 14
(Coated)

FIGURE 16 - Tensile Tested Samples of Base and Coated Material
Top: Room Temperature Tests - Nos. 8 and 11
Bottom: 2400°F Tests (1589°K) - Nos. 9 and 14

reveals loss of the coating occurred on the room temperature tests, while it cracked severely but adhered to the gauge section on the 2400° F tests. The stage of elastic strain alone was observed sufficient to completely spall the coating from the gauge section on room temperature tested samples, thus, it did not contribute to strength.

The coated samples also displayed a lower elongation at 2400° F compared to the base material. This manifested itself primarily in the inability to fully develop the deformation stage of plastic instability. This is not an indication of property change caused by coating, but, instead, reflects rapid oxidation of the substrate in the air test environment resulting from coating failure at the 0.05/min. tensile test strain rate.

An interesting comparison can be made between the tensile data obtained for the base material tested at room temperature, and that reported for the same material[6], shown in Table 1. A lower yield strength was measured on this program due to the absence of yield point behavior. The samples represented by these tests were all removed from the same piece of T-222 sheet, and differed only in surface preparation, those tested on this program having received the treatment given material in preparation for coating. As described in Table 2, preparation for coating involved barrel finishing, sandblasting and pickling. Presumably, surface compression by the mechanical abrasive treatments eliminated yield point behavior.

Creep Tests. Creep tests were performed in air at 2400° F, on four samples in the as-coated condition, and on the two coated specimens air exposed 304 hours at 2400° F. In addition, creep behavior of base material was examined in ultrahigh vacuum, $<10^{-8}$ torr, after heat treatment in this environment to the thermal condition of coating. This inert environment test was included in the study to determine if the thermal conditions of the coating process affected air environment creep behavior, and permit by direct comparison evaluation of whether coating or atmospheric element contamination was sufficient to affect creep properties of coated material.

Testing was performed at stress levels from 4 ksi to 12 ksi. Stress changes were incorporated in some tests to expand the evaluation of stress dependency of creep. Stress on

coated samples was based upon substrate dimensions measured prior to coating, and no compensation was made for change in dimensions due to reaction with the coating during the test, or for any load support afforded by the coating. The amount of substrate recession due to interaction with the coating at 2400° F was measured, and will be discussed in a later section. The creep strength of the coating at 2400°F is likely very slight compared to the substrate.

Creep data are presented in Table 12. The first test performed was on sample 26 at 8 ksi. This as-coated specimen was tested for 500 hours and displayed a 0.0130%/hr. creep rate throughout the entire period. Elongation of 7.0 percent was measured directly from the tested sample, corresponding closely with 6.8 percent, the value of the last creep strain measurement. A photograph of the tested sample is displayed in Figure 17 where comparison is made to an as-coated specimen.

The next creep test was performed on sample 27, starting at 8 ksi. Creep at a constant rate of 0.011%/Hr. was recorded at this stress up to 187 hours test time, at which point a stress increase to 10 ksi was initiated. A constant creep rate of 0.018%/Hr. was measured at 10 ksi until 355 hours total test time when test stress was changed to 12 ksi. Creep data was recorded at 12 ksi to within 1 hour of specimen failure, occurring at 437 hours total test time, and a creep rate of 0.043%/Hr. was observed. Failure, however, occurred well outside of the gauge length through one of the head sections. Gross substrate oxidation had occurred at the region, reducing the section and causing failure. Substrate oxidation also occurred at the head section opposite that where the specimen failed, but did not progress completely through the cross section.

A photograph of sample 27 is shown in Figure 18 superimposed above its temperature profile. The profile was determined on a subsequent creep test by measuring temperature at several axial positions along one half of the sample. The temperature gradient shown for the other half of the sample is a mirror reflection of the measured data.

TABLE 12 - Creep Test Data Obtained at 2400°F (1589°K)

Sample Number	Sample Condition	Test Stress		Transition[1.] Time & Stain		Minimum Creep Rate	Test Duration	Total % Elongation	
		ksi	$N/m^2 \times 10^7$	Hrs.	%	%/Hr.	Hrs.	Test	Sample
26	As coated	8	5.5	N.O.	—	0.0130	500[2.]	6.8	7
27	As coated	8	5.5	N.O.	—	0.0110	187		
		10	6.9	N.O.	—	0.0180	187[3.] to 355		
		12	8.2	N.O.	—	0.0430	355[3.] to 437[4.]	8.6	9
38	As coated	4	2.7	(75)	0.4	0.0039	213		
		6	4.1	N.O.	—	0.0062	213[3.] to 381		
		8	5.5	N.O.	—	0.0108	381[3.] to 500	3.4	2.9
37	As coated	4	2.7	(100)	0.9	0.0032	446[4.]	1.9	2
15	304Hrs/2400°F	4	2.7	15	0	N.O	18.5[5.]	1.8	
16	304Hrs/2400°F	4	2.7	13.9	0	N.O.	21.5[5.]	3.9	
VT	6.	8	5.5	N.O.	—	0.0094[7.]	500	3.8	3.8

1. ( ): 1st to 2nd stage creep. ____: 2nd to 3rd stage. N.O. : not observed.
2. Test stopped at 500 hours.
3. Stress changed to indicated value at this time
4. Sample failure occurred at this time by oxidation through a head section.
5. Sample failure occurred at this time by oxidation through a gauge end radius.
6. A sample of the T-222 substrate heat treated to the thermal condition of coating in ultra high vacuum and tested in this environment.
7. 0.0050 %/Hr ≤ Creep Rate ≤ 0.0094%/Hr. for 0 ≤Test Time ≤325Hrs.
   Creep Rate = 0.0094%/Hr for 325 ≤ Test Time ≤ 500 Hrs.

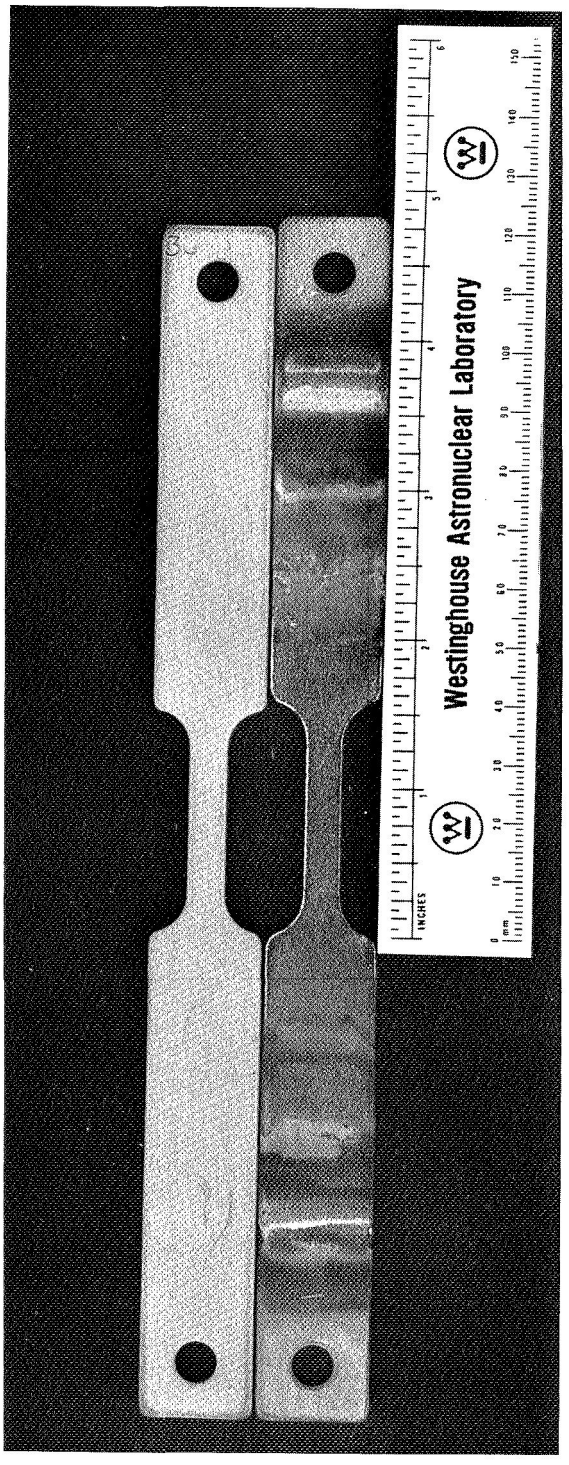

FIGURE 17 - Comparison of Creep Sample 26 with an As-Coated Sample

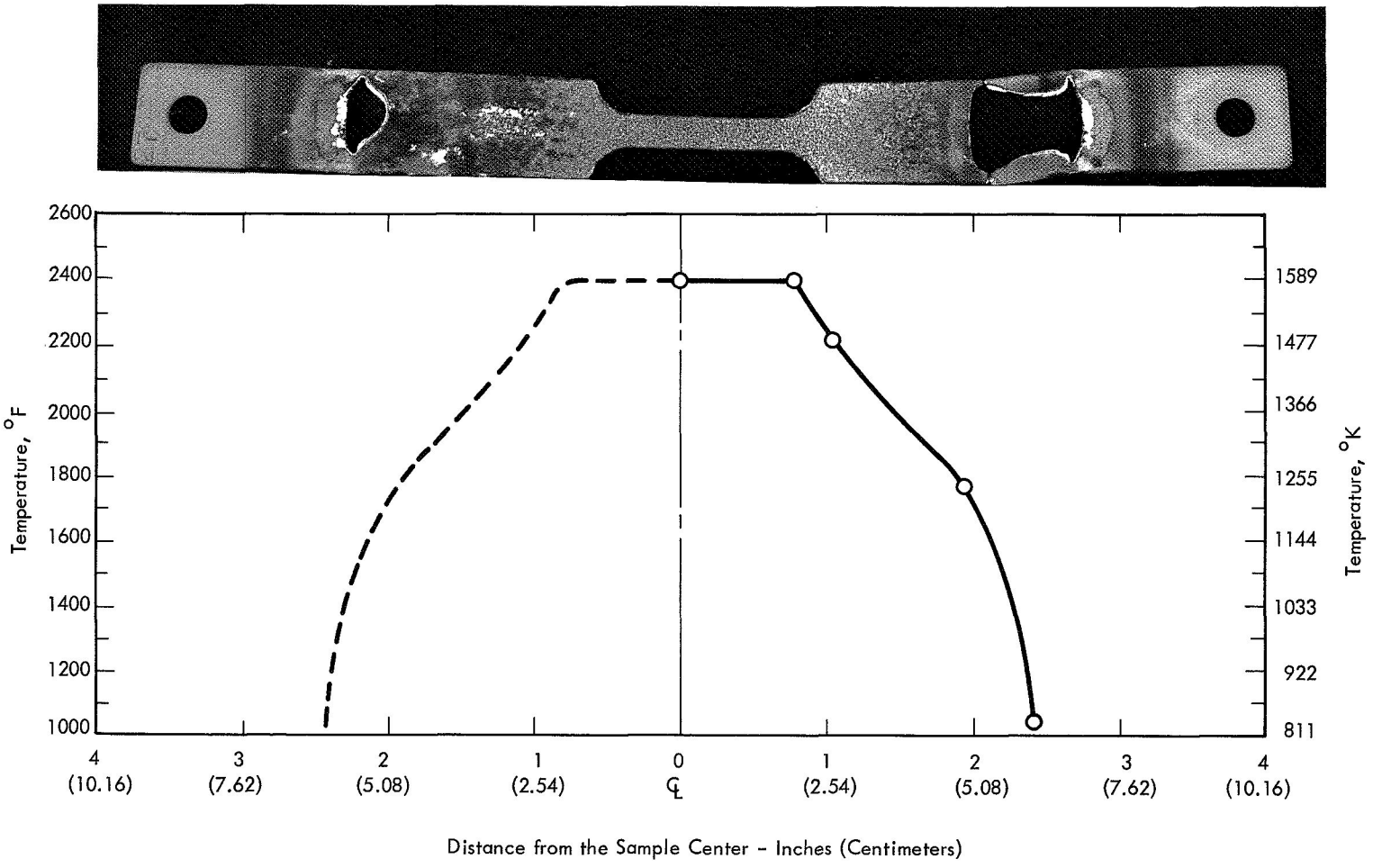

FIGURE 18 - Appearance and Temperature Profile of Creep Sample 27

The areas where oxidation occurred on sample 27 are too large to permit an absolute estimate of the failure origins to be made. It would seem inconceivable, however, to consider oxidation as starting at the higher temperature region of the failure sites, then progress to the extent observed in the direction of lower sample temperatures.

If the small failure site were reflected through a mirror plane placed at the center of the gauge section, it would correspond to size, shape and position of the colder end of the larger oxidized site. This suggests a similar failure origin at each region, which by judgment from the small area would lie about 1-1/2 inch from the specimen end. Coating failure at a temperature in the vicinity of 1000° F is indicated.

Elongation measured directly from the tested sample, 9 percent, compared very close to the last strain measurement, 8.6 percent, taken one hour before failure. Because of this, it is concluded that although oxidation occurred at the specimen head sections, it did not affect creep behavior measured during the test. It is likely that oxidation began at the center of the head section width, and spread across this dimension and in the direction of higher sample temperatures leaving, for the greater part of the test, sufficient sound material around the site so as to have no affect on measured creep rates.

Of the other two samples tested in the as-coated condition, one, number 37, also failed by oxidation through a head section. The estimated failure origin, shape of the oxidized region, and time of failure, were all similar to that observed on sample 27. Sample 37 was tested at 4 ksi and displayed a creep rate of 0.0032%/Hr. Elongation determined from direct sample measurement was within 0.1 percent of the last strain measurement, indicating, as was concluded for sample 27, that oxidation did not affect creep behavior.

Creep behavior of the other sample tested in the as-coated condition, number 35, was measured at 4, 6, and 8 ksi. Testing was carried out for a total of 500 hours, and data consistent with that discussed above was obtained.

Examination of sample 38 after testing revealed substrate oxidation beginning at an edge site located 1-3/8 inches from one end. Oxidation had proceeded into the sample at the site to a 3/16 inch depth. The location of oxidation on the sample, and the estimated origin of oxidation on creep specimens 27 and 37, fell within the same general sample area. Sample temperature at the failure region was relatively low, approximately 1000° F, indicating failure might be associated with the "pest" mechanism. On the other hand, coating failure on these samples occurred at a location where failure originated on many samples during 1400° F and 2400° F oxidation testing. This seems to indicate, as was previously suggested, that the specimens could have been particularly susceptible to coating failure in the vicinity as a result of something associated with the coating process.

Samples 15 and 16, which were exposed 304 hours at 2400° F, were tested at 4 ksi. Both failed after just a few hours of testing by oxidation through a radius at the end of the gauge section. A photograph of sample 15 showing the oxidation which occurred is presented in Figure 19.

Visual evidence that prior air exposure at 2400° F had created a coating defect at the eventual creep failure site was not obtained on sample 15. On the other hand, evidence that substrate oxidation had started within a gauge section radius was observed on sample 16 — Table 6 and Figure 11. Gross oxidation of sample 16 did occur at the suspect defect site during creep testing, but it also occurred at one other gauge section radius. The high failure susceptibility of the coating at these radius sites, suggested in discussion of Oxidation Behavior, appears to be emphasized by these results.

A point that could be overlooked in discussion of creep behavior is that the as-applied coating survived exposure for much longer times at 2400° F on creep tests than on oxidation tests at 2400° F. The difference must reflect the strong influence cyclic exposure, employed on the oxidation tests, has on coating life.

FIGURE 19 - Appearance of Creep Sample 15

Creep sample VT, heat treated in ultrahigh vacuum to the thermal conditions of coating, was tested in this environment at 8 ksi and 2400° F for 500 hours. Specimen extension began at a rate of 0.005%/Hr. and steadily increased to 0.0094%/Hr. after approximately 325 hours test time. Creep proceeded at the 0.0094%/Hr. rate for the 325 to 500 hour span of test time. A total creep strain of 3.8 percent was obtained.

Creep rates measured on the ultrahigh vacuum test fell within the same order of magnitude of those obtained at the same stress and temperature on coated and air tested samples, indicating that behavior of coated material was principally controlled by intrinsic substrate change, not coating or environmental affects. Observation of a changing creep rate over the initial 325 hours of the vacuum test is not considered a display of different creep behavior from that observed on air tested samples. Instead, it is believed simply to reflect a more sensitive strain measurement technique employed on the test, which allowed the gradual creep rate change to be detected.

Creep rate data obtained on the program is plotted against test stress in Figure 20. Data comparison is made to information reported for T-222 during alloy development[5,6], and by independent investigators[8, 9, 10]. The comparison information represents vacuum environment tests at conditions where rupture did not occur in 500 hours*, and where rupture occurred in 1 to 60 hours**. All reference tests were performed on material recrystallized at time-and-temperature conditions consistent with complete solutioning of carbon present in the alloy. For the most part, final heat treatment of one hour at 3000° F was employed.

Minimum constant creep rate is plotted in Figure 20, with exception of information shown for the ultrahigh vacuum creep test performed on this program (sample VT), and references 8 and 9. The constant creep rate occurring between 325 and 500 hours test time, which was the

*Referred in later discussion as long time tests. References 8, 9, and 10.

**Referred in later discussion as short time tests. References 5 and 6.

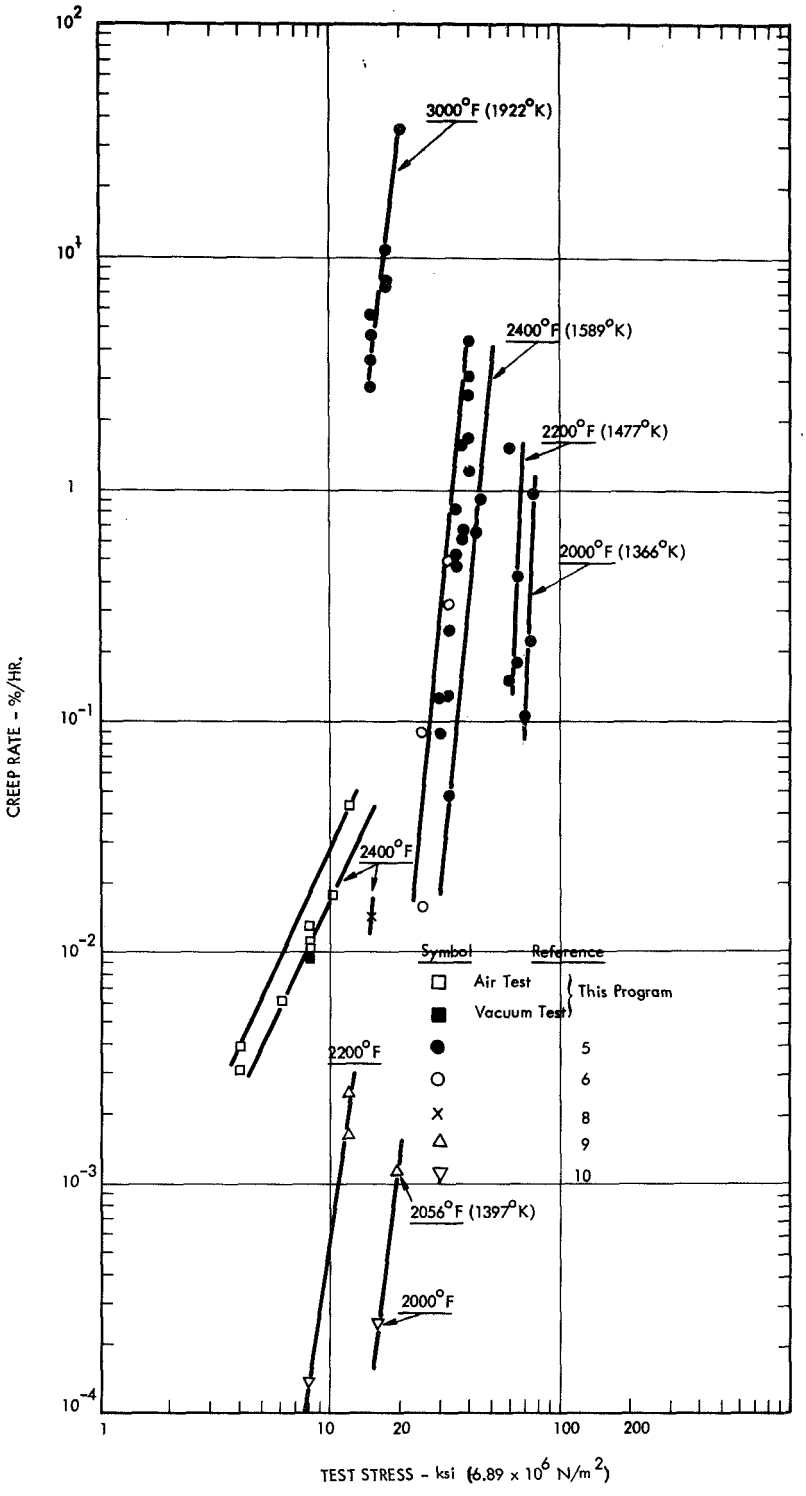

FIGURE 20 - Stress Dependency of Creep Rate for T-222 Tested in Vacuum and Air Environment

highest observed, is plotted for sample VT. A continuously increasing creep rate occurred on the tests reported on in references 8 and 9, and average creep rate to 1 percent strain was used to represent this information. Creep rates did not change by a large amount on any of these tests, as a result, other methods of representing behavior would not seriously shift the position of the data points.

Creep rates obtained in this program are higher than would be expected by straight line extrapolation of the short time 2400° F comparison test data. Furthermore, a lower stress dependency of creep rate was observed in this work than characteristic of the comparison information. These deviations from anticipated behavior may be related, in part, to the difference of material conditions prior to test. The creep behavior noted in this program might also reflect a major change in stress dependency of creep rate over the range of stress represented by the data. An indication in this respect can be observed by comparing the creep rates obtained at a given temperature on tests employing less than 20 ksi, with those measured at the same temperature on higher stress tests.

The results shown in Figure 20 are plotted in Figure 21 in accordance with the linear dependency of log $\dot{\epsilon}/D$ and log σ/E,* shown by Sherby to be obeyed by pure metals[11]. Also displayed in the figure for comparison is creep data for pure tantalum[12]. Values of modulus and diffusivity used to normalize the information were those incorporated by Begley et al, in a recent analysis of creep and fracture in refractory metals[13].

Presentation of the results in this manner reveals considerable scatter. Part of this variation is undoubtedly related to differences in test techniques and metallurgical factors, i. e., differences in composition, heat treatment, grain morphology, dislocation density,

---

* $\dot{\epsilon}$: Creep rate σ : Stress D: Diffusivity E: Modulus

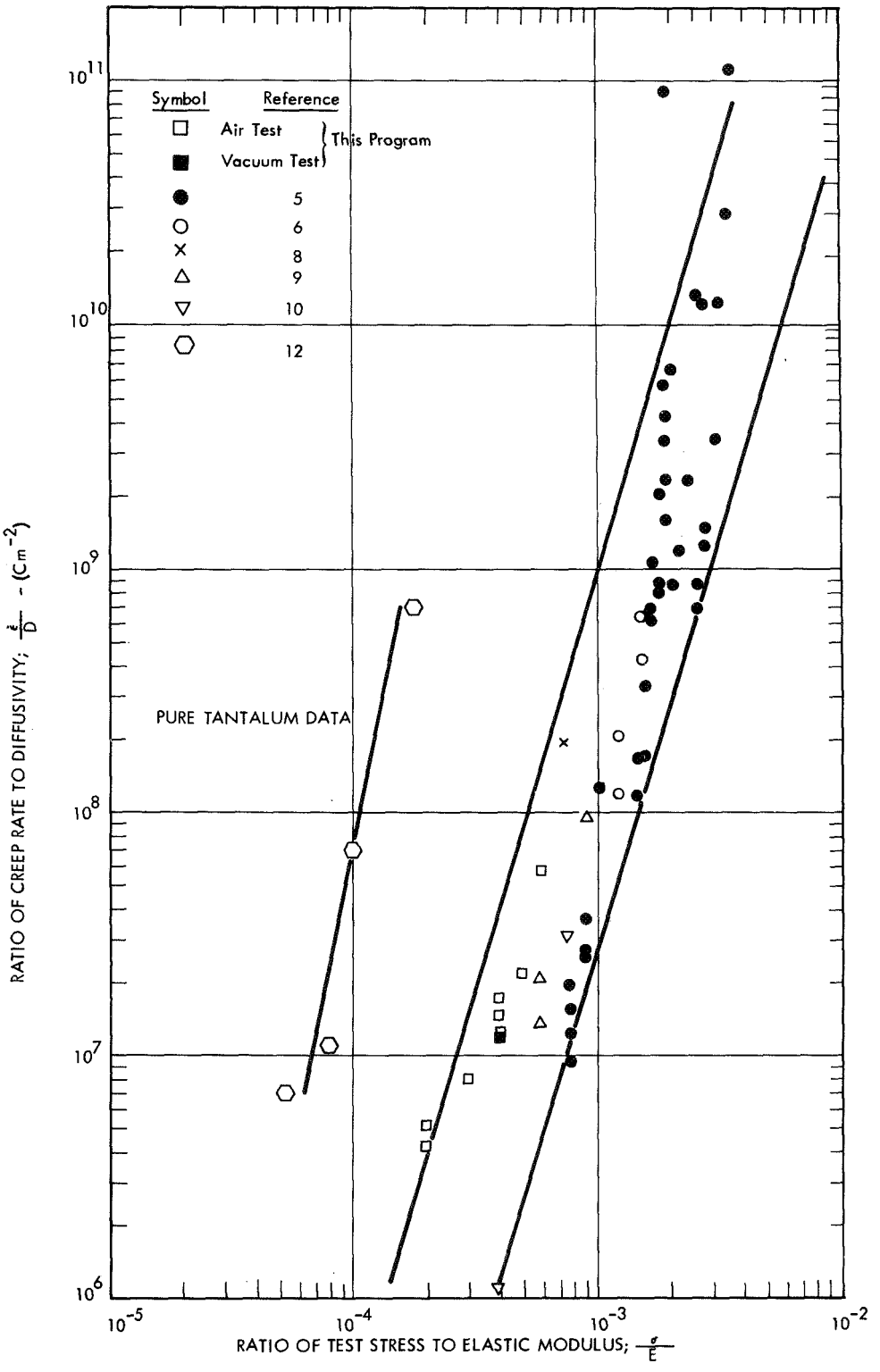

FIGURE 21 - Sherby Plot for T-222 Tested in Vacuum and Air Environment

strain measurement methods and test environments, to name a few. As an example, an ultrahigh vacuum environment, $\leq 10^{-8}$ torr, was employed on the long time tests (References 8, 9, and 10), while vacuum of 10^{-5} to 10^{-6} torr was used for the short time tests (References 5 and 6).

Weertman[14] showed a slope of 3 to 4 might be expected for the Sherby plot of an alloy, a value between 4 and 5 being likely for a pure metal. Consistent with this predicted behavior, is the slope value of 3.3 obtained for lines shown in Figure 21, which provide a reasonably tight band around the information. Creep behavior observed for coated and air tested material, when analyzed on the Sherby basis, appears fairly consistent with that expected by analogy with tests performed under the presumably inert condition of vacuum. Admittedly, the air test results do lie on the weak side of the band, but this might reflect property loss due to thermal history rather than from substrate interaction with coating or atmospheric elements.

The air creep test and comparison vacuum test data are presented in Figure 22 in the usual Larson-Miller form. Time to 1 percent creep is used for the Larson-Miller parameter. With exception of one data point, the information generally defines two curves, one for short time tests, the other for long time tests. Interestingly, superior overall creep behavior would be predicted from extrapolation of the short time test results. In this respect, the plot emphasizes the change in stress dependency of creep rate suggested previously — Figure 20.

Chemical Analysis. Analysis for carbon, oxygen and nitrogen contents was performed on the T-222 substrate of samples representing various elevated temperature air exposure treatments. Comparison of the data was made to the levels present in the base material sheet, the substrate after silicide coating, and the base material sample heat treated and tested in ultrahigh vacuum. Preparation for analysis of coated samples involved sandblast removal of the coating, followed by acid pickling until the substrate was thinned by a few thousandths of an inch.

Identification of samples examined and results of chemical analysis are reported in Table 13.

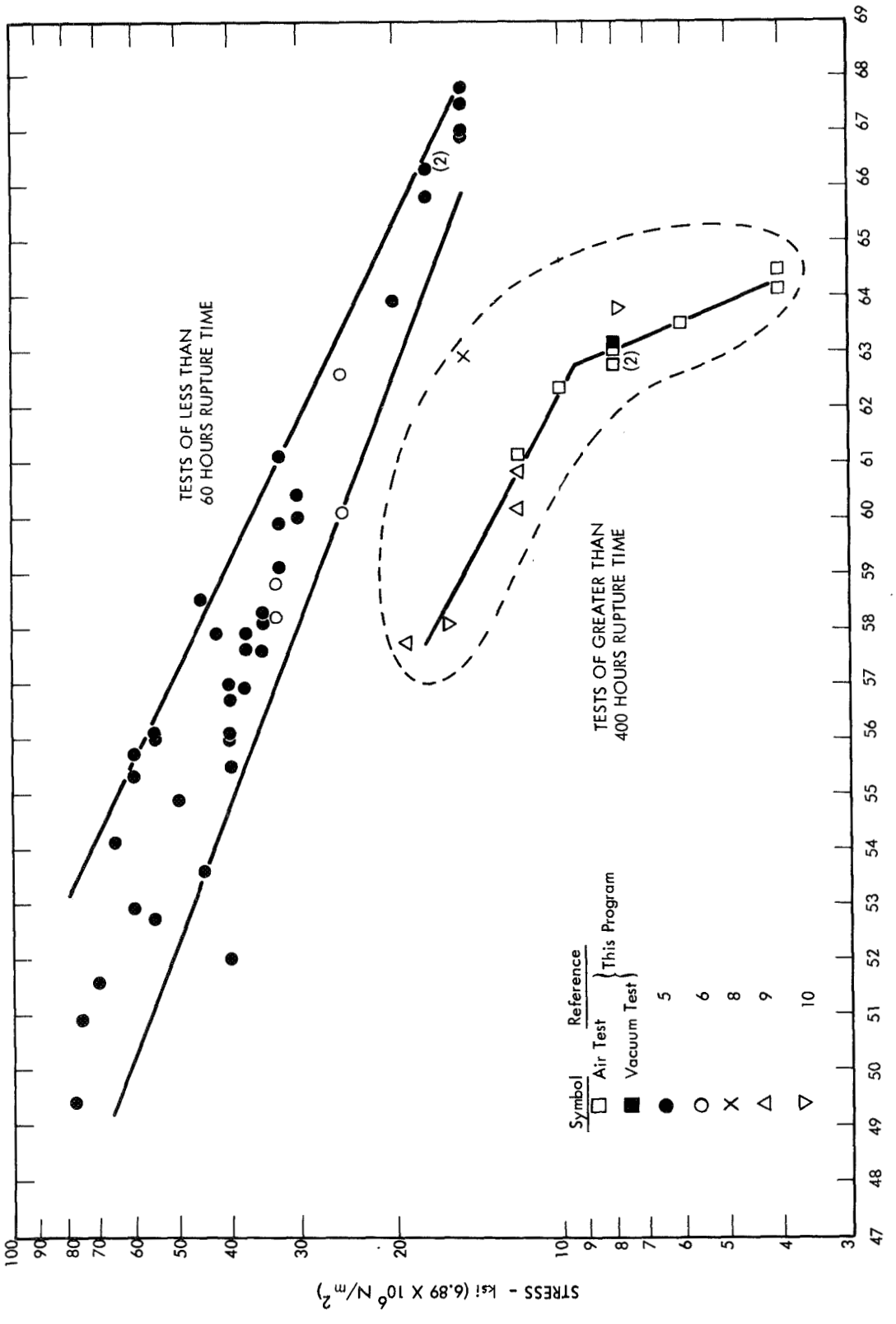

FIGURE 22 - Larson-Miller Plot for T-222 Tested in Vacuum and Air Environment

TABLE 13 - Substrate Impurity Analysis

Sample Identification	Exposure[1] Condition	Interstitial Level; ppm		
		Carbon	Oxygen	Nitrogen
Tensile 7	Substrate material	120	30	15
Bend 6	As-coated	150	270	44
Tensile 28	191 Hrs/2400°F	170	260	68
Bend 16	304 Hrs/2400°F	170	250	65
Bend 22	355 Hrs/1600°F + 610 Hrs/1400°F	140	370	39
Bend 14	10 Hrs/2400°F + 600 Hrs/1400°F	170	370	90
VT	Ultra high vacuum creep test	110	25	14

1. 2400°F - 1589°K
   1600°F - 1144°K
   1400°F - 1033°K

Consistently higher oxygen, nitrogen and carbon levels were detected in the as-coated substrate and the substrate of samples representing the various exposure conditions, compared to that characteristic of the starting base material and the ultrahigh vacuum tested sample. Some variations in level of these elements were observed for the coated and oxidized samples, but this is believed due more to sample preparation for analysis than actual difference. Because of this, the information implies that an increase in interstitial element level occurs in the T-222 substrate during coating, but little further change develops during subsequent exposure in air at 1400° F, 1600° F and 2400° F.

Ammon and Begley[15] examined the effect of carbon, oxygen and nitrogen content on the properties of T-111, a low interstitial level tantalum-base alloy of normal composition, Ta-8w/oW-2w/oHf. Compositions containing up to 500 ppm oxygen displayed little change in tensile, stress rupture, or bend behavior from that characteristic of the T-111 alloy. Creep and tensile strength were found to be similarly increased by either carbon and/or nitrogen addition up to about 0.02 w/o without loss of bend ductility; major strengthening being developed at the 0.01 w/o level. This implies that the level of substrate contamination suggested in the results of chemical analysis should not seriously change mechanical property behavior from that intrinsic to T-222, appearing to confirm the overall results of mechanical property tests performed on the program.

Structure Studies

Samples representing various conditions of elevated temperature air exposure were examined to define coating and substrate changes and interaction. Samples oxidized at 2400° F displaying coating failure in times spanning 21 to 304 hours, and a few creep tested specimens, provided the material for examination.

Primary Barrier Development. Microstructures across the coating thickness on samples air exposed at 2400° F for 10 and 284 hours*, are shown in Figure 23. Included for comparison in the figure is the as-coated condition.

*Bend sample 12 and tensile sample 17 — Table 6.

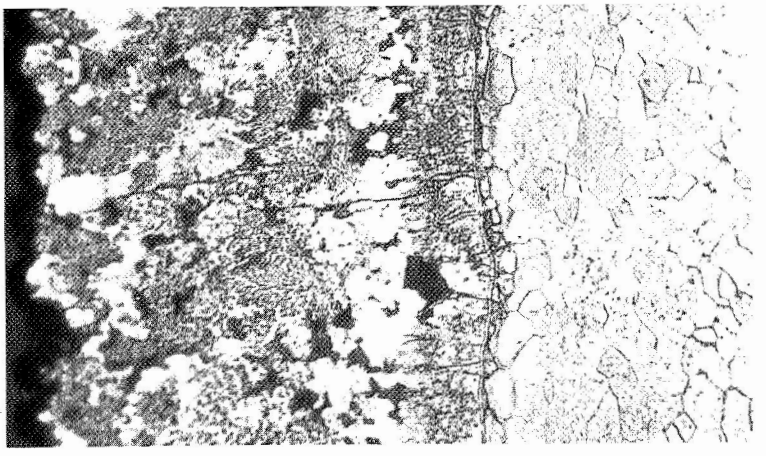

As-Coated

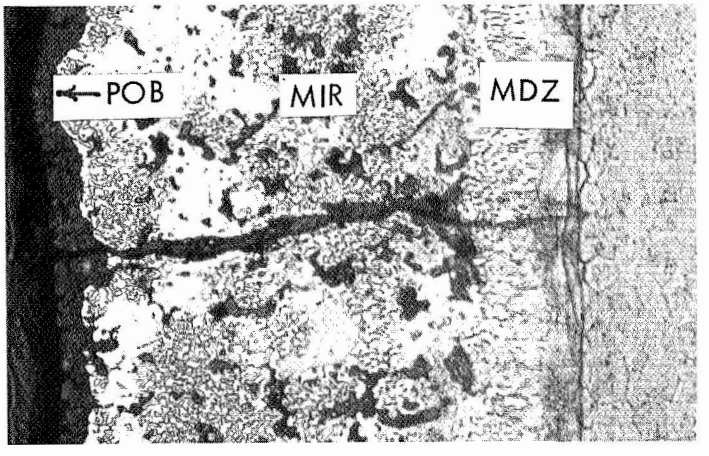

10 Hrs/2400°F

POB: Primary Oxide Barrier

MIR: Metallic-Intermetallic Reservoir

MDZ: Metallic Diffusion Zone

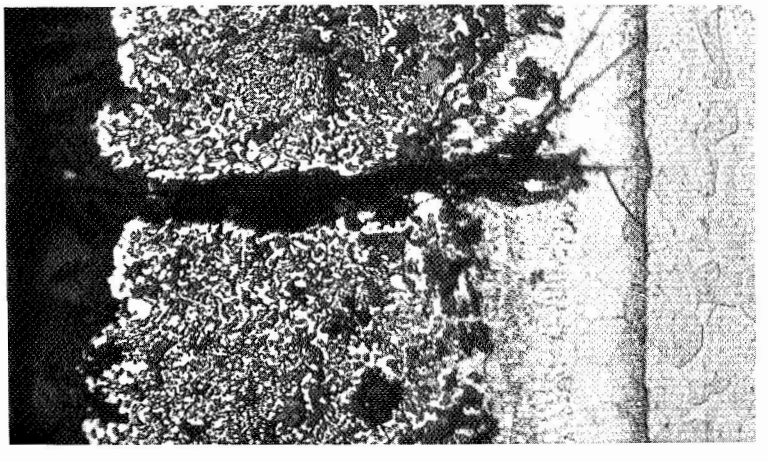

284 Hrs/2400°F

FIGURE 23 - Primary Oxide Barrier Formation at 2400°F (1589°K) Mag: 300X

Many cracks were uncovered in the metallic-intermetallic reservoir and metallic diffusion zone on these samples. Fissures were particularly wide in the metallic-intermetallic reservoir, but oxidation was found across and inside of them. Formation of these coating fissures is undoubtedly a result of thermal stress induced by cyclic exposure, and is believed to be the cause of measurement of more rapid oxidation over the 2 hour exposure periods compared to those of longer duration - Figure 13. Assuming oxidation is accelerated until the fissures are plugged, then the rate measured over short periods would be higher than measured over long periods, since the time taken by the sealing process would occupy a greater percent of the short period.

Oxide development within the gauge section of creep sample 27, strained 9 percent during testing at 2400° F, is depicted in Figure 24. Oxidation was noted across and within large fissures traversing the metallic-intermetallic reservoir, as was found on the samples exposed without application of stress. Many metallic diffusion zone cracks, however, were also observed plugged with oxide on creep sample 27. Two of these cracks are shown in Figure 24. Note that transgranular cracks emanate from the metallic diffusion zone fissures and propagate a short distance into the T-222 substrate.

The progress of primary oxide development was also studied by microscopy, and x-ray diffraction and electron microprobe analyses performed, in situ, on the primary oxide surface formed during 2400° F air exposure. Results of this examination are presented in Figure 25 and 26, and Table 14.

Change of coating surface microstructure developed by 24 through 500 hour air exposure at 2400° F*, is shown in Figure 25. Development of a two phase, particle-in-matrix, structure occurs during oxidation at 2400° F, with the amount of particle phase increasing with increased time-at-temperature. Cracks in the primary oxide barrier are also a common structural feature.

---

*Samples examined: Tensile samples 12, 13, 18, 33 — Table 6
Creep sample 26 — Table 12

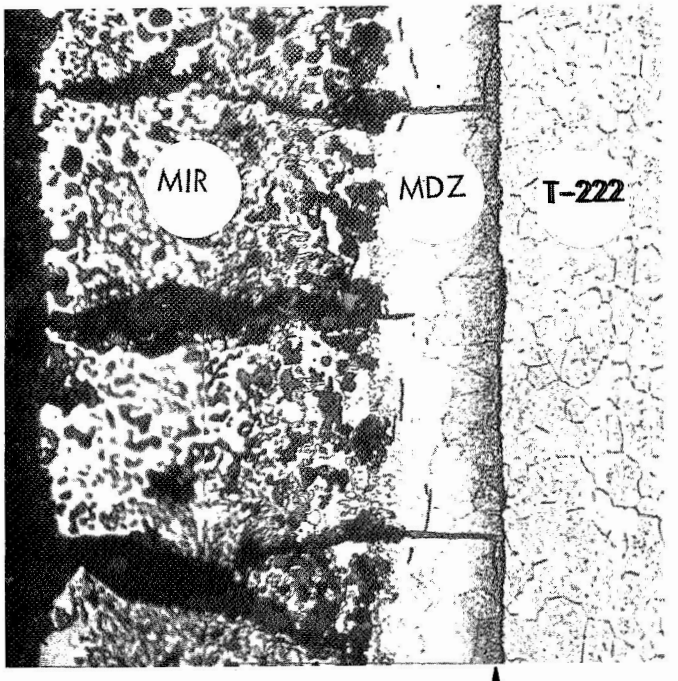

MIR: Metallic-Intermetallic Reservoir

MDZ: Metallic Diffusion Zone

300X

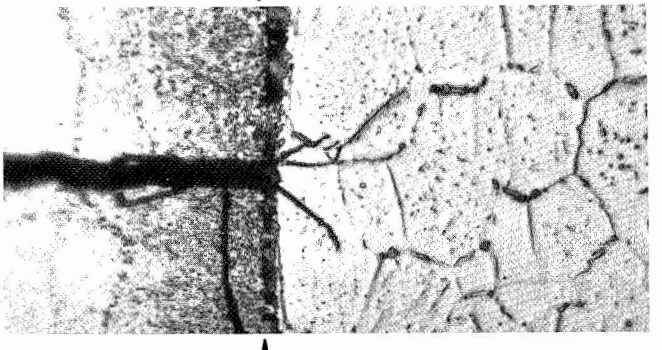

1000X

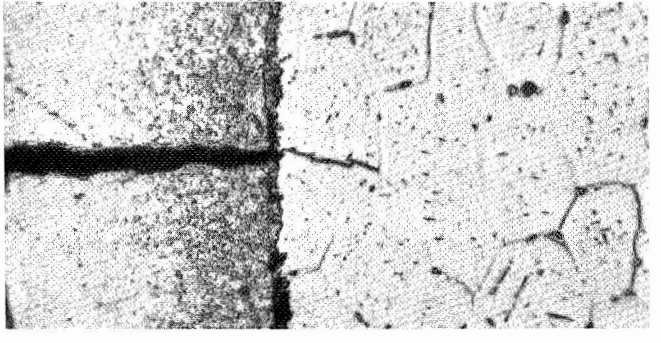

1000X

FIGURE 24 - Oxide Formation on Creep Sample 27

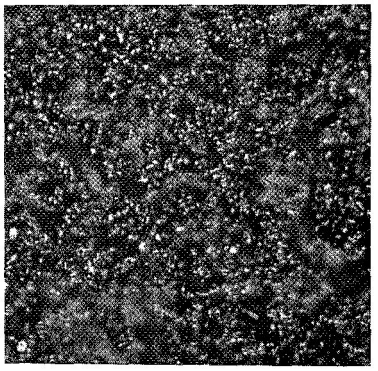

As-Coated

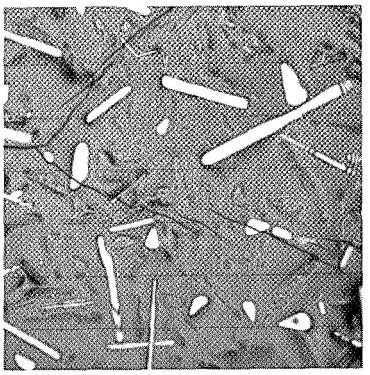

195 Hrs/2400°F

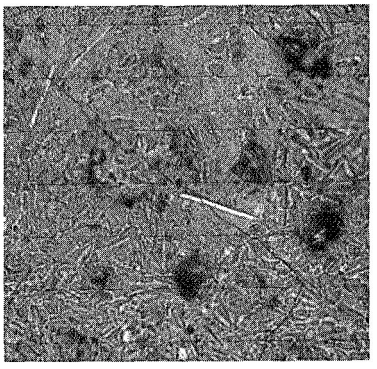

24 Hrs/2400°F

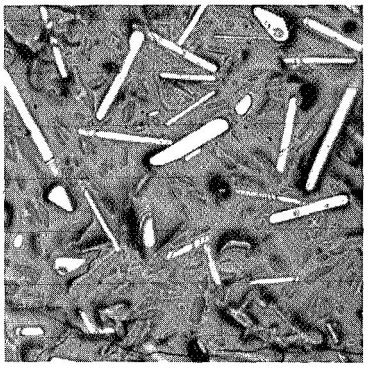

304 Hrs/2400°F

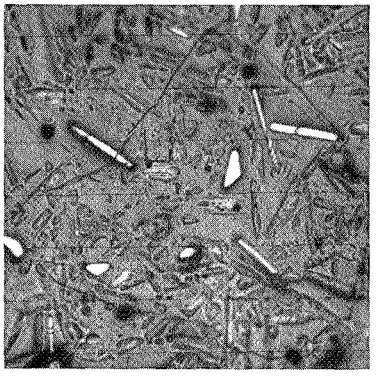

155 Hrs/2400°F

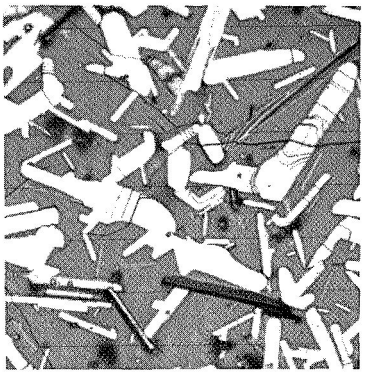

500 Hrs/2400°F

FIGURE 25 - Structure Developed at the Primary Oxide Surface by Oxidation at 2400°F
Mag: 200X

Electron microprobe analysis for the presence of major coating and substrate elements in the two phase surface structure, Figure 26*, revealed the particle phase to be titanium rich, and the matrix silicon rich. Other elements present in the as-applied coating, tungsten, vanadium and molybdenum, were not detected at the primary oxide surface. Similarly, tantalum and hafnium, elements common only to the substrate, did not migrate through the coating to its surface during exposure of the sample.

X-ray diffractometer analysis was performed on the surface developed after 10, 24, and 134 hours air exposure at 2400° F**. The results are reported in Table 14. Favorable comparison of the diffraction data was obtained with the ASTM standards for rutile and silica,*** implying the primary oxide structure formed at 2400° F is basically that of TiO_2 particles in a SiO_2 matrix. Reflection was particularly strong for the (200) and (110) planes in the TiO_2 phase indicating the particles form with these crystallographic planes parallel to the plane of the sheet. Wimber and Stetson[2] obtained similar x-ray diffractometer results from a coating, close to the study composition, oxidized at 2400°F. Tungsten, vanadium and molybdenum, elements that form oxides which volatilize at relatively low temperatures, are apparently eliminated from the coating surface during oxidation at 2400°F.

Substrate Structure Changes. Photomicrographs characterizing the structure of the T-222 substrate throughout its thickness are presented in Figures 27 through 30 for the as-coated condition, and the conditions developed by air exposure for 10, 284 and 437 hours at 2400° F. Photomicrographs representing the T-222 structure prior to coating are displayed in Figure 31 for comparison. Bend sample 12 and tensile sample 17 were used to represent the 10 and 284 hours-at-temperature conditions — Table 6. The 437 hour time-at-temperature condition was obtained from creep sample 27 — Table 12. It should be noted that time-at-temperature was accumulated on bend sample 12 and tensile sample 17 in the cyclic manner used for oxidation testing, whereas exposure of creep sample 27 occurred under stress and was continuous.

---

*Sample examined: Bend 17 — Table 6
** Samples examined: Bend Samples 12 and 17, Tensile Sample 18 — Table 6
*** Low Cristobalite

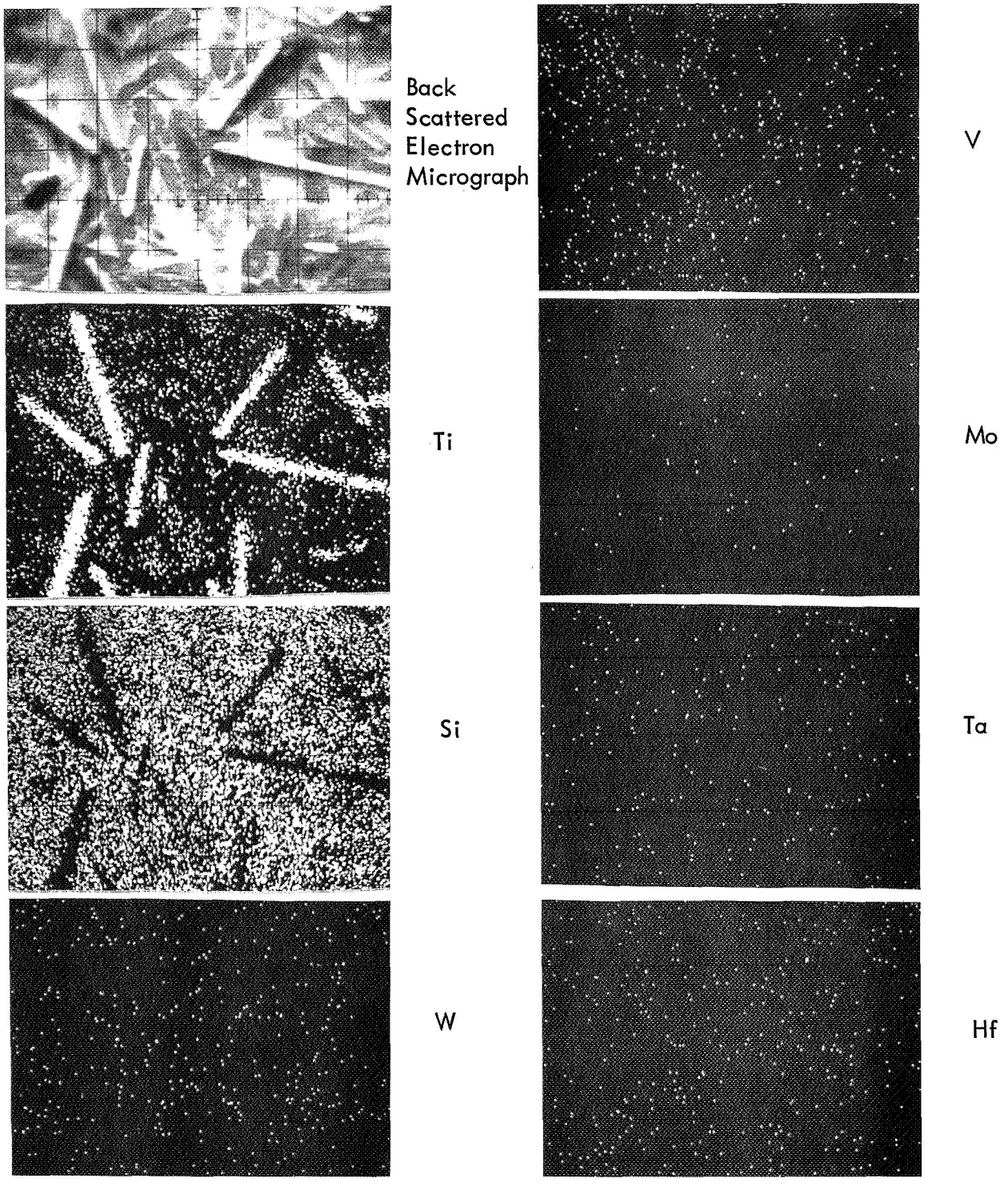

FIGURE 26 – Concentration of Elements at the Primary Oxide Surface Developed by Oxidation at 2400°F. Bend Sample 17 Oxidized 134 Hrs/2400°F.
Mag: 500X

TABLE 14 - X-Ray Diffraction Analysis of the Coating Surface Oxidized at 2400°F

Total Air Exposure Time at 2400°F						ASTM Standards					
10 Hours		24 Hours		134 Hours		Low Cristobalite		Low Tridymite		Rutile	
d	I[1]	d	I	d	I	d	I	d	I	d	I
		4.31	W	4.30	M			4.328	90		
				4.08	M			4.107	100		
4.05	S	4.06	M	4.05	M	4.05	100				
3.90	VW	3.90	VW	3.90	VW			3.867	20		
3.40	VW	3.81	W	3.81	W			3.818	50		
3.24	VW	3.24	S	3.24	S					3.245	100
3.15	VW			3.15	VW	3.135	11				
2.96	W	2.94	VW	2.96	W			2.975	25		
2.86	W	2.86	VW	2.86	W	2.841	13				
								2.776	8		
								2.500	16		
2.48	W	2.49	VW	2.48	W			2.490	14		
										2.489	41
						2.485	20				
								2.308	16		
2.29	W	2.26	VW	2.26	W					2.297	7
2.17	W	2.18	VW							2.188	22
								2.086	8		
										2.054	9
2.02	M	2.02	W	2.02	M			2.049	8		
1.96	VW	1.96	VW	1.96	W	1.870	7				
1.86	VW	1.86	VW	1.86	VW			1.695	12		
										1.687	50
								1.635	8		
										1.624	16
1.60	VW	1.62	W	1.62	W			1.600	10		

1. Diffractometer Peak Intensity Estimates: S - Strong
M - Moderate
W - Weak
VW - Very Weak

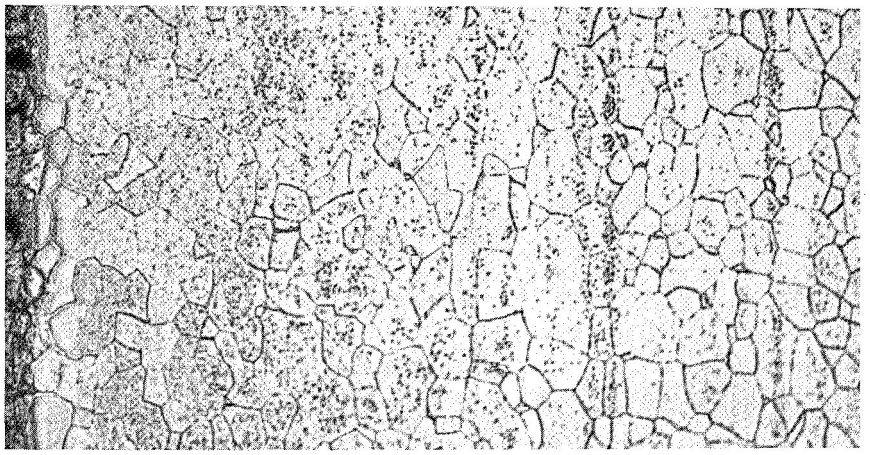

Coating–Substrate Interface

400X

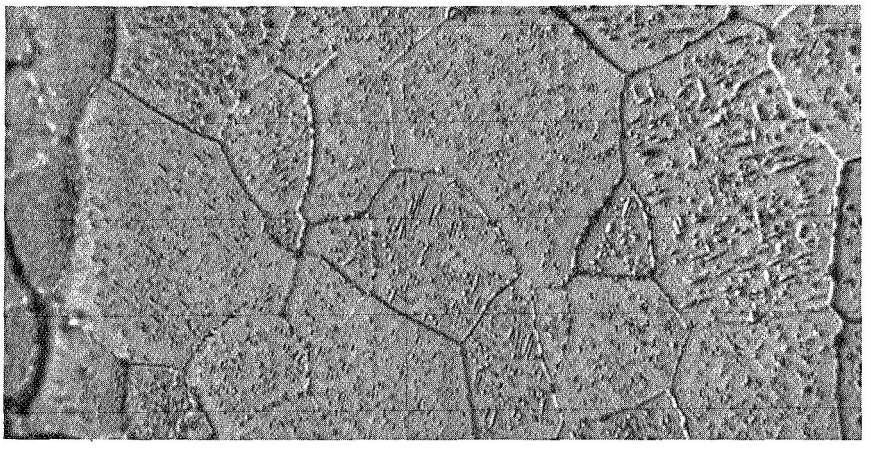

1500X

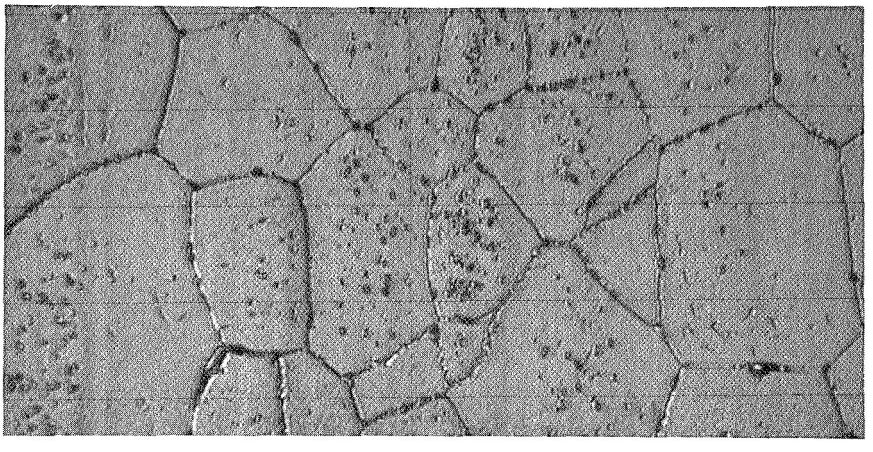

1500X

FIGURE 27 – Microstructure of The T-222 Alloy Substrate After Coating
Top & Middle: Structure into the Substrate from its Interface with the Coating
Bottom: Structure at Center Thickness of the Substrate

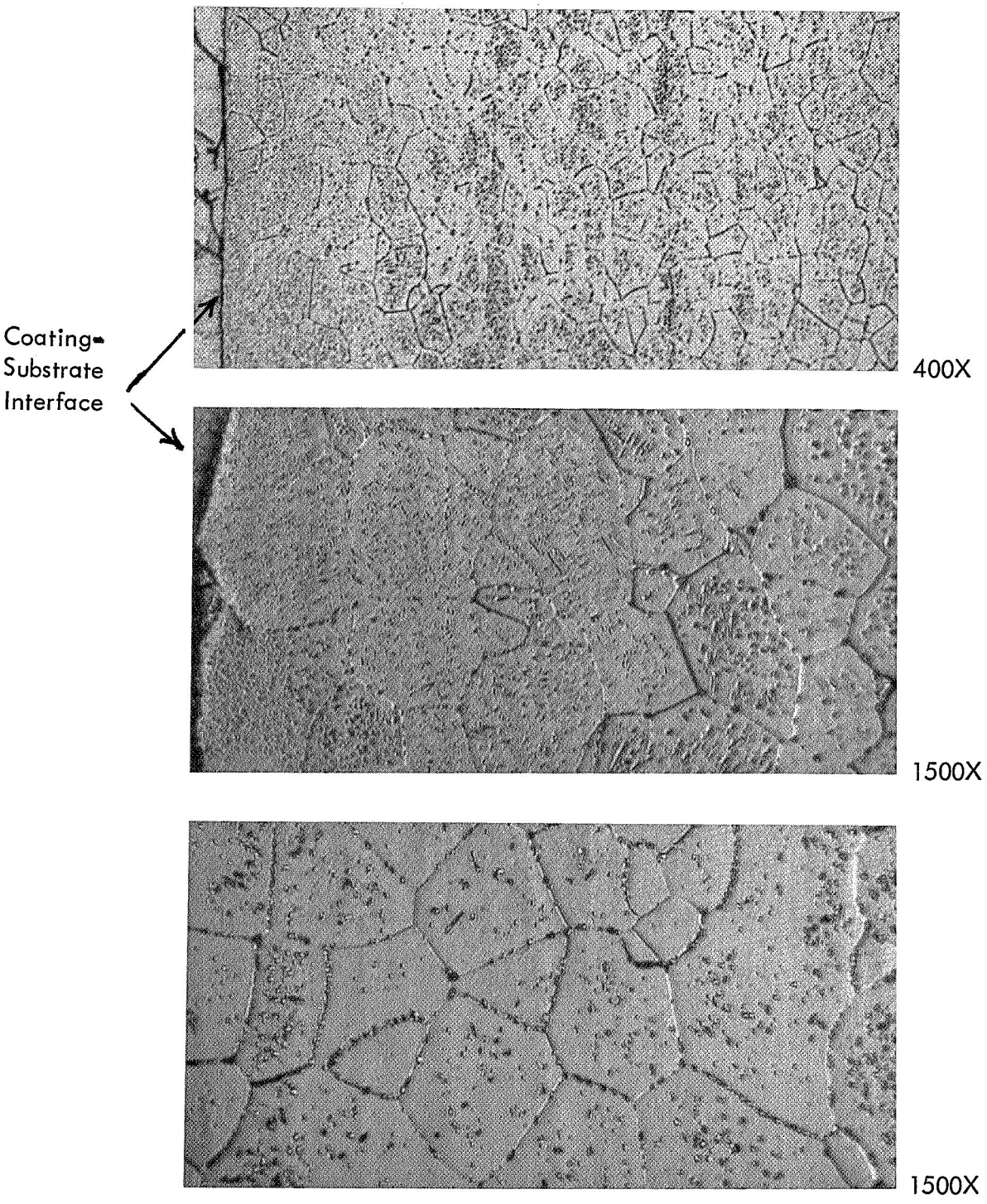

FIGURE 28 - Microstructure of the T-222 Alloy Substrate After Coating and Oxidation at 2400°F for 10 Hours.
Top & Middle: Structure into the Substrate from its Interface with the Coating
Bottom: Structure at Center Thickness of the Substrate
Bend Sample 12

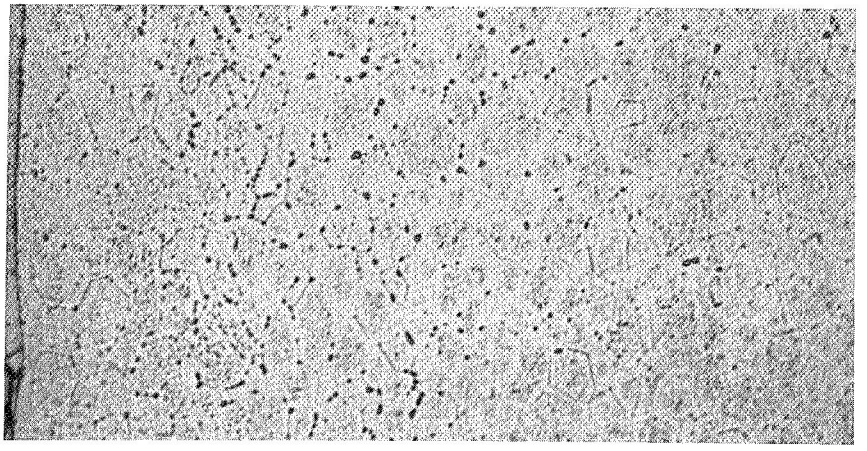

Coating-Substrate Interface

400X

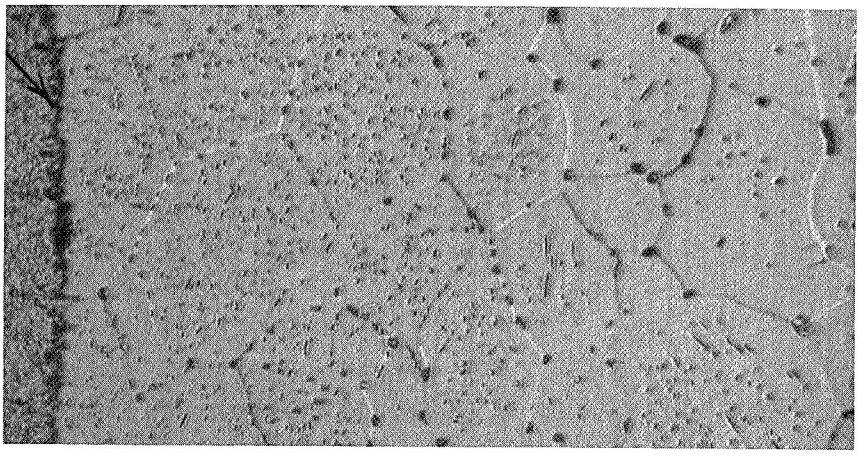

1500X

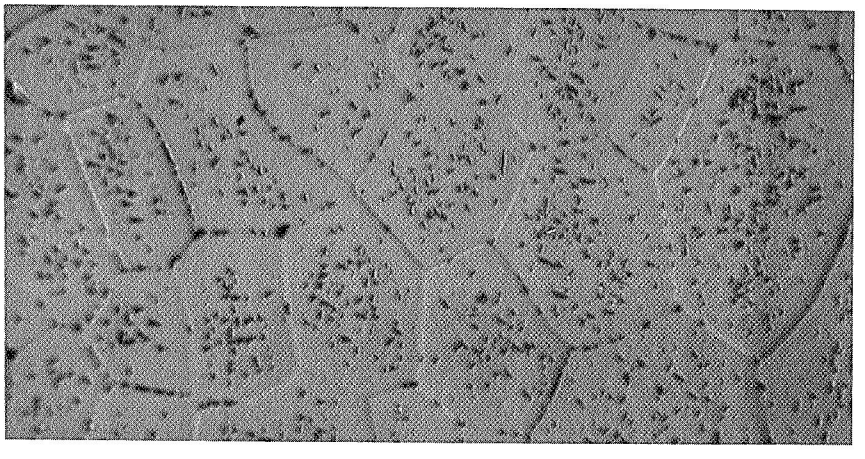

1500X

FIGURE 29 - Microstructure of the T-222 Alloy Substrate After Coating and Air Exposure at 2400°F for 284 Hours
Top & Middle: Structure into the Substrate from its Interface with the Coating
Bottom: Structure at Center Thickness of the Substrate
Bend Sample 17

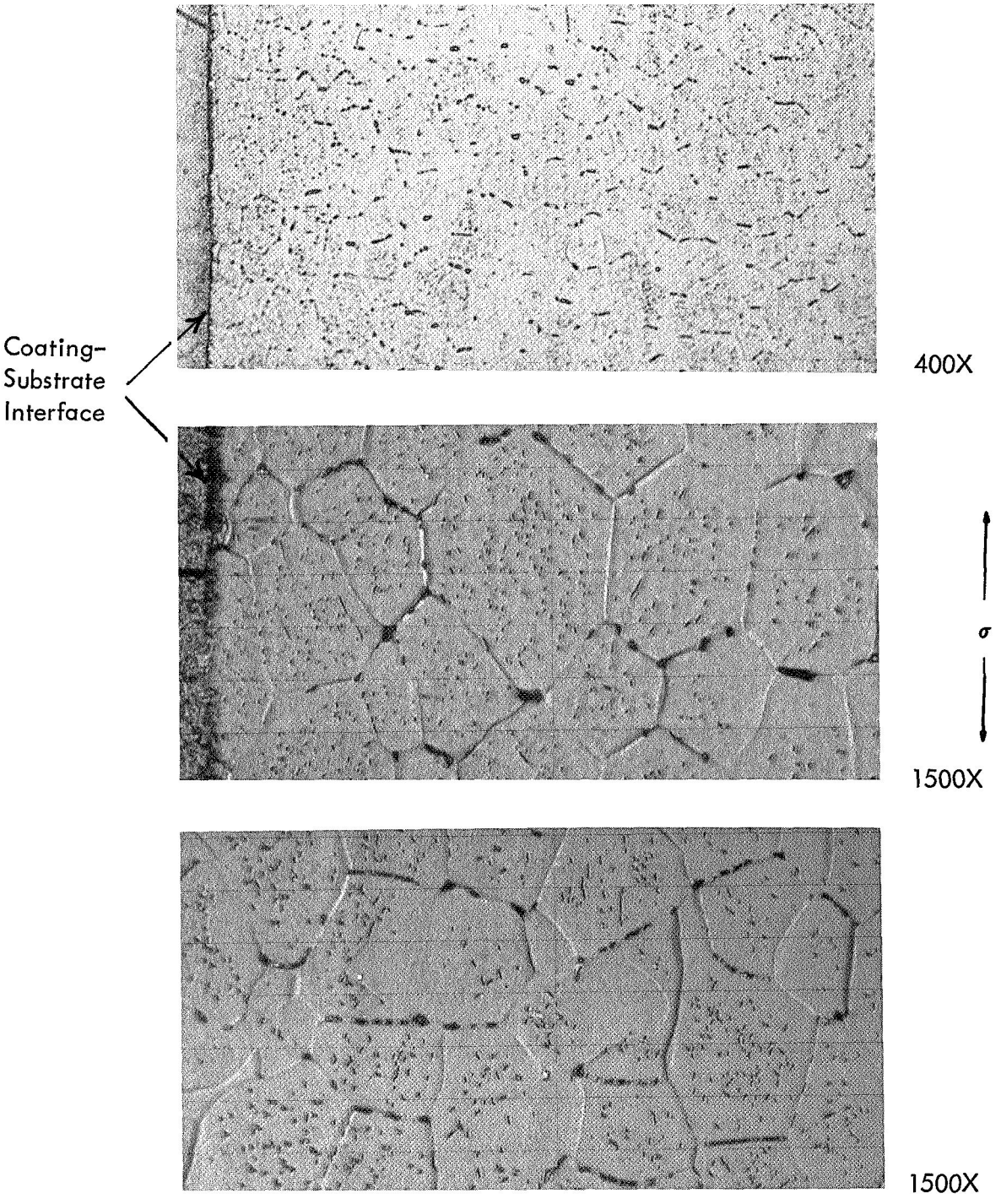

FIGURE 30 - Microstructure of the T-222 Alloy Substrate After Coating and Air Exposure at 2400°F for 437 Hours
Top & Middle: Structure into the Substrate from its Interface with the Coating
Bottom: Structure at Center Thickness of the Substrate
Creep Sample 27

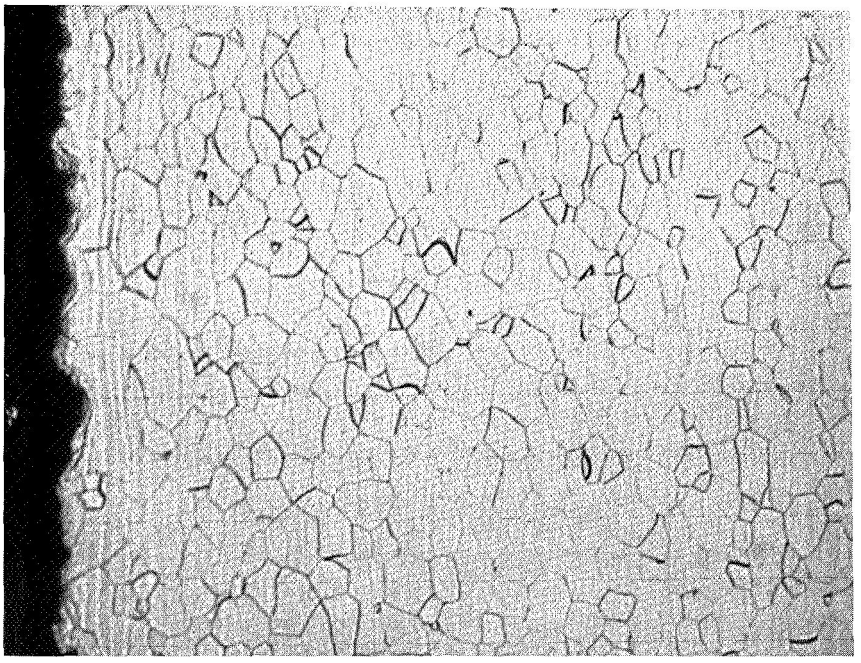

400X

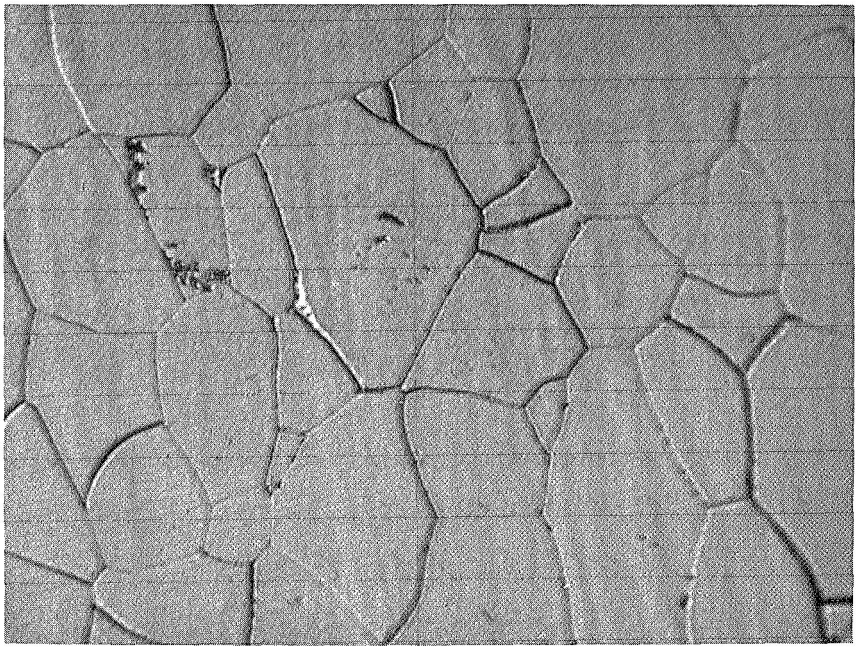

1500X

FIGURE 31 - Microstructure of the T-222 Before Coating
Condition: 1 Hr/3000°F Anneal
Top: Structure into Thickness for 0.010"
Bottom: Representative Bulk Microstructure

Microstructures heavy with precipitation, both at grain boundaries and within grains, characterize the as-coated condition and those representing air exposure at 2400° F. As previously mentioned, these conditions will cause aging of the solution treated T-222 substrate (Figure 31), accounting for much of the precipitation observed.

A significantly greater population of within grain precipitates was observed for the as-coated condition in the vicinity of the substrate-coating interface. This might be due to interstitial element contamination introduced during the coating process as indicated by the results of chemical analysis — Table 13. Greater within grain precipitation was also a general feature of the 10 hour/2400° F exposure condition in the vicinity of the substrate-coating interface, but was relatively uniform throughout the substrate on the 284 hour and 437 hour exposed samples, reflecting homogenization with increased time-at-temperature.

Grain boundary precipitation consisting of small closely spaced particles was a general feature throughout the entire substrate thickness for the as-coated and 10 hour/2400° F conditions. A few large precipitates located principally at grain boundary triple points near the coating-substrate interface were also found in the 10 hour/2400° F sample.

Precipitation at grain boundaries in the sample representing 284 hour/2400° F air exposure partly resembled that prevalent in the as-coated and 10 hour/2400° F samples, i. e., closely spaced small particles. However, many large precipitates located primarily at grain boundary triple points in the vicinity of the coating-substrate interface were present in this sample. A similar amount of large, individual precipitates located at grain boundary triple points near the coating-substrate interface were also found in the sample representing 437 hours air exposure at 2400° F. Closely spaced particles also formed along grain boundaries throughout the entire substrate on the 437 hour/2400° F sample. These precipitates were somewhat larger than those associated together along grain boundaries in the as-coated, 10 hour/2400° F and 284 hour/2400° F samples.

Microstructure of the base material sample heat treated in ultrahigh vacuum to the thermal conditions of coating, then creep tested in the environment at 2400° F and 8 ksi for 500 hours, is presented in Figure 32. Precipitation to a much lesser degree than found in creep sample 27, similarly tested but in air environment, was observed in sample VT. The carbon, oxygen and nitrogen levels in this sample were identical to that in the T-222 sheet prior to testing, while the content of these elements was undoubtedly higher in the coated and air tested material — Table 13. This must account for the difference in amount of precipitation.

The morphology of within grain precipitates in sample VT was similar to that found in creep sample 27. Fairly large grain boundary precipitates were also found associated together in this sample, as was observed in creep sample 27, but large individual precipitates were not present at grain boundary triple points. It follows from this that the large triple point particles found prevalent in the vicinity of the coating-substrate interface on the 284 hour/2400° F and 437 hour/2400° F samples, are associated with contamination during coating and/or subsequent oxidation testing.

The similar amount of these large particles in the 284 hours/2400° F and 437 hours/2400° F samples, appears to support the conclusion arrived at from chemical analysis; namely that little change in contaminant level occurred with time at exposure temperature. Because of this, and the result of chemical analysis showing increase of oxygen content was most pronounced after coating, it follows that these particles are oxides. Presence in the substrate of the reactive metal hafnium suggests HfO_2 formation. The absence of these particles in the as-coated microstructure, and presence of just a few after 10 hours at 2400° F, implies particle growth with time-at-temperature is required to distinguish the phase.

By analogy to work identifying equilibrium precipitate phases in T-222[4,5], the matrix and grain boundary phase observed in sample VT would principally consist of the face centered cubic hafnium rich monocarbide, (Hf, Ta, W) C*. Development

* a/o Hf approximately 75 percent.

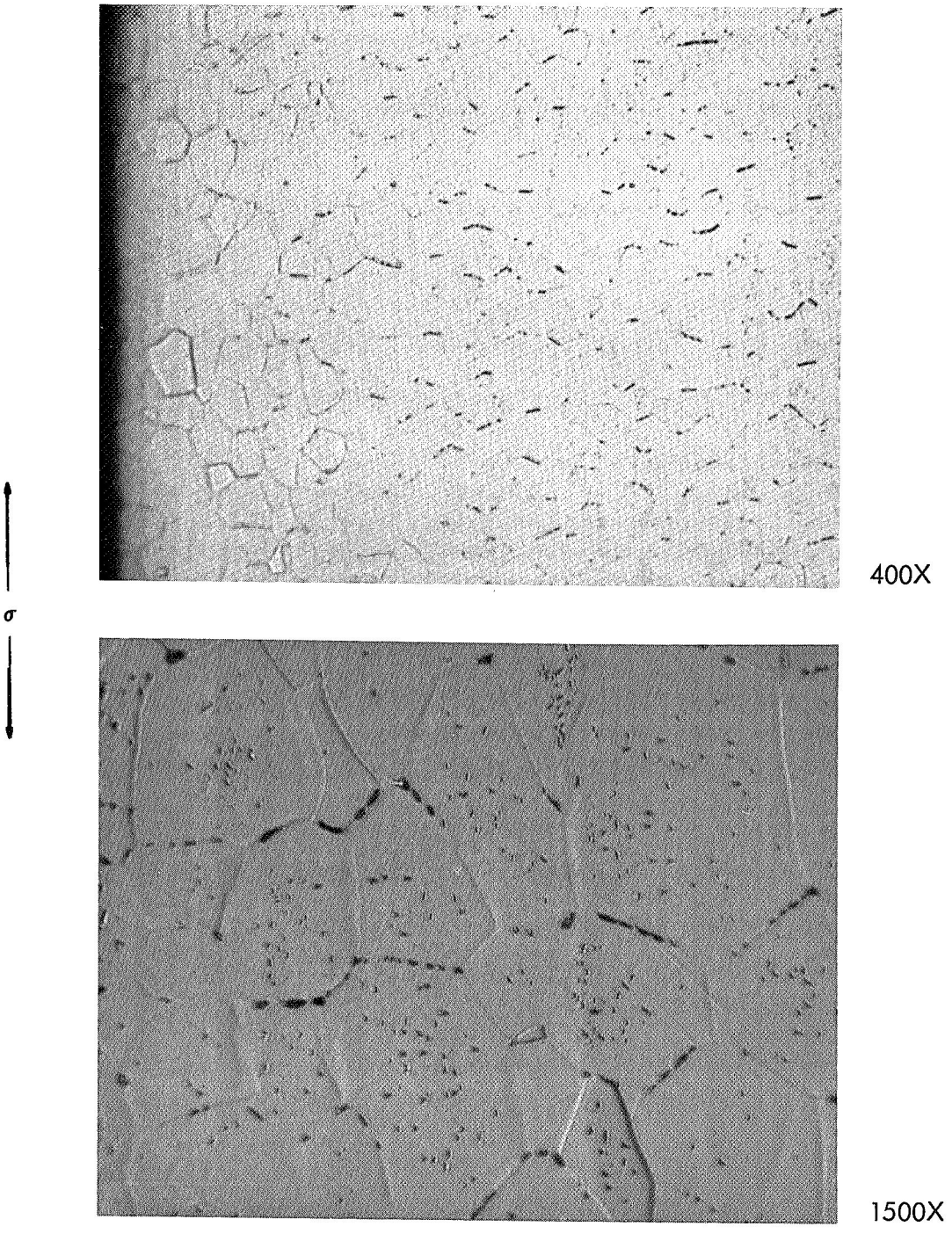

FIGURE 32 - Microstructure of Creep Sample VT
Top: Structure from Surface into Sample Thickness for 0.010"
Bottom: Representative Bulk Microstructure

of the relatively large precipitates associated together along boundaries in this sample might reflect a favored site for growth of the phase. Some indication that grain boundaries do indeed act in this manner can be obtained by close examination of the photomicrographs for sample VT in Figure 32. Boundaries oriented left-to-right in the photomicrographs were transverse to the axis of stress imposed during testing, and appear to contain more precipitate phase than those oriented with the stress axis. Grain boundaries oriented left-to-right in the photomicrographs of creep sample 27, shown in Figure 30, were similarly transverse to the test stress axis, and also appear to contain more precipitate.

Stress is likely to promote separation of transverse oriented grain boundaries, which might be viewed as a process of vacancy condensation. An excess of vacancies in the region of these boundaries could favor the sites for formation and/or growth of precipitates. For example, formation of (Hf,Ta,W)C would require a major increase of hafnium content at the site. This would occur by diffusion, and be promoted by the presence of excess vacancies in the region of the precipitate site. Perhaps this type of mechanism, as well as a longer time-at-temperature, accounts for larger precipitates associated together along grain boundaries in the 437 hour/2400° F air test and 500 hour/2400° F vacuum test samples, compared to precipitates similarly associated in the samples representing shorter time-at-temperature.

Substrate Hardness Changes. Hardness data were obtained on the samples discussed in the above section, and are reported in Table 15. Included in Table 15 is the hardness level of the base material.

All conditions representing air exposure at 2400° F, as well as the as-coated condition, displayed lower hardness than the base material. This is certainly due in part to aging induced by the treatments. Softening due to removal of some hafnium from solid solution in the alloy by combination with oxygen introduced from contamination, is also possible. Evidence of a hardness decrease with increased oxygen content was obtained by Ammon and Begley[15] for the T-111 alloy, Ta-8 w/o W-2 w/o Hf, in the as-cast condition. On the other hand, hardening can occur in these alloys through formation of a coherent oxide precipitate by oxygen contamination introduced under certain temperature and pressure conditions.

TABLE 15 - The Effect of Coating and Exposure on Substrate Hardness

Impression Location	Sample Condition											
	Base Material		As Coated		Air Exposed 10 hrs/2400°F		Air Exposed 284 hrs/2400°F		Air Exposed 437 hrs/2400°F		Vacuum Exposed 500 hrs/2400°F	
Mils[1]	KHN[3]	DPH[4]	KHN	DPH	KHN	DPH	KHN	DPH	KHN	DPH	KHN	DPH
T.B.[2]	---	---	---	---	1500	---	1500	---	1500	---	---	---
2	---	---	282	---	300	---	267	---	275	---	251	---
3	---	---	289	---	300	---	269	---	267	---	254	---
4	---	---	---	---	290	---	264	---	281	---	260	---
5	---	---	272	---	302	---	272	---	278	---	251	---
7	---	---	261	---	278	---	260	---	266	---	255	---
10	---	---	263	---	294	---	269	---	269	---	250	---
15	315	283	279	243	304	257	262	247	265	251	246	240

1. Mils into the substrate from the ternary barrier-substrate interface. 1 mil = .0025 cm
2. Hardness of the ternary barrier at a location 1 mil from its interface with the substrate
3. Knoop hardness at 100 gm load
4. Diamond pyramid hardness at 10 Kg load

Significant hardness gradients were not detected on any of the samples, although somewhat more erratic behavior was observed for the as-coated and 10 hour/2400° F conditions; probably a reflection of the variation of precipitation noted in these samples.

Slightly higher hardness was obtained for the 10 hour/2400° F condition compared to the as-coated condition, while the samples oxidized for 284 hours and 437 hours at 2400° F displayed a similar but slightly lower hardness than developed by 10 hour treatment. These small differences probably reflect change of precipitate phases from those formed under the conditions of coating to those stable at 2400° F, as well as precipitate growth with time-at-temperature. As an example, phase identification studies[5] have shown that the dimetal carbide precipitate* is stable in T-222 solution treated and aged at 2000° F, while aging at 2400° F produces the monocarbide** phase.

Little difference was observed between the hardness levels of the samples representing air exposure at 2400° F, and that of the ultrahigh vacuum heat treated and tested sample. To some degree, this confirms the mechanical property and analytical results which indicated atmospheric contaminants did not reach a serious level during coating or subsequent oxidation testing. An absolute conclusion in this respect, however, would be arguable since, as exemplified previously for oxygen, contaminants may effect hardness differently depending upon specific conditions.

Coating and Substrate Interaction. Those samples employed to characterized substrate microstructure after coating and air exposure at 2400° F, were also examined to define the amount of coating and substrate interaction. Substrate recession due to ternary barrier growth, and interdiffusion of major coating and substrate elements, were examined.

Measurements of substrate recession due to coating and exposure at 2400° F for 10, 284, and 437 hours, are presented in Figure 33. These data are plotted against the square root of time-at-temperature in Figure 34.

---

*$(Ta,W,Hf)_2C$ $|Ta| > |W| > |Hf|$

**$(Hf,Ta,W)C$ $|Hf| > |Ta| > |W|$

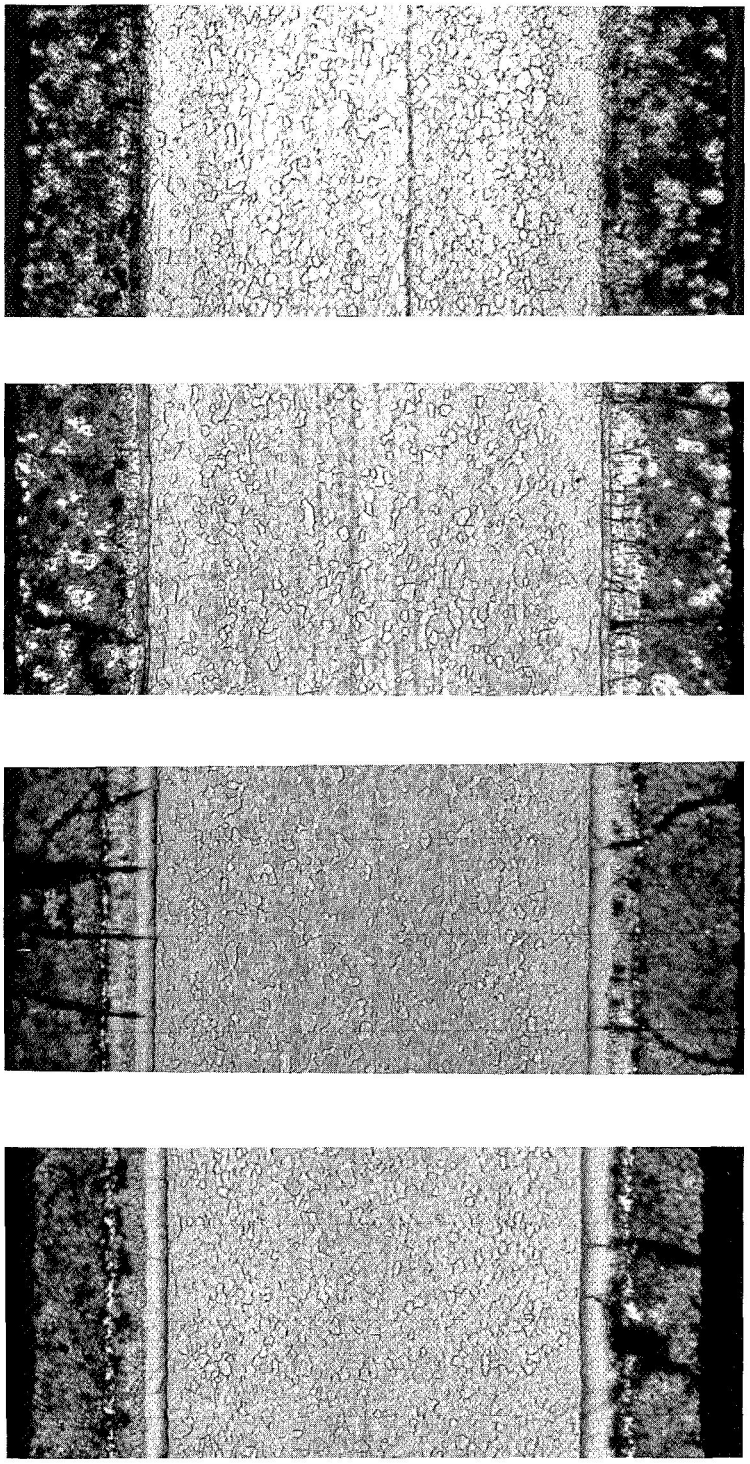

Condition	Substrate Thickness	
	Original	Final
As-Coated	0.0309"	0.0301"
Coated + 10 Hrs/2400°F	0.0313"	0.0292"
Coated + 284 Hrs/2400°F	0.0313"	0.0281"
Coated + 437 Hrs/2400°F	0.0315"	0.0270"

FIGURE 33 - Substrate Recession Due to Coating and Oxidation at 2400°F
Mag: 80X 0.001" = 0.025 mm

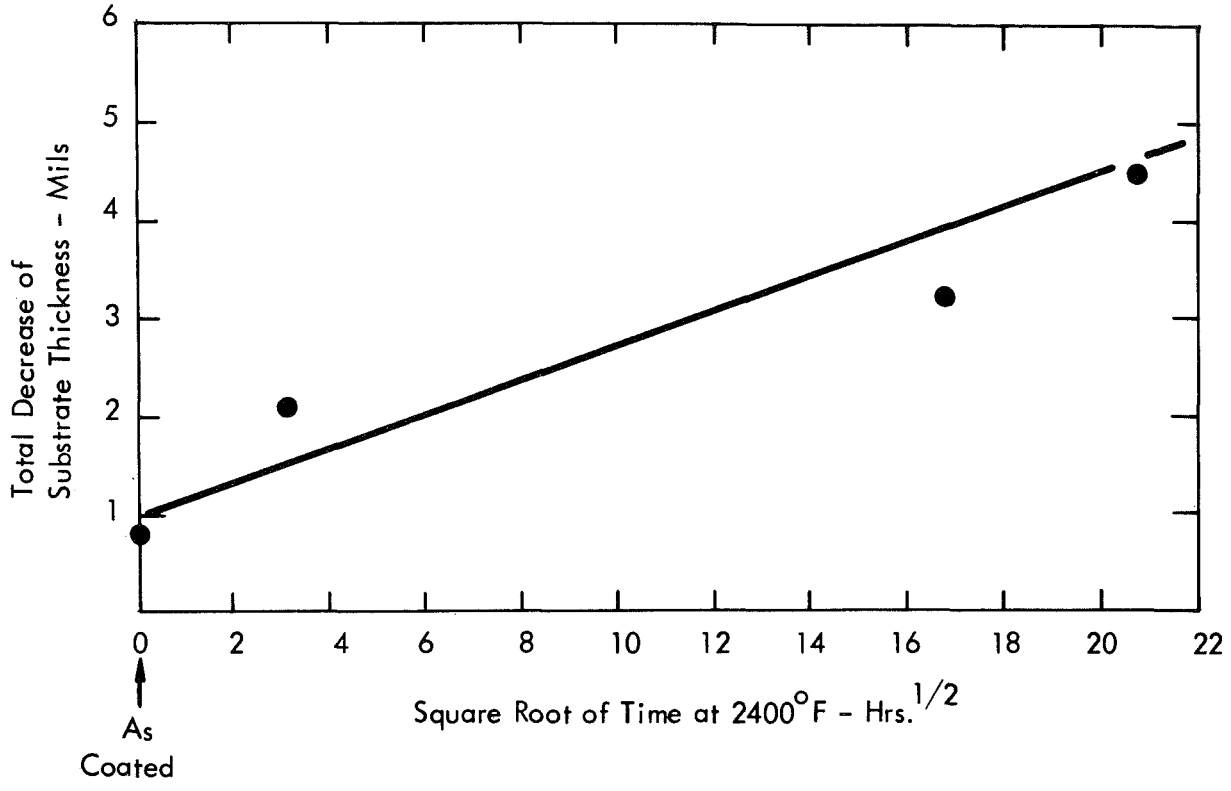

FIGURE 34 - Substrate Recession as a Function of the Square Root of Oxidation Time at 2400°F

A 0.0008" decrease in total unaffected substrate thickness was measured as a result of the coating process. Exposure for 10 hours at 2400°F caused an additional 0.0013" change in this dimension, while 284 hours and 437 hours at 2400°F resulted in 0.0024" and 0.0037" total recession, respectively. This information shows a reduction of unaffected substrate cross sectional area roughly of 15 percent will occur from coating followed by 400 to 500 hours oxidation at 2400°F, the conditions common to the majority of creep tests performed on the program.

Interdiffusion of major coating and substrate elements was examined by electron microprobe analysis, for the as-coated condition, and that developed after 10 hours and 437 hours at 2400° F. This was done by tracing element concentrations across the entire coating thickness and into the substrate for a short distance. Results showing the sample areas examined and element concentrations revealed are shown in Figures 35 through 37.

The intensity of characteristic radiation was determined for each element at two points along the path traced, one marked (A) in the coating, the other marked (B) in the substrate. These intensities are reported as a percentage of that determined from pure standards. In this manner, the approximate amount of an element in weight percent can be judged at these locations in the trace path. It should be understood, however, that at best these values are only very approximate. Correction for absorption and reinforcement of characteristic radiation due to the presence of other elements, for porosity at the area examined, or for change in standard intensity values due to surface oxidation, to name a few, was not made.

Considering the as-coated condition, the elements silicon, titanium and vanadium, which are common to the coating only, were found to decrease to zero level in the vicinity of the structurally obvious interface between the metallic diffusion zone and substrate — Figure 35. Of these elements, silicon appears to drop sharply in concentration at this interface, while the levels of titanium and vanadium gradually change in the region of the metallic diffusion zone close to the interface. Molybdenum concentration in the coating decreased to zero level in the region between the metallic diffusion zone and metallic-intermetallic reservoir.

Titanium, vanadium and molybdenum were observed in greatest concentration roughly midway into the metallic-intermetallic reservoir in the as-coated condition. Tungsten level was relatively constant across the metallic-intermetallic reservoir, except for a sharp drop at the region where titanium, vanadium and molybdenum were concentrated. A decrease of tungsten level, an element common to both coating and substrate, was also found in the metallic diffusion zone.

The metallic diffusion zone developed by coating consists primarily of tantalum and silicon, as was indicated from previously discussed x-ray diffraction and microprobe analyses. This region, which defines the limit of interpenetration of coating and substrate elements, is 0.002 to 0.003 inches thick, and begins roughly 0.005 inches below the coating surface.

Exposure for 10 hours at 2400°F widened the metallic diffusion zone to 0.003 to 0.004 inch thickness, but penetration of coating elements beyond the structurally obvious interface of this region with the unreacted substrate, was not detected - Figure 36. Silicon concentration was found to decrease in two abrupt steps in the vicinity of the interface between substrate and the metallic diffusion zone. Change of concentration of other elements across the metallic diffusion zone was fairly similar to that found in the as-coated condition.

Evidence that 10 hour air exposure at 2400° F promotes concentration of titanium at the extremes of the metallic-intermetallic reservoir was obtained, while relatively constant levels of tungsten and molybdenum were found in this region. Vanadium content of the metallic-intermetallic reservoir varied somewhat more than tungsten and molybdenum.

Air exposure at 2400° F for 437 hours widened the metallic diffusion zone to 0.004 to 0.005 inches — Figure 37. Part of this region consists of a layer obvious in the microstructure appearing, from examination of the tantalum and silicon traces, to consist of two silicides of tantalum. The two abrupt changes in silicon level near the interface between metallic diffusion zone and substrate noted after 10 hours at 2400° F, is apparently evidence of formation of these adjacent reaction products. Penetration of coating elements into the substrate beyond its obvious interface with the metallic diffusion zone was not observed.

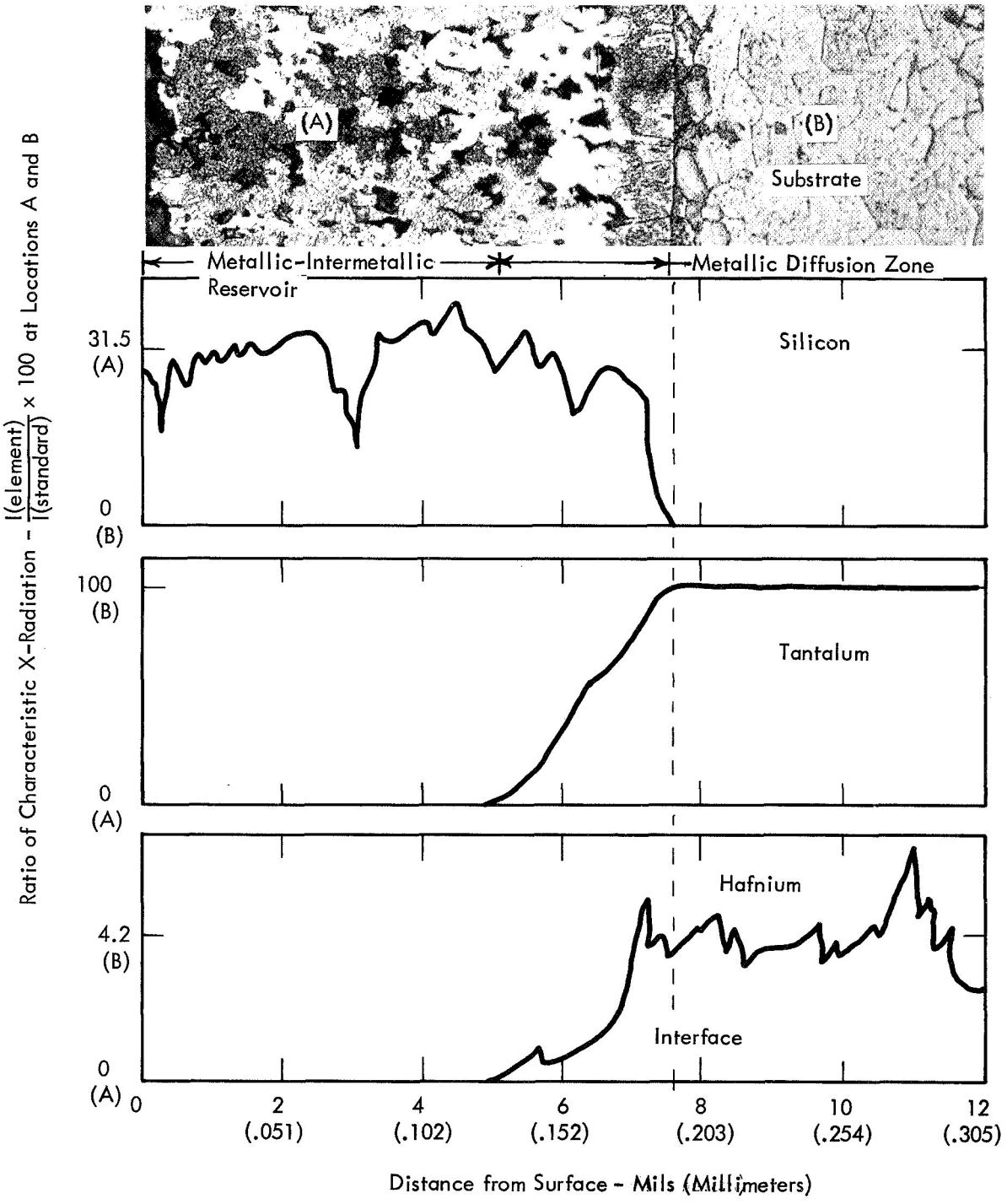

FIGURE 35 - Electron Microprobe Traverses of As-Coated Condition

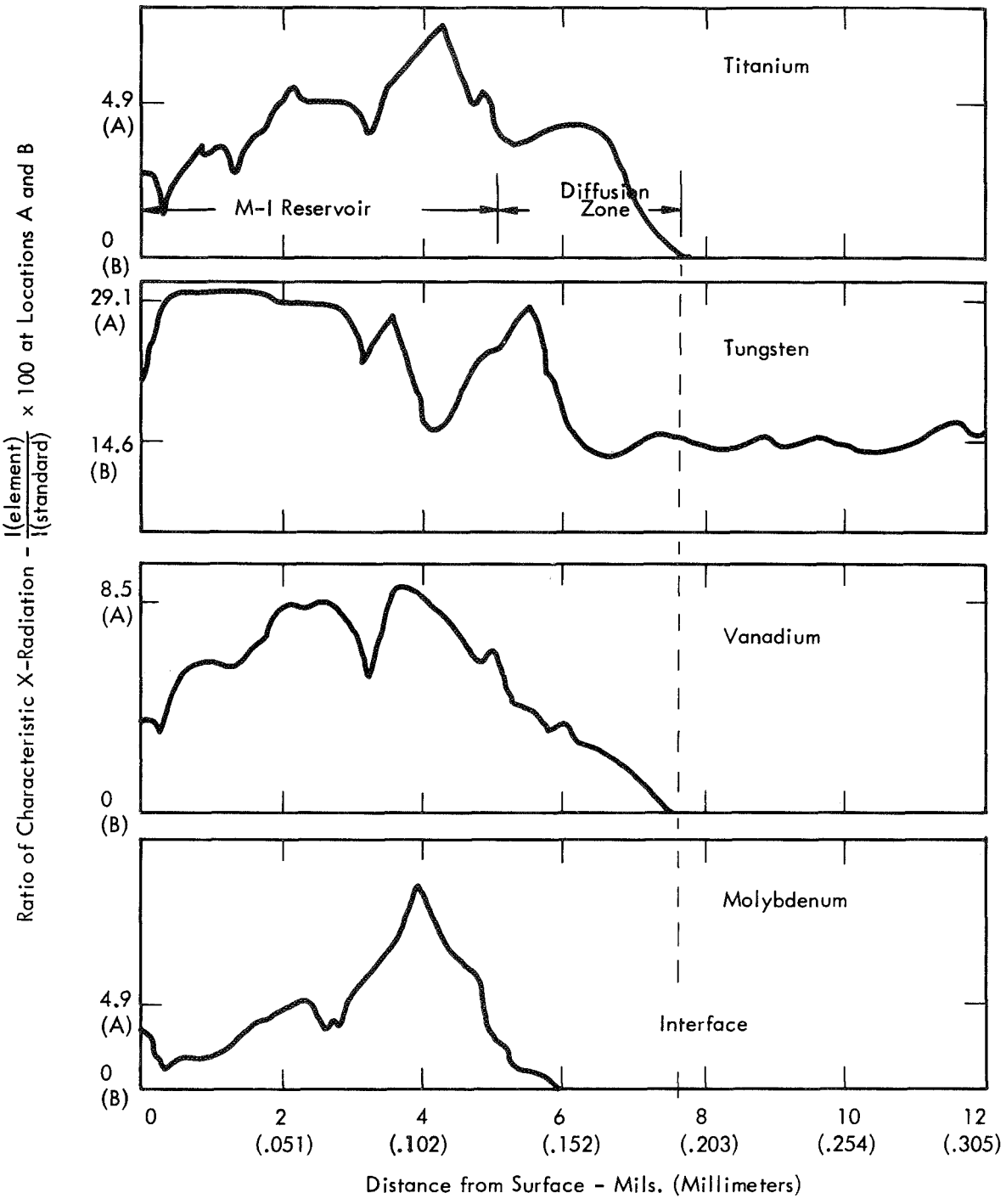

FIGURE 35 (Continued) - Electron Microprobe Traverses of As-Coated Condition

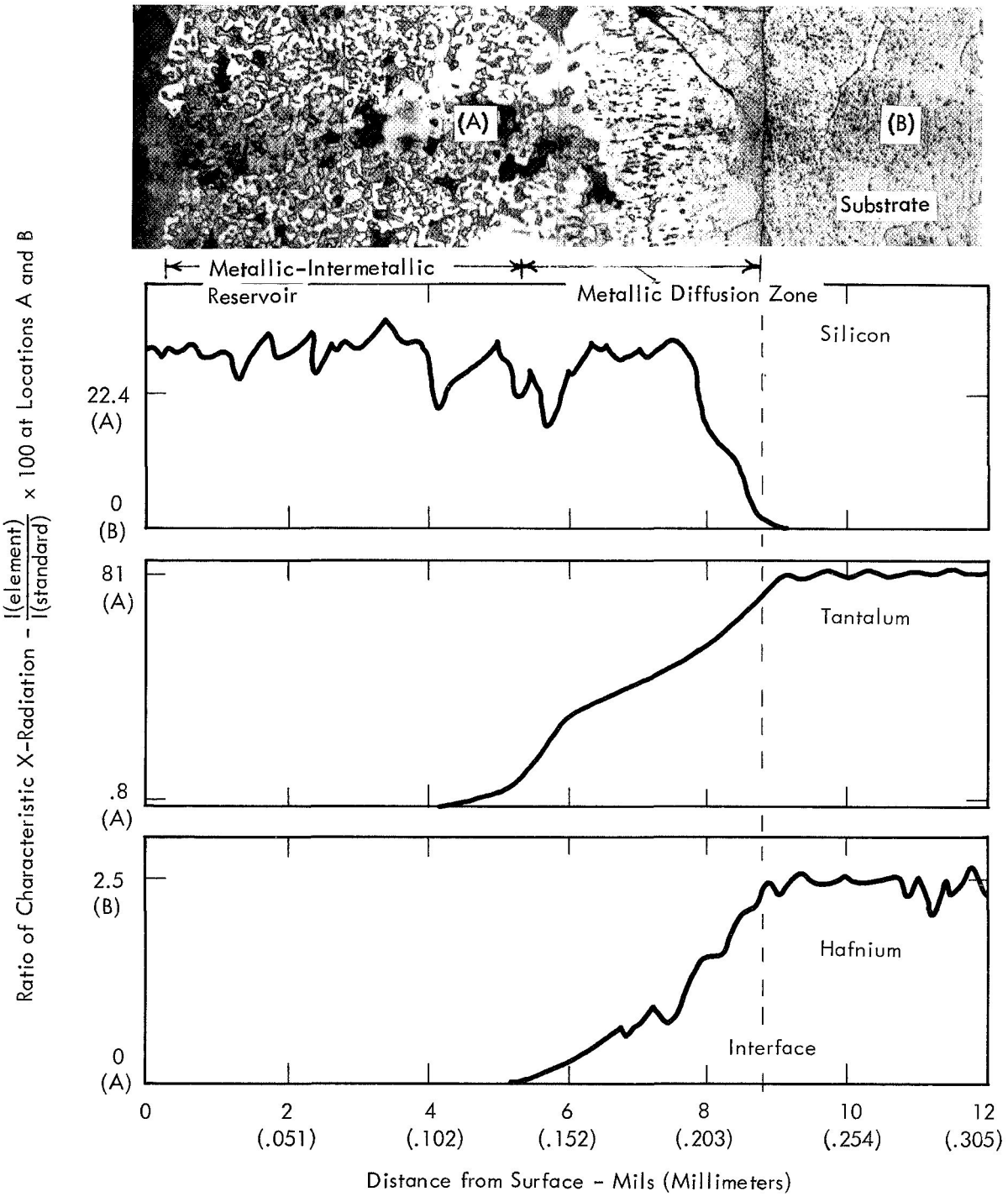

FIGURE 36 - Electron Microprobe Traverses After 10 Hours/2400°F Oxidation. Bend Sample 12.

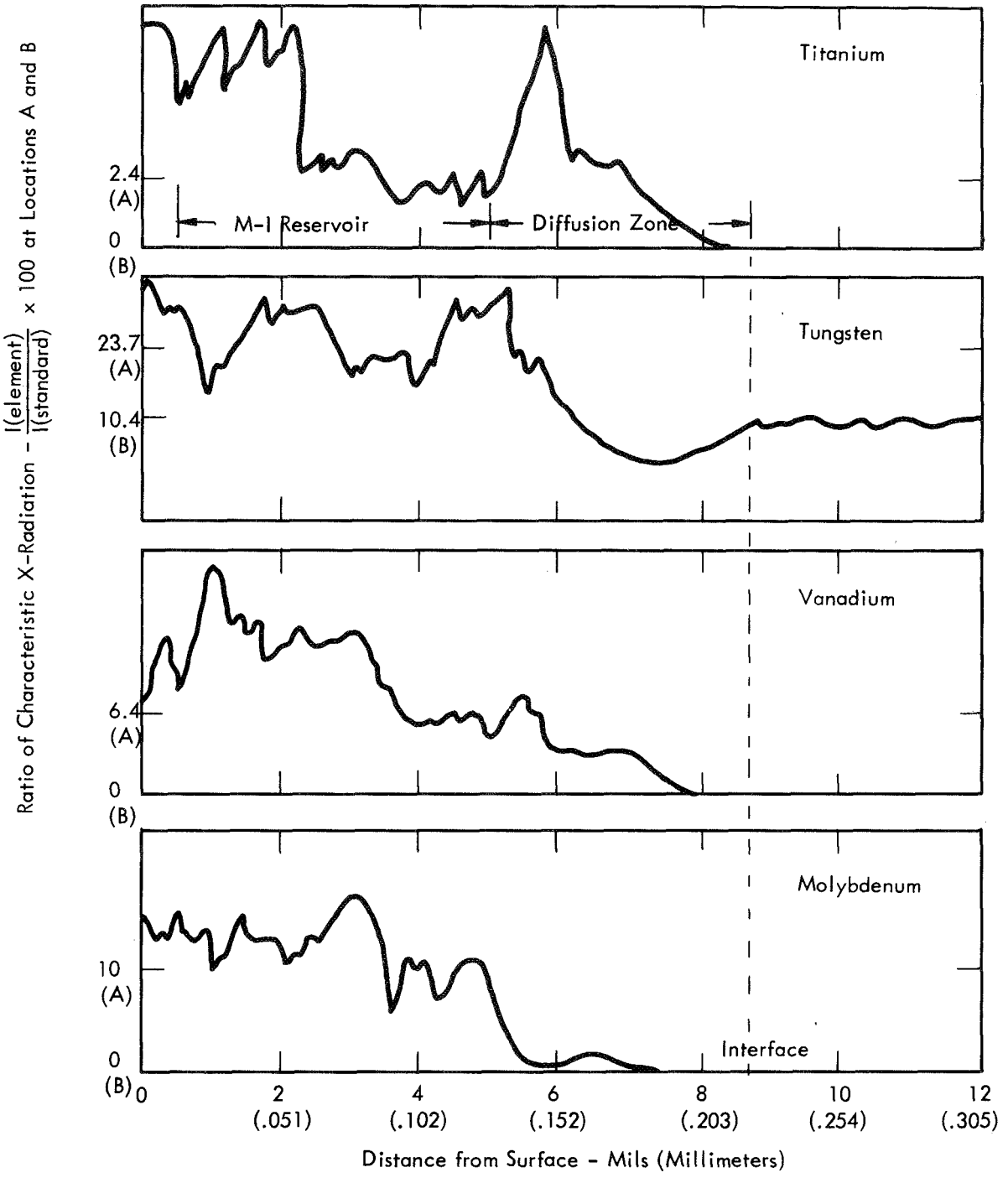

FIGURE 36 (Continued) - Electron Microprobe Traverses After 10 Hours/ 2400°F Oxidation. Bend Sample 12.

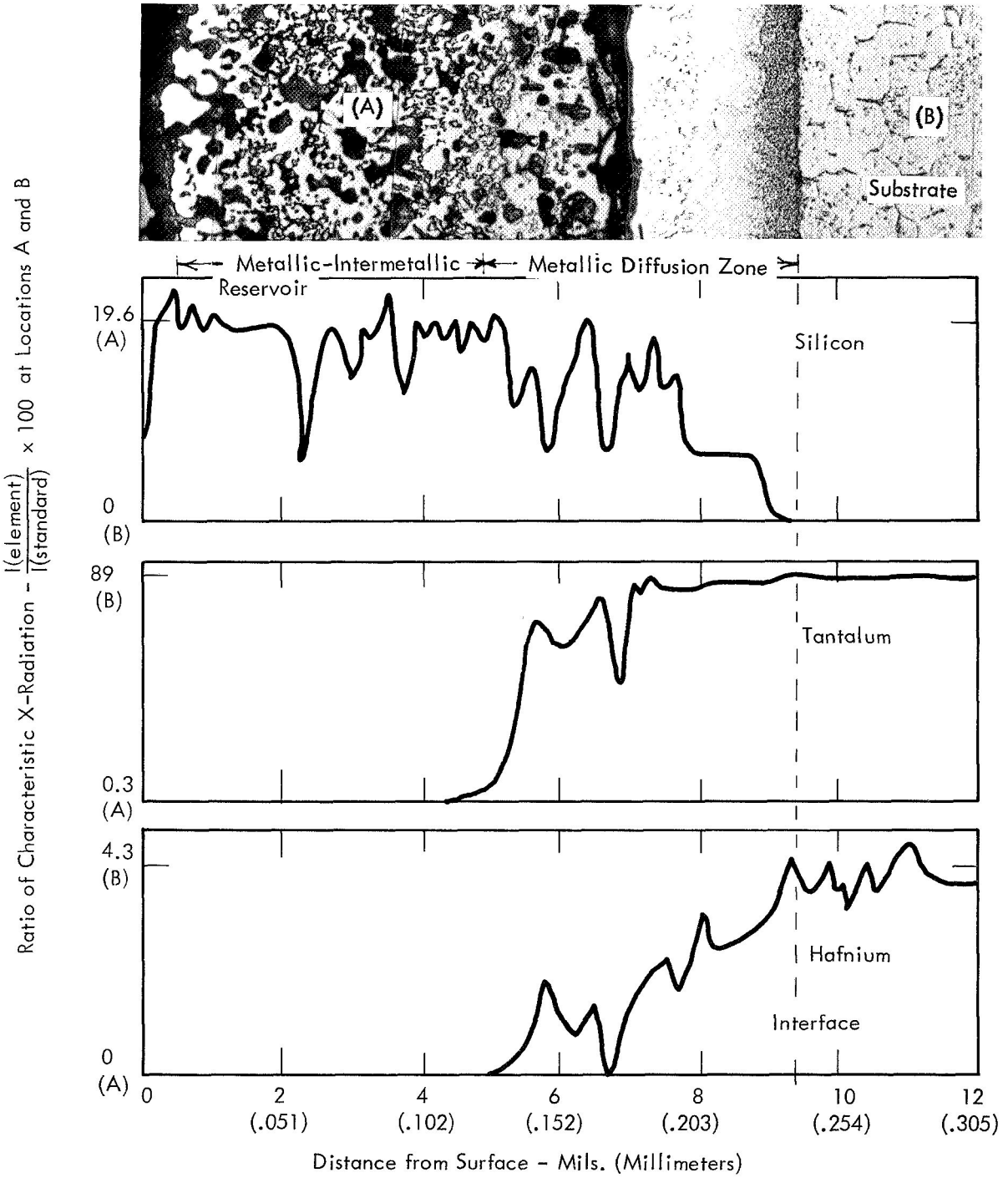

FIGURE 37 - Electron Microprobe Traverses After 437 Hrs/2400°F Oxidation. Creep Sample 27.

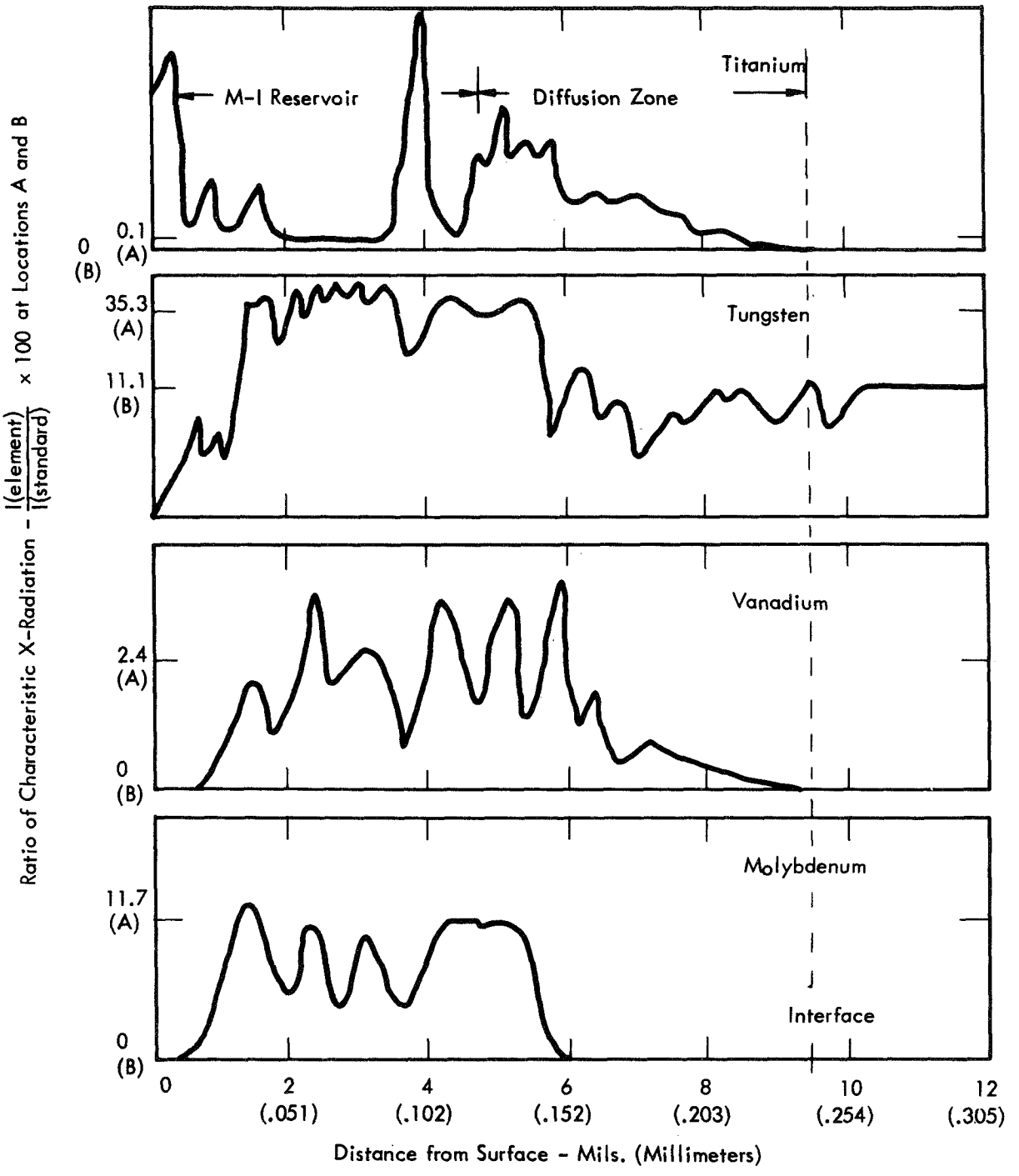

FIGURE 37 (Continued) - Electron Microprobe Traverses After 437 Hours/2400°F Oxidation. Creep Sample 27.

Titanium was found concentrated in the vicinity of the coating surface, and in the region of transition between the metallic-intermetallic reservoir and metallic diffusion zone, after 437 hours at 2400° F. Tungsten, vanadium and molybdenum were depleted near the coating surface for this condition.

Concentration of titanium near the coating surface is not detection of the few TiO_2 particles which can be seen in the primary oxide barrier cross section. These particles are too small and too few to cause the concentration response observed. Instead, a layer rich in titanium, presumably TiO_2, is believed to have formed beneath the primary oxide barrier, i.e., at the outermost extreme of the metallic-intermetallic reservoir. The high titanium concentration response appears to have occurred from the large white particle obvious in the path of the microprobe trace, located at the coating surface.

It is sufficient to say that quantitative judgment of element concentration changes in coating and substrate developed during oxidation at 2400° F, without benefit of multiple evaluations performed at several sample locations, meets with serious objections. Qualitative evaluation, as presented above, based on single microprobe traces obtained at one location, however, is believed representative of the general conditions developed. An example of how correct element concentration revealed by these traces is can be obtained by reference to Figure 38. Shown in the figure is an x-ray scan photograph of titanium characteristic radiation obtained across the coating and part of the substrate, on the sample oxidized 437 hours at 2400° F. Concentration of titanium in the vicinity of the coating surface, and within the region of transition from metallic-intermetallic reservoir to metallic diffusion zone, is obvious.

One interesting aspect of the microprobe examinations is the observation of concentration spikes in that portion of the traces for hafnium which span the substrate. This is taken to be evidence that hafnium rich precipitates are present in the substrate, as was suggested in discussion of substrate structure changes.

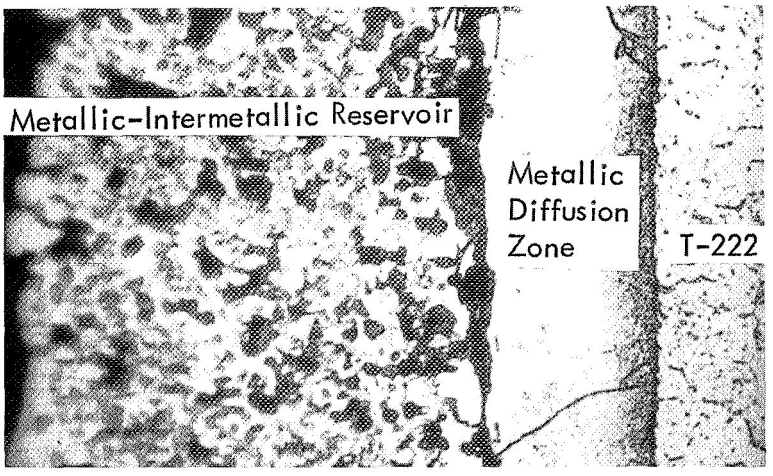

Light Photomicrograph

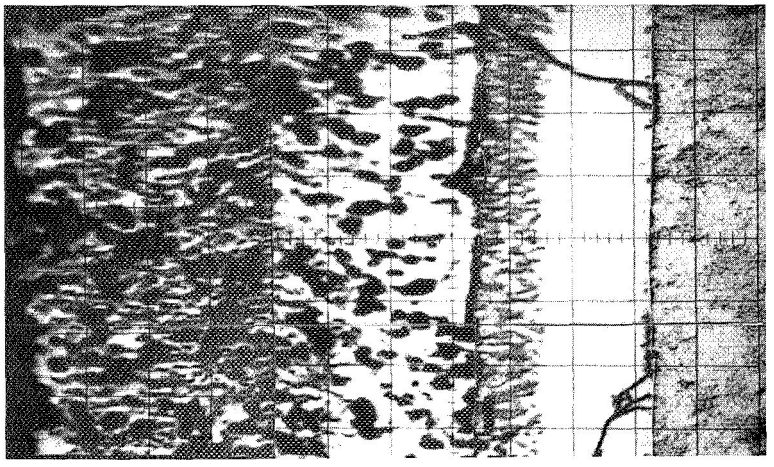

Back Scattered Electronmicrograph

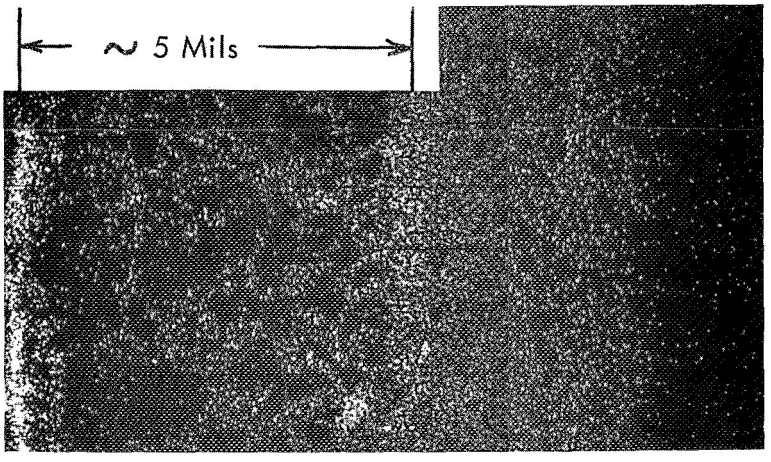

X-Ray Scan for Ti Characteristic Radiation

FIGURE 38 - Titanium Concentration in the Coating After 437 Hours Oxidation at 2400°F. Mag: 375X Creep Sample 27

Characterization of Creep Sample 38. As previously mentioned, air environment creep testing imposed a temperature gradient along the sample length — Figure 18. Because of this, study of a creep sample was undertaken to define coating and substrate changes and interaction developed over a wide temperature range. Characterization was performed on creep sample 38, principally employing microscopy, x-ray diffraction, and microprobe analysis.

This sample had been creep tested for 500 hours at 2400° F without fracture - Table 12. Coating failure and a small amount of substrate oxidation was found on the sample, however, at a point 1-3/8 inches from one end. The coating surface also exhibited a crazed appearance within the head section opposite that where oxidation had started, occupying an area roughly 1.2 to 1.6 inches from the nearest end. Except for these apparent differences, the macroscopic appearance of the sample on one side of the gauge center was a mirror image of the other half, and its overall appearance was similar to that of other specimens creep tested in air environment. That portion of the sample on which the coating remained protective for the test duration was examined in this study.

The sample, along with the temperature profile imposed by the creep test, is shown in Figure 39. The surface had a powder-like appearance between the position of 0.81 inch and approximately 2.0 inches from the end. The position of 0.81 inch represents the location of the end of the grip employed on the test. A dense surface was developed over the sample length between the 2 inch position and the gauge section.

Microstructures observed on the coating surface at several of the positions identified in Figure 39 are displayed in Figure 40. Structure could not be clearly defined at positions where a powder-like surface was present — positions A through C. Note that although the coating region at position C appears crazed (see Figure 39), the 50X picture of this region presented in Figure 40 revealing two craze marks, shows them as dark lines rather than cracks. Closer examination of these marks confirmed that they were not associated with cracks.

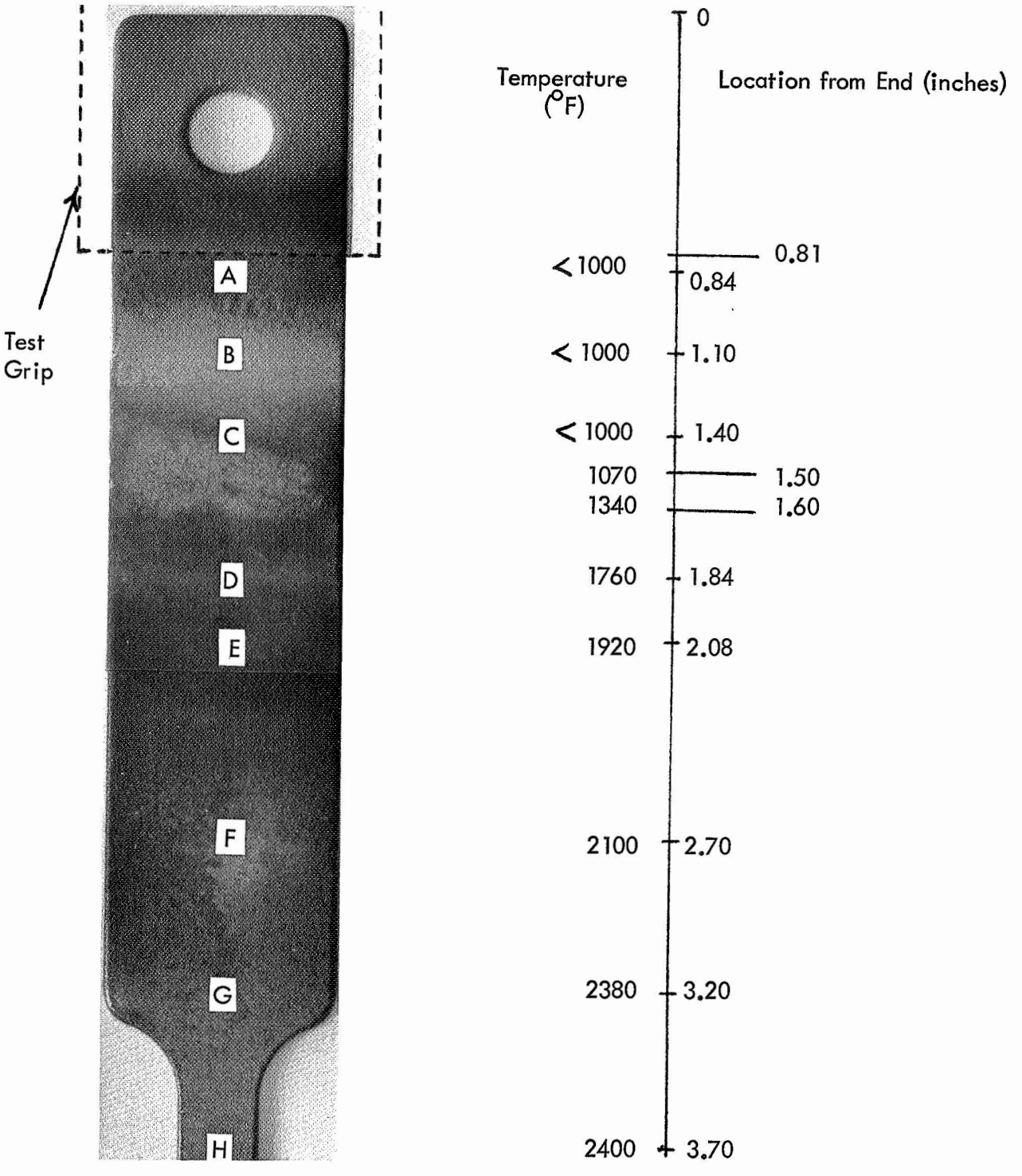

FIGURE 39 - Temperature Distribution and Surface Appearance Along Creep Sample 38. Air Test 500 Hours/2400°F

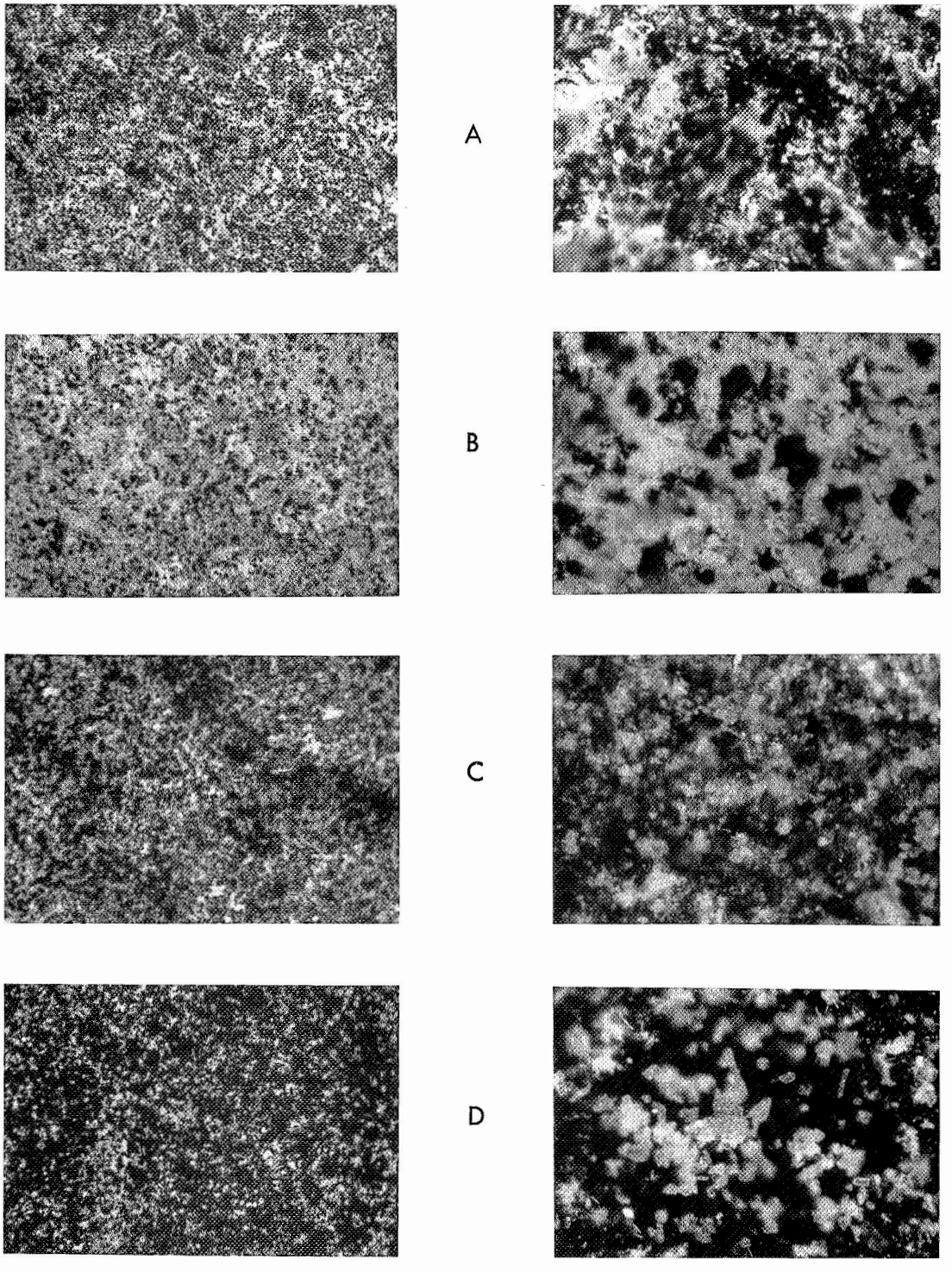

FIGURE 40 - Structure of the Coating Surface on Sample 38.
A-D: Positions Identified in Figure 39.
Left: 50X Polarized Light Illumination
Right: 200X Polarized Light Illumination

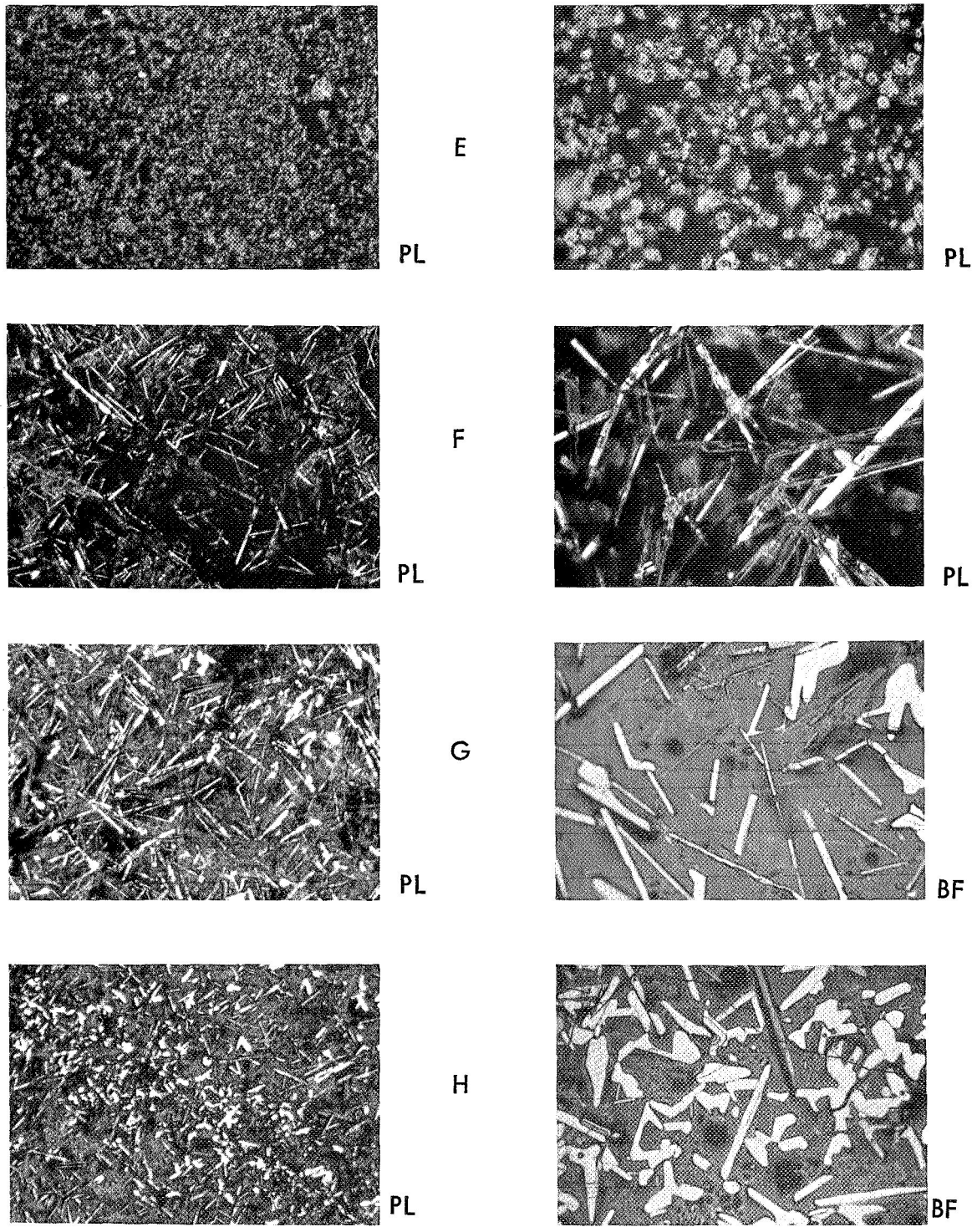

FIGURE 40 (Continued) - E-H: Positions Identified in Figure 39.
Left: 50X Right: 200X
PL: Polarized Light BF: Bright Field

The structures observed at positions D through H are clearly those of two phases, particle-in-matrix. Overall analysis indicates increased exposure temperatures favor development of this two-phase structure, with the discontinuous phase forming as nodules at low temperatures and platelets at high temperatures. The amount of particle phase also appears to increase with increasing temperature. Structure at position H representing 500 hours at 2400° F, is essentially identical to that presented in Figure 25, representing similar exposure on creep sample 26.

The results of microprobe analysis obtained at several of the surface positions identified in Figure 39 are displayed in Figures 41 through 45. Again, analysis of the structure at positions where a powder-like surface was present could not be made because of its irregularity. The indication that development of a two-phase structure is promoted by increased exposure temperature noted in the microstructural results, however, is verified by the microprobe data. It is apparent from this analysis that, in general, the particle phase is titanium rich and the matrix silicon rich. Data showing some particles to be both titanium and silicon rich was obtained at position F — Figure 45.

A small amount of molybdenum, and perhaps also vanadium, was observed in the particles formed at positions representing exposure temperatures of 1920° F and lower — positions B through E. Neither of these elements, however, is present at the coating surface in large amounts at temperatures above about 1000° F. It is difficult to establish the partitioning between precipitate and matrix of the element tungsten, but like vanadium and molybdenum, little of this element was found at positions representing temperatures above about 1000° F — position C.

The elements tantalum and hafnium, which are present initially only in the T-222 alloy substrate, were observed in a significant amount at two of the positions examined, positions C and F — Figures 42 and 45. Two tantalum rich specks were noted in the area studied at position C. The coating in the overall area occupied by positions B and C has

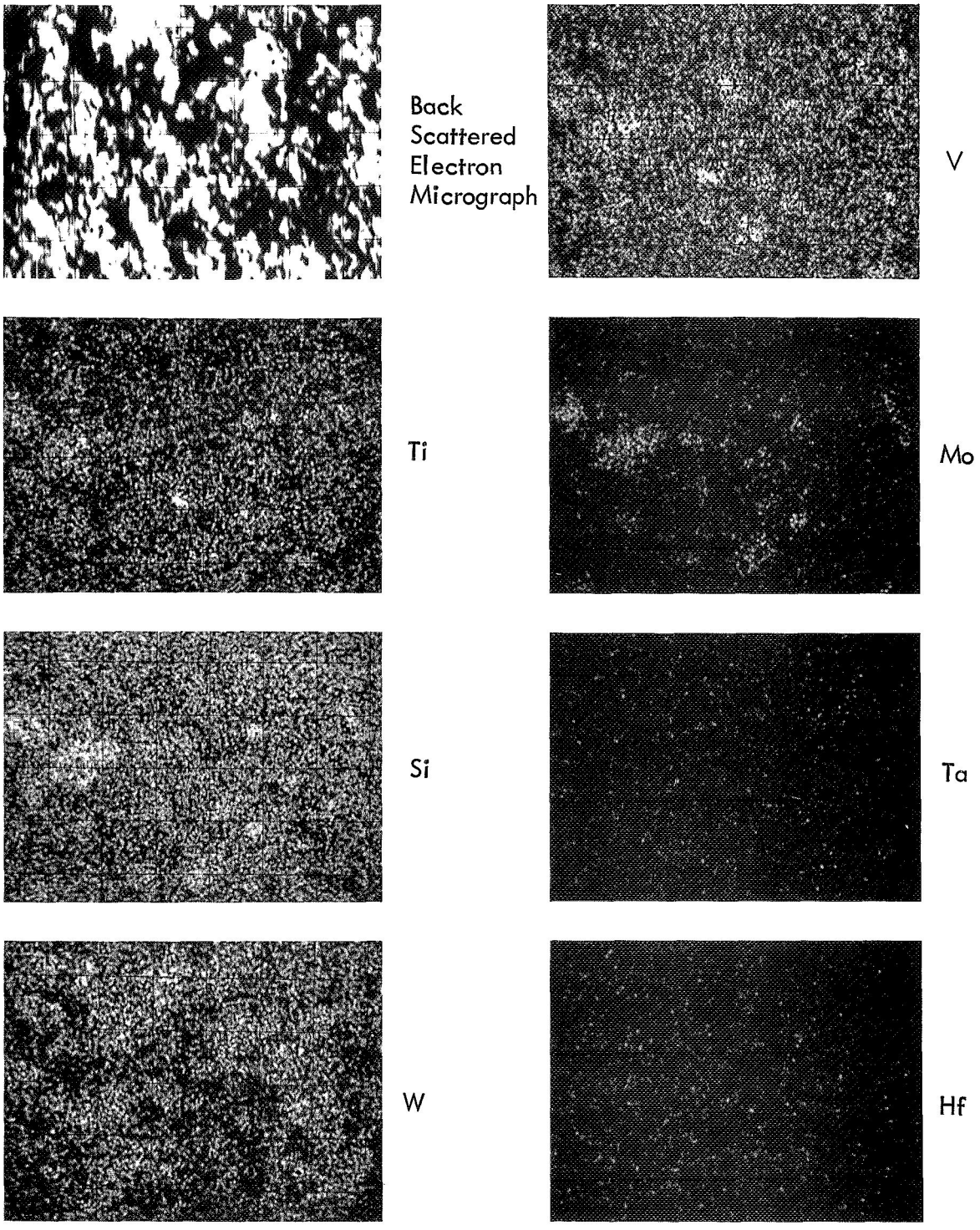

FIGURE 41 - Element Concentrations at the Coating Surface Revealed by X-Ray Scans at Position B on Creep Sample 38. Mag: 400X

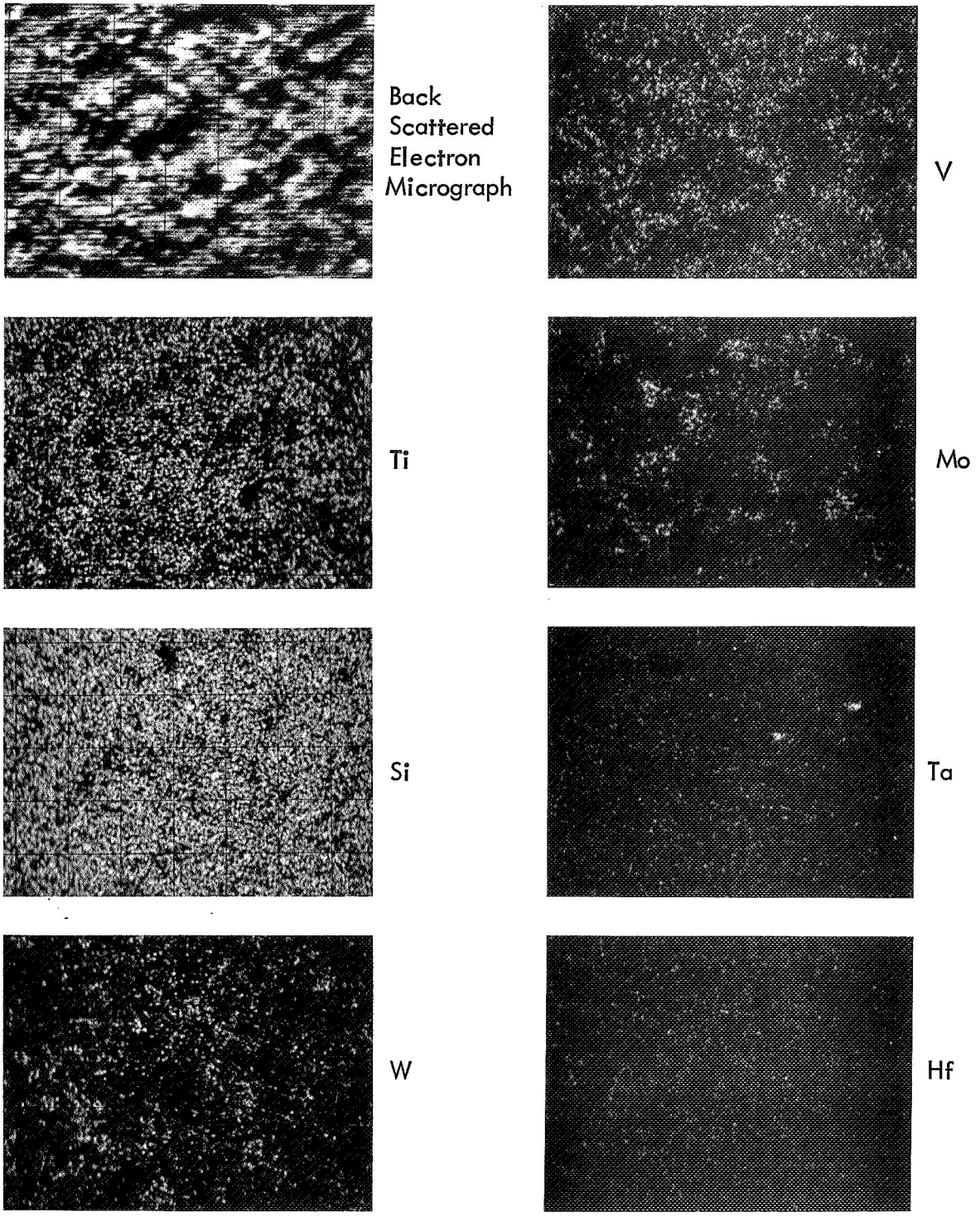

FIGURE 42 - Element Concentrations at the Coating Surface Revealed by X-Ray Scans at Position C on Creep Sample 38. Mag: 400X

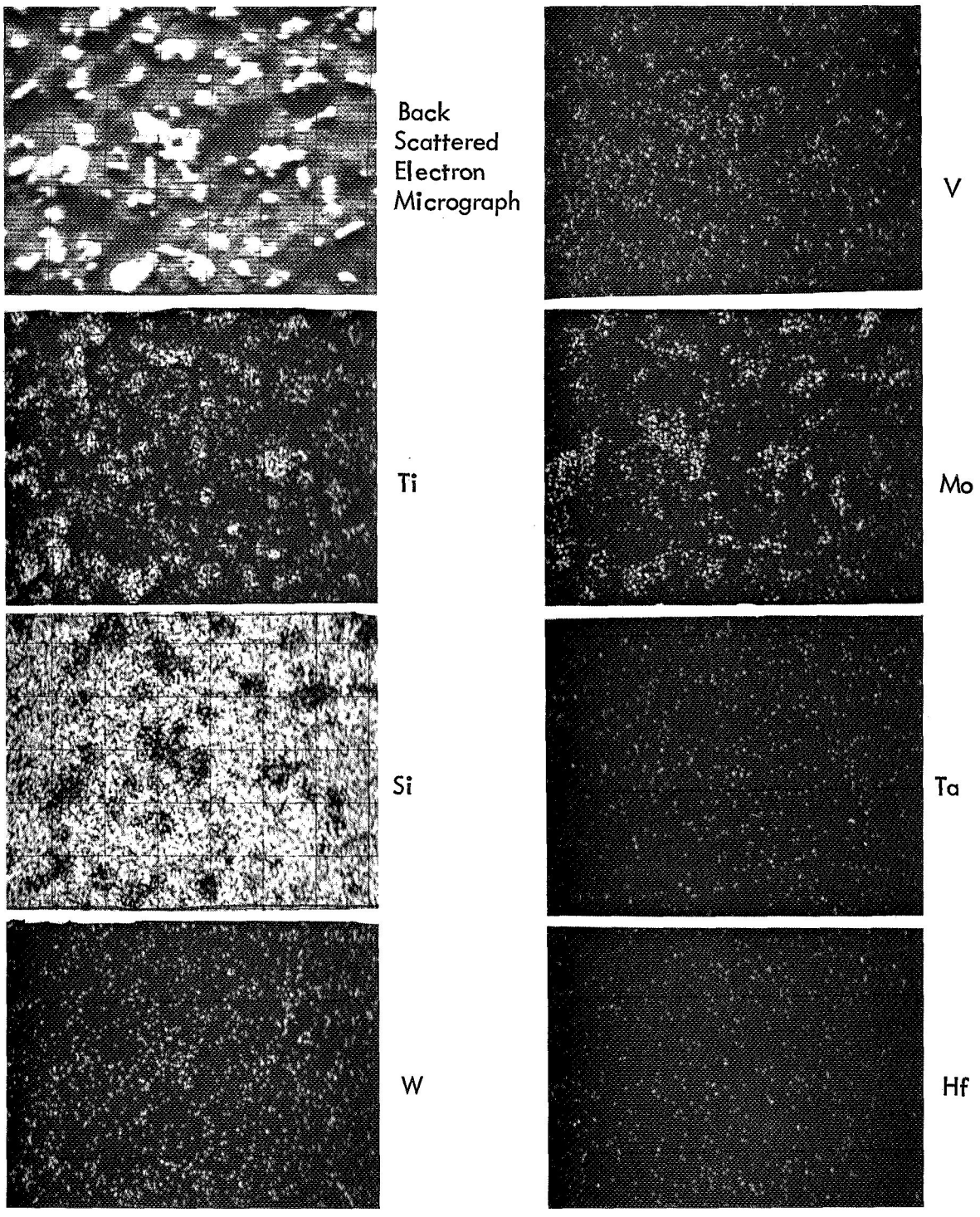

FIGURE 43 – Element Concentrations at the Coating Surface Revealed by X-Ray Scans at Position D on Creep Sample 38 Mag: 400X

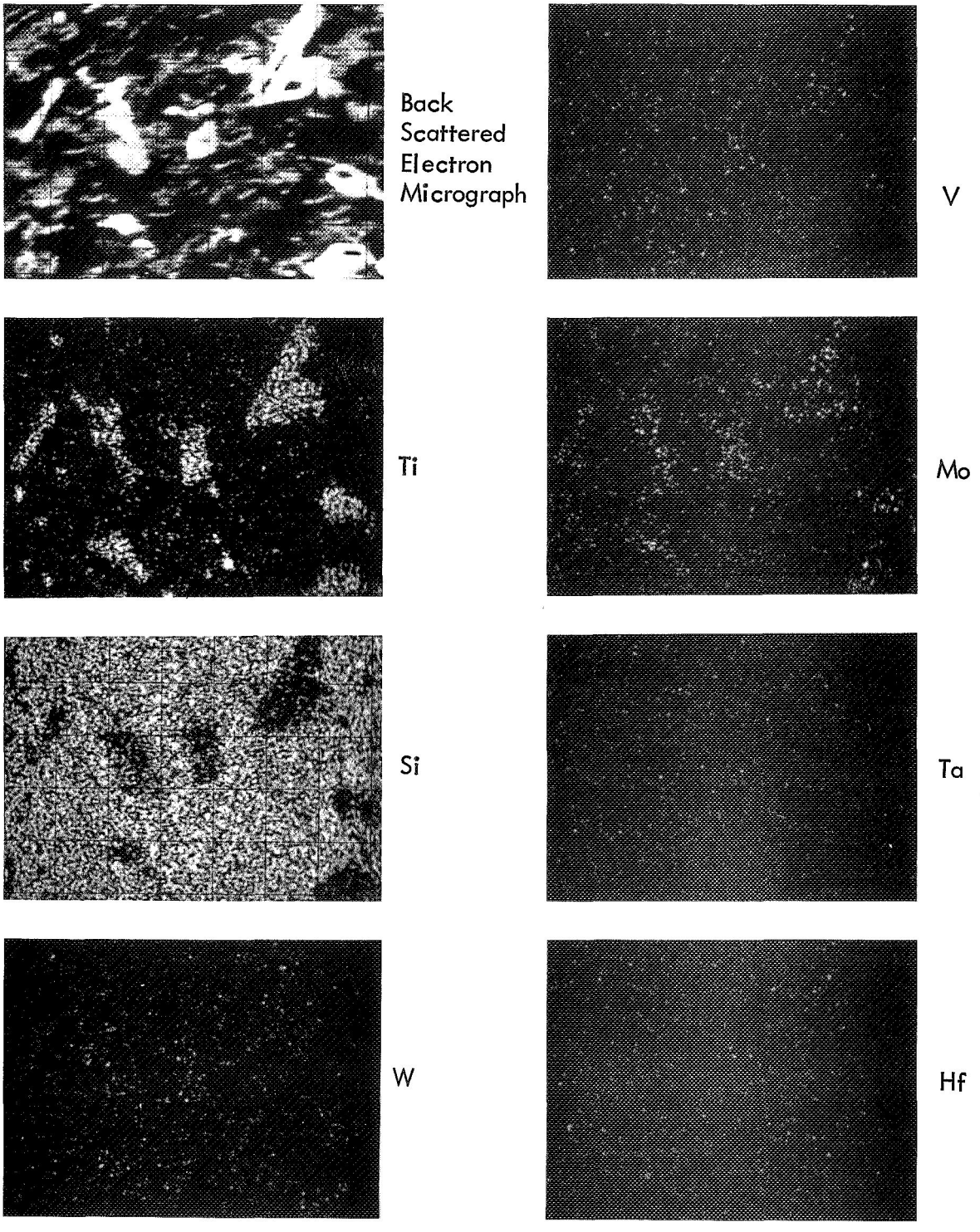

FIGURE 44 - Element Concentrations at the Coating Surface Revealed by X-Ray Scans at Position E on Creep Sample 38 Mag: 400X

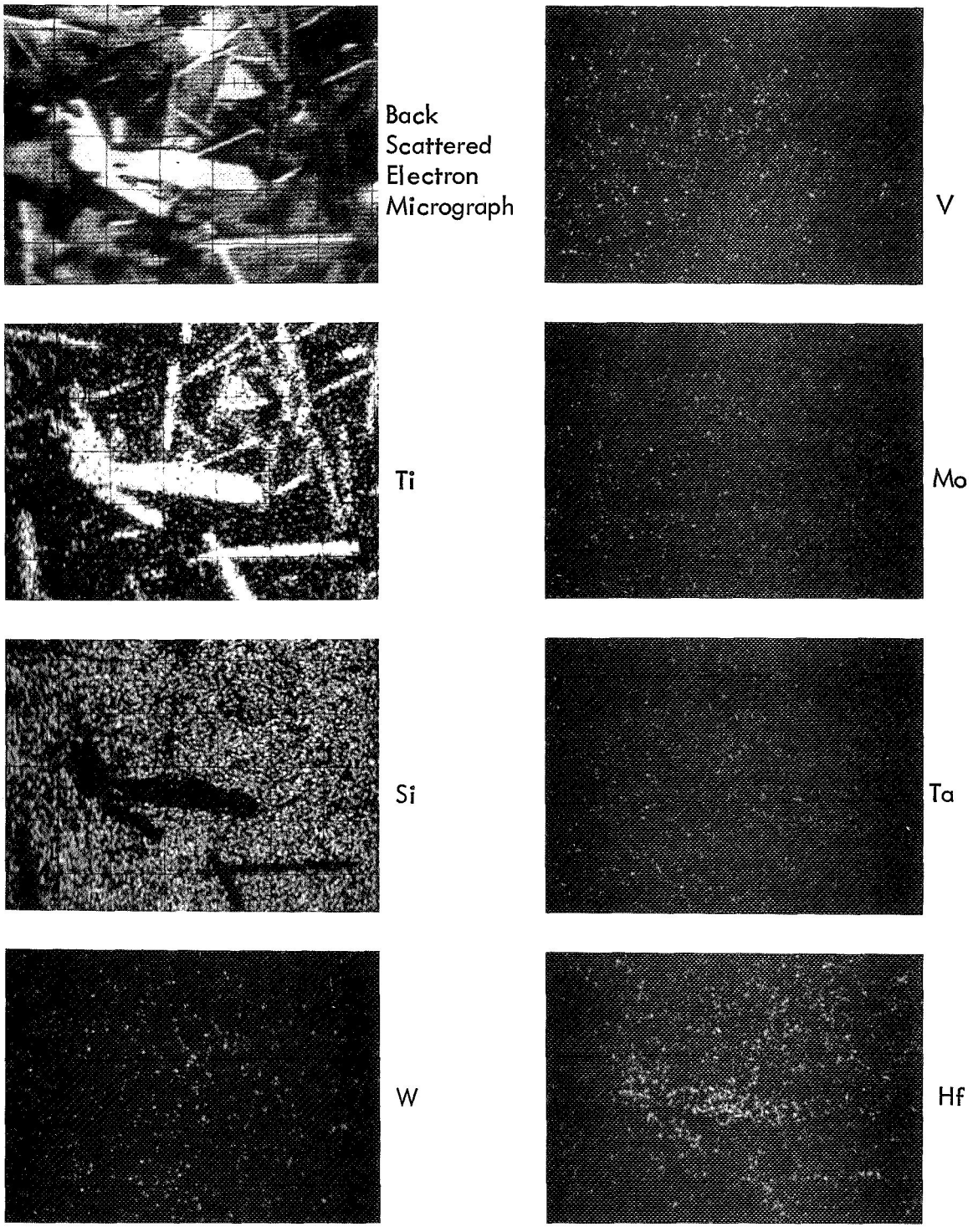

FIGURE 45 - Element Concentrations at the Coating Surface Revealed by X-Ray Scans at Position F on Creep Sample 38 Mag: 400X

been previously observed to be very susceptible to failure during the course of a creep test, or during oxidation tests at 1400° F or 2400° F. Observation of tantalum rich locales at the area examined within position C is, therefore, not surprising, and suggests formation of tantalum oxide at small sites of coating failure.

A small amount of hafnium was detected in a few of the large particles formed at the coating surface within position F. This position was exposed to 2100° F for the 500 hour test. Microprobe examination on the particle-in-matrix surface structure formed after 134 hours air exposure at 2400° F, did not uncover the presence of any hafnium — Figure 26. Furthermore, study of coating and substrate interdiffusion after air exposure for 437 hours at 2400° F, revealed no trace of hafnium to within about 0.005" of the coating surface — Figure 37. This information implies that hafnium diffusion from the T-222 substrate to the coating surface could not have occurred at position F, unless the coating was unusually thin at the locale examined or, perhaps hafnium was introduced to the coating as a process of material containment.

Results obtained from x-ray diffractometer analysis performed at the positions identified in Figure 39 are summarized in Table 16. The diffraction pattern intensity observed for a compound at a given position is compared in the table to the maximum intensity observed, which was given the value 100. Compound intensities were not corrected for absorption or reinforcement.

Tungstic Oxide, WO_3, was detected at positions B and C. As previously noted, coating failure on test samples was found to be particularly prevalent within the overall area bound by these regions. Because of this, and the previously noted presence of WO_3 at the surface of a coating which failed in a short time when exposure at 1400° F (Table 7), an association of the mechanism of coating failure during creep testing and failure during oxidation at 1400° F, is suggested. Creep sample 38, however, was exposed in air under a temperature gradient, unlike the samples oxidized at 1400° F where isothermal conditions were employed. As a consequence, detection of WO_3 at positions B and C might simply reflect deposition of the oxide volalitized in the process of oxidation at higher temperature regions of the sample. This point will be amplified in later text.

TABLE 16 - X-Ray Diffraction Analysis of the Coating Surface On Creep Sample 38

Location from Sample End (inches)	Temperature (°F)	Compounds Present and Their Relative Intensity[2]					
		$[(Ti,V)_x(W,Mo)_{1-x}]Si_2$	$(W,Mo)Si_2$	TiO_2	WO_3	SiO_2(C)	SiO_2(T)
.84 (A)[1]	T < 1000	72	65	0	0	7	0
1.10 (B)	T < 1000; T > at .84"	39	18	5	100	7	0
1.40 (C)	T < 1000; T > at 1.1"	100	40	7	16	44	0
1.50	1070	--	--	--	-	-	-
1.84 (D)	1760	33	95	8	0	56	0
2.08 (E)	1920	28	100	10	0	84	0
2.70 (F)	2100	17	70	58	0	89	100
3.20 (G)	2380	0	60	73	0	77	45
3.70 (H)	2400	0	50	100	0	100	0

(1) Positions identified in Figure 39.

(2) Comparison of diffractometer pattern strength at the location to the maximum strength observed at a location, uncorrected for absorbtion or reinforcement.

SiO_2 (C) = Crystobalite

SiO_2 (T) = Trydimite

The x-ray diffraction results indicate increased exposure temperature promotes titanium oxide and silica formation, suggesting that these compounds are the principal particle and matrix phases revealed by the microstructure and microprobe examinations. Formation of silica at position C is initially surprising since the sample temperature in this vicinity was only approximately 1000° F, and silica was not detected at the coating surface of a sample after air exposure for 2 hours at 1400° F (Table 7). The condition at position C, however, represents 500 hours time-at-temperature, apparently enough time for a large amount of silica to form.

The complex disilicides characteristic of the as-applied coating were also detected by x-ray analysis. This does not contradict the microprobe data which showed little, if any, vanadium, tungsten or molybdenum present at positions exposed to higher than about 1000° F. Instead, this principally reflects the deeper penetration of x-radiation used for diffraction analysis as compared to that of the electron beam used on the microprobe, the x-rays easily penetrating beneath the silica surface to detect the compounds present in the coating reservoir. Of course, observation by microprobe analysis of particles containing both titanium and silicon at position F, Figure 45, may be an indication that some $\left[(Ti, V)_x (W, Mo)_{1-x}\right] Si_2$ is still present at the coating surface. The failure to detect vanadium, molybdenum, or tungsten in this phase, however, contradicts this conclusion, although their concentrations could be below the detectability limits of the microprobe. On the other hand, the titanium and silicon rich phase could be a titanium silicide. Many of the diffraction lines for the silicides of titanium coincide with those for the complex silicides characteristic of the coating, making it difficult to distinguish between these possibilities.

Creep sample 38 was also sectioned and prepared metallographically to view the cross section along the specimen axis between points 0.75" to 2.75" from the end. This permitted coating and substrate thickness, structure, and interaction, to be evaluated over air exposure conditions representing 500 hours at temperatures from below 1000° F to 2100° F. Specific study was made at sample positions A through F — refer to Figure 39.

The results of microstructure, thickness measurements, and hardness, made at these sample positions, are displayed in Figures 46 through 51. Small hardness impressions apparent in the view showing total cross section at each sample position are fiducial marks made to assist location for metallography.

Comparison of total thickness measured at each position reveals position A to be roughly 0.005 inch thinner than the others — Figure 46. Close examination of the mirror image of position A at the other end of creep sample 38, showed the coating at this position to also be noticeably thinner than elsewhere. Other coated samples creep tested on the program were similarly examined and found thin at this region. Total thickness measured at position B was also slightly lower than elsewhere — Figure 47.

Cracks running parallel to the surface are apparent in the outer portion of the metallic-intermetallic reservoir at position A. Cracking is also apparent at position B, but to a much lesser degree than at A - Figure 47. This appears to imply that the coating was not deposited thin in this vicinity of the sample but, instead, was thinned by a process which caused spalling.

Tungsten oxide was found on the coating surface at positions B and C where the coating cross section was relatively sound, but not at position A- Table 16. If this compound were associated with a "pest" disintegration mechanism, it would be logical to expect to detect it at position A where cracking and spalling of the coating occurred. It follows that the compound was likely deposited from vapor, not formed where detected.

X-ray diffraction analysis was performed on material easily removed by scraping the coating at the mirror image of position A on the opposite end of the sample, Chemical change associated with the spalling process was not revealed by the results, which proved identical, in all respects, to that observed for the metallic-intermetallic reservoir of an as-coated sample. An explanation for cracking and spalling of the coating at position A, therefore, was not obtained.

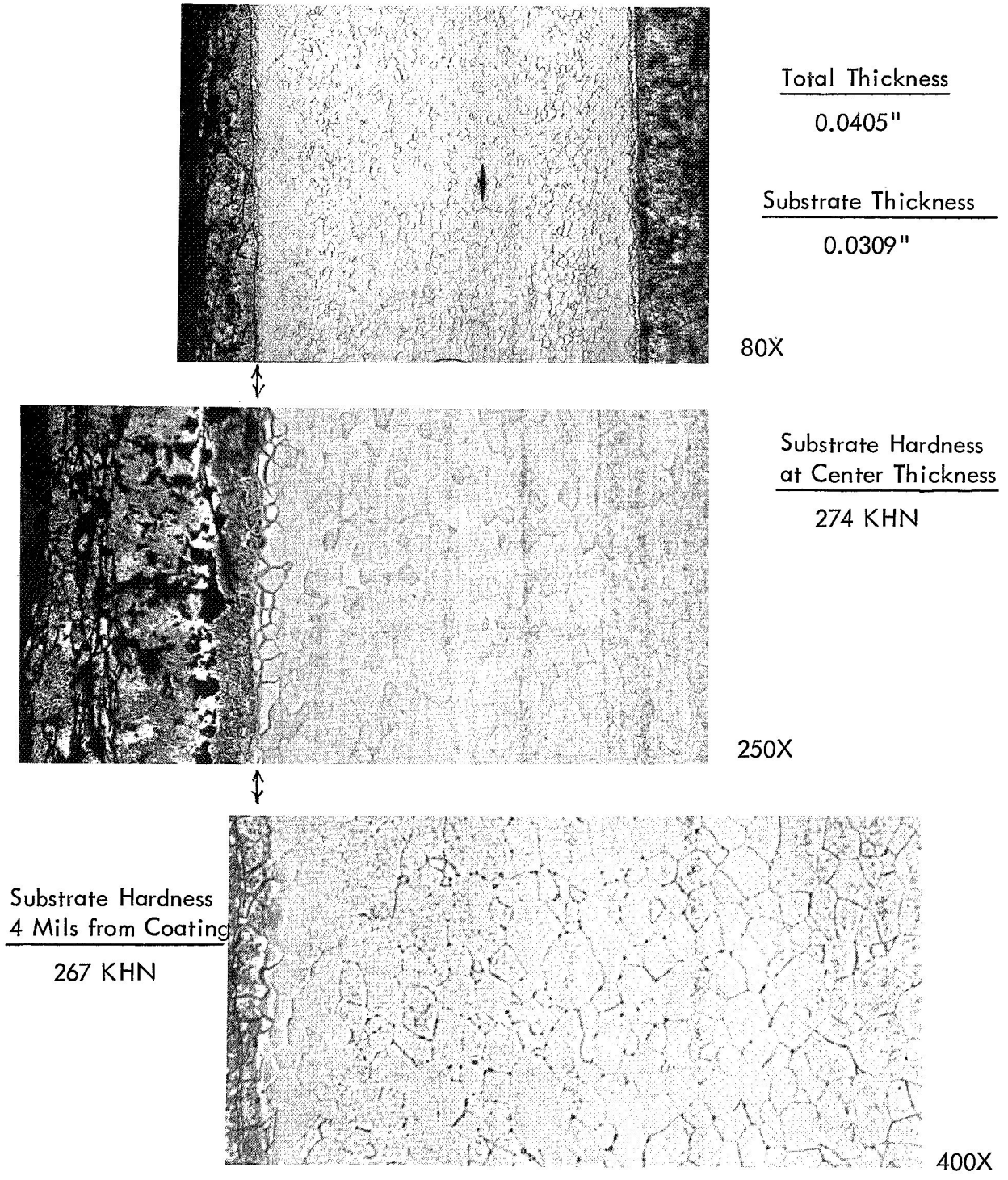

FIGURE 46 - Coating and Substrate Structure at Position A on Creep Sample 38.
Refer To Figure 39

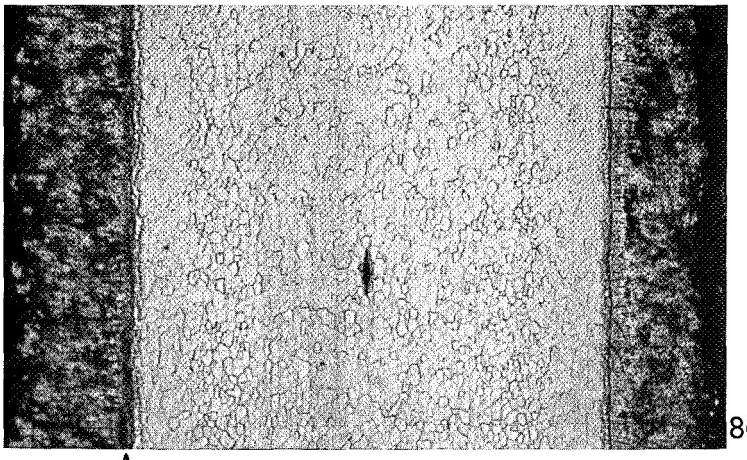

Total Thickness

0.0450"

Substrate Thickness

0.0309"

80X

Substrate Hardness at Center Thickness

260 KHN

250X

Substrate Hardness 4 Mils from Coating

258 KHN

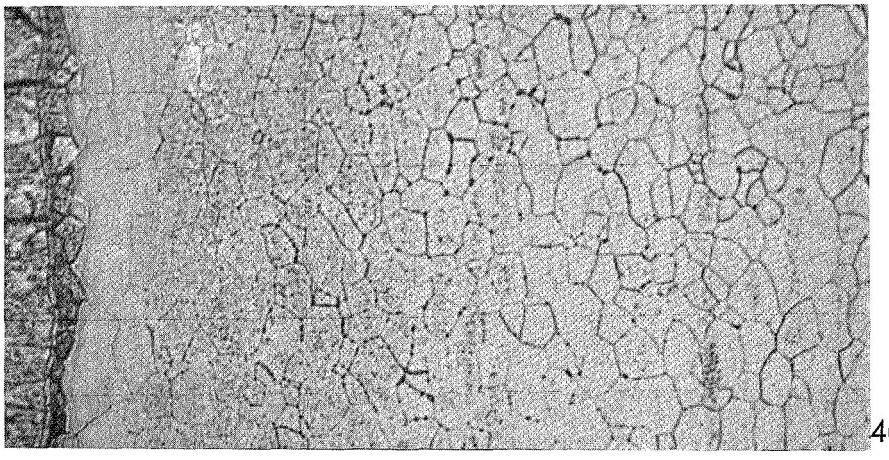

400X

FIGURE 47 - Coating and Substrate Structure at Position B on Creep Sample 38
Refer to Figure 39

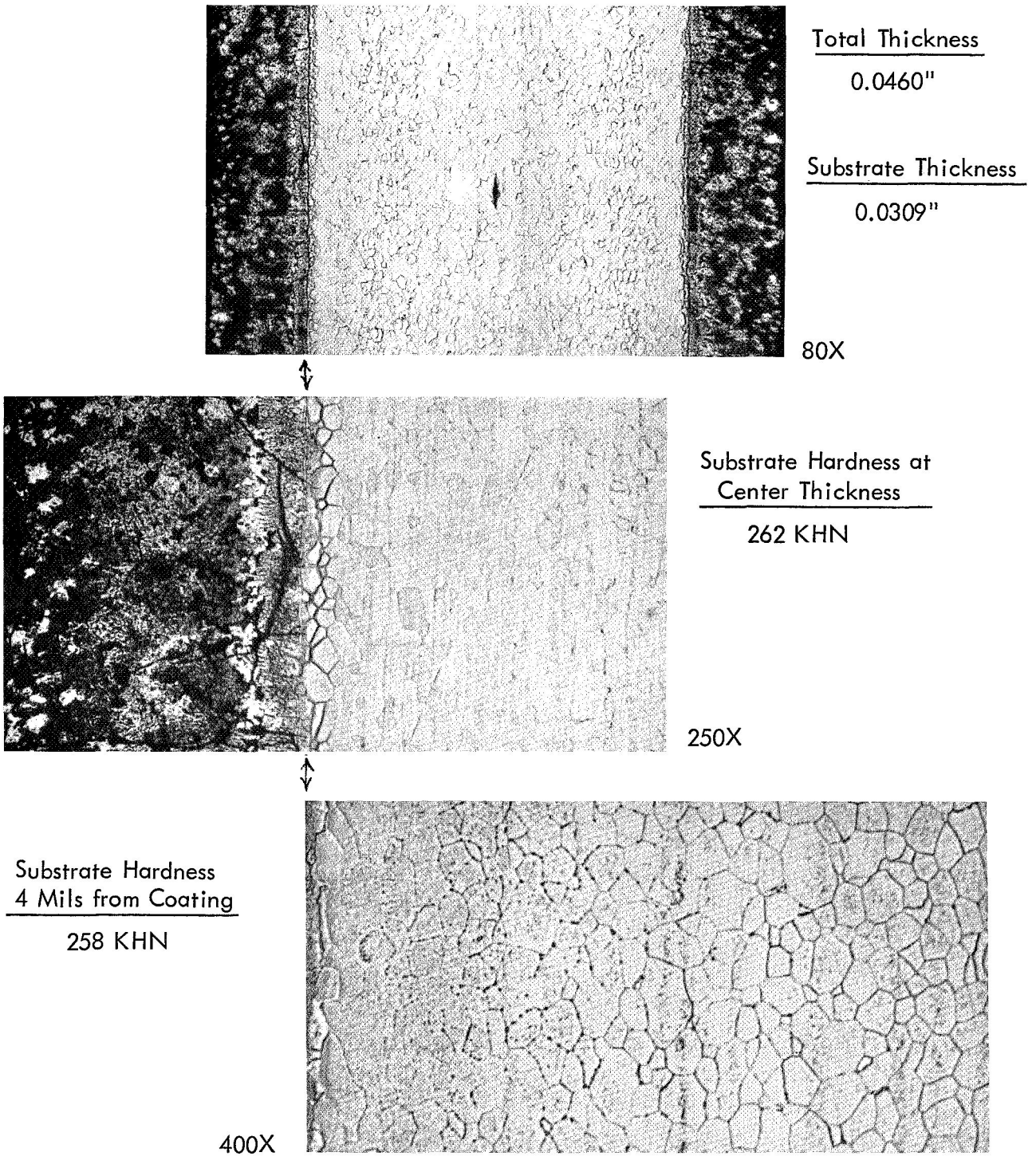

FIGURE 48 - Coating and Substrate Structure at Position C on Creep Sample 38
Refer to Figure 39

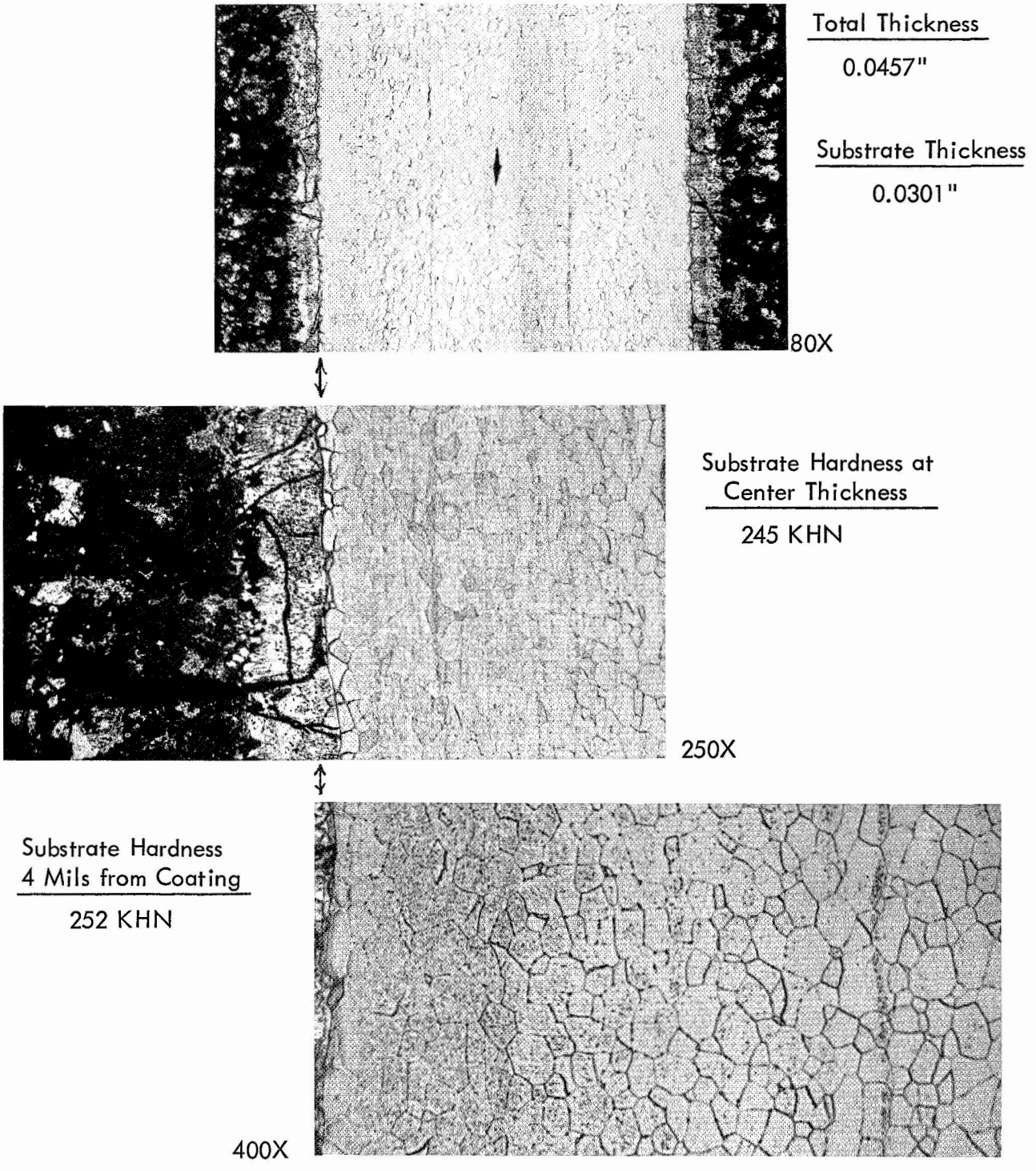

FIGURE 49 - Coating and Substrate Structure at Position D on Creep Sample 38
Refer to Figure 39

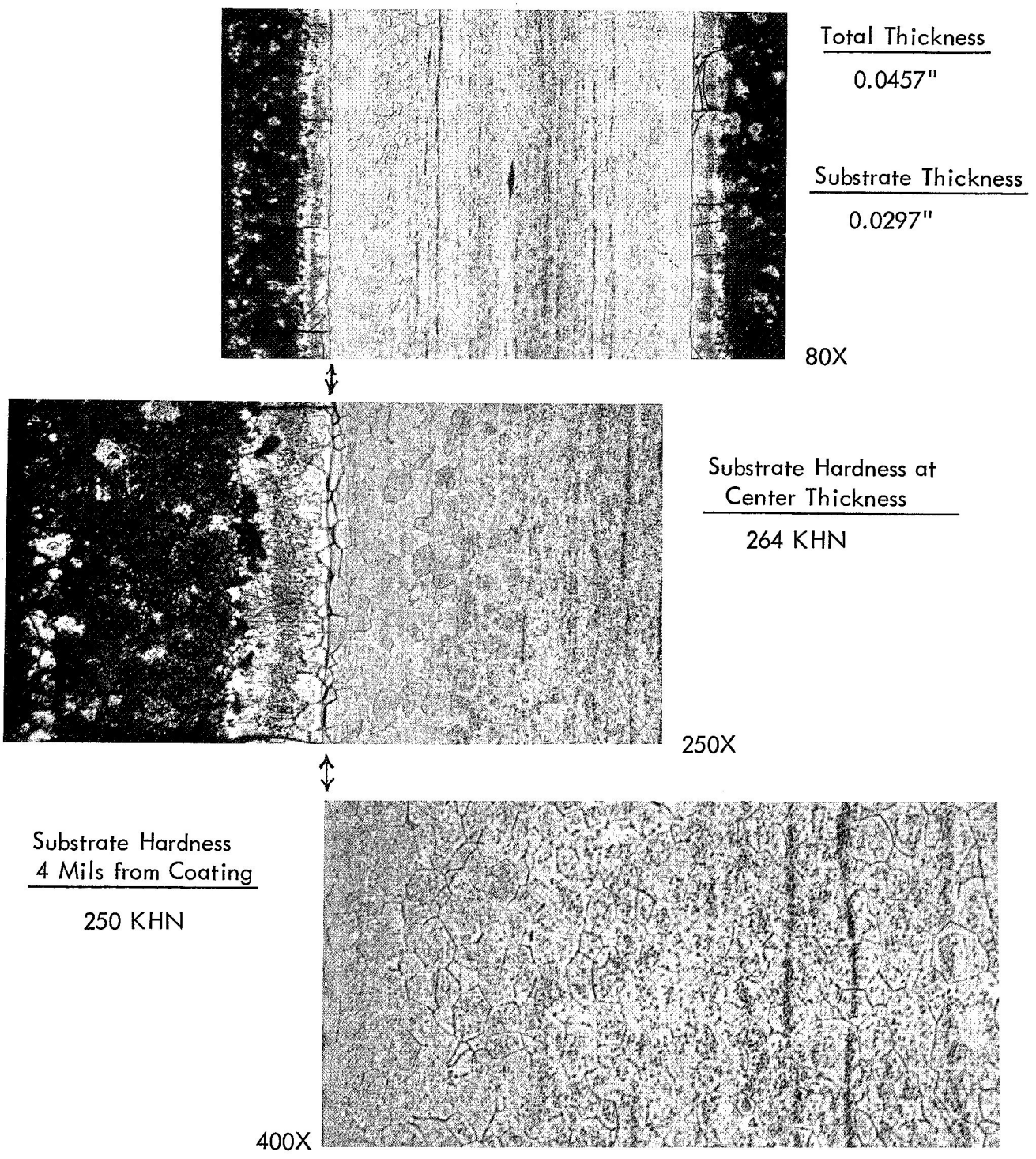

FIGURE 50 - Coating and Substrate Structure at Position E on Creep Sample 38
Refer to Figure 39

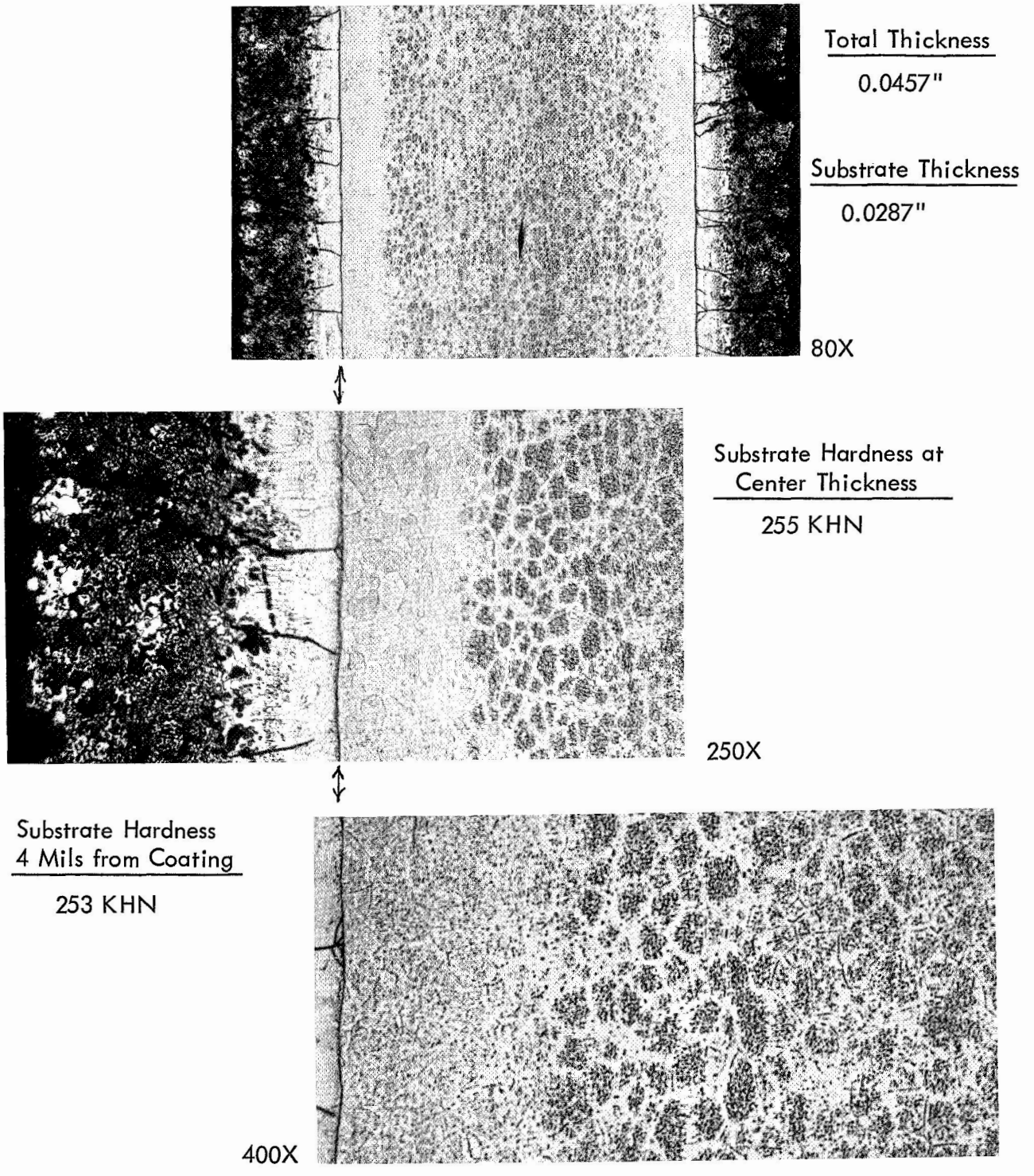

FIGURE 51 - Coating and Substrate Structure at Position F on Creep Sample 38
Refer to Figure 39

Substrate thickness measurements displayed in Figures 46 through 51 show a progressive increase in degree of coating-substrate interaction for positions D through F. On the other hand, little change in substrate thickness from that of the as-coated condition developed due to the exposure conditions imposed at positions A through C, as judged from the constant substrate measurement observed at these points. Comparison of the substrate dimension at these locations, 0.0309", with the sample thickness before coating which was 0.0314", yields a 0.0005" recession due to coating. Total substrate recession of 0.0008" was measured from an as-coated sample — Figure 33. The difference in these recession values probably reflects the inaccuracy of determining a change small enough to be within the range of error associated with the measured quantities.

Substrate recession measured as a function of temperature from sample 38, is plotted in Arrhenius form in Figure 52. The points for 1760° F, 1920° F and 2100° F represent measurements made at sample positions D, E and F — Figures 49 to 51. Points representing lower temperatures were obtained by substrate measurement at locations between positions C and D where temperature was accurately known. Examination of substrate recession on sample 38 was not made at temperature locations beyond position F, 2100° F. The slope of the high temperature position of the curve of recession vs. temperature presented in Figure 52, however, was guided by recession measured after 437 hours at 2400° F, 0.0045" — Figure 33. This part of the curve was drawn to intersect 2400° F* at a value of substrate recession of 0.0050", compensating for the longer, 500 hour, exposure time of sample 38.

An increase of coating-substrate reaction rate with increased temperature, occurring at approximately 1600° F, is apparent from the data presented in Figure 52. The change to a greater rate is coincident, therefore, with temperature below which the coating displayed erratic protective behavior. Perhaps increased coating-substrate interaction, i.e., major development of a metallic diffusion zone, and improved substrate protection against oxidation, are somewhat associated, although admittedly improved protectiveness is more likely a result of rapid silica formation on the coating at higher temperatures.

*$1/R^{\circ} \times 10^{-4} = 3.5$

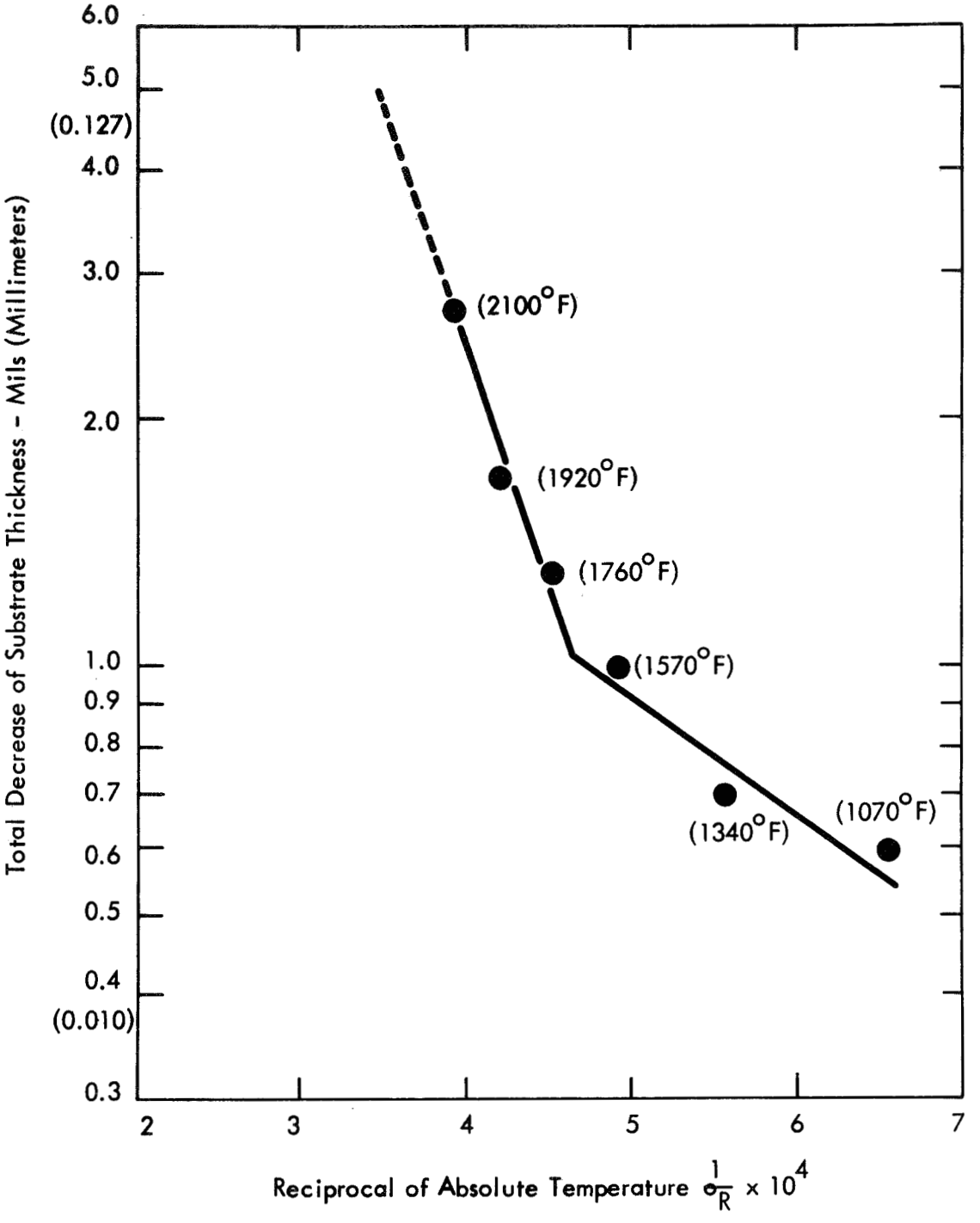

FIGURE 52 - Substrate Recession as a Function of 500 Hour Oxidation Temperature Creep Sample 38

Hardness measurements made in the substrate at positions A through F, reported in Figures 46 through 51, show a close correspondence of hardness level near the coating-substrate interface and at center thickness. Furthermore, the level of hardness measured at these positions compares well with that determined from samples air exposed for various times at 2400° F, and generally concluded to be free of serious interstitial element contamination (Table 15), although as previously mentioned different contaminants change hardness in opposite directions.

An increase in the amount of precipitation in the T-222 substrate with higher exposure temperatures is obvious from the photomicrographs shown in Figures 49 through 51. Assuming major contamination not to be present, this simply reflects thermally induced precipitation and growth of carbide particles stable in the alloy at the represented conditions.

Photomicrographs showing the coating cross section at positions A, B, C, E, and F, identified in Figure 39, are presented at 500X magnification in Figures 53 through 57. Coating locations representing single or multiphase areas in the metallic-intermetallic reservoir, and in some cases the primary oxide barrier, are identified in the photomicrographs, and results of microprobe analysis performed at these locations are given below each picture. Microprobed data was obtained for major coating and substrate elements, and are reported as a ratio of detected element intensity to intensity from a pure standard. As previously mentioned in discussions of similar microprobe information (Figures 35 - 37), use of this data to indicate weight percent of an element would meet with several serious criticisms.

Close examination of each photomicrograph reveals that a continuous primary oxide barrier was developed at positions C, E and F. Microprobe examination at locations within the primary barriers detected primarily silicon, which, along with the results of x-ray diffraction (Table 16), indicates the layers consist principally of silica. Detection of some tungsten, titanium and vanadium at the primary barrier location examined for position C, and some tungsten at the spot surveyed for position E, is believed due to presence nearby of

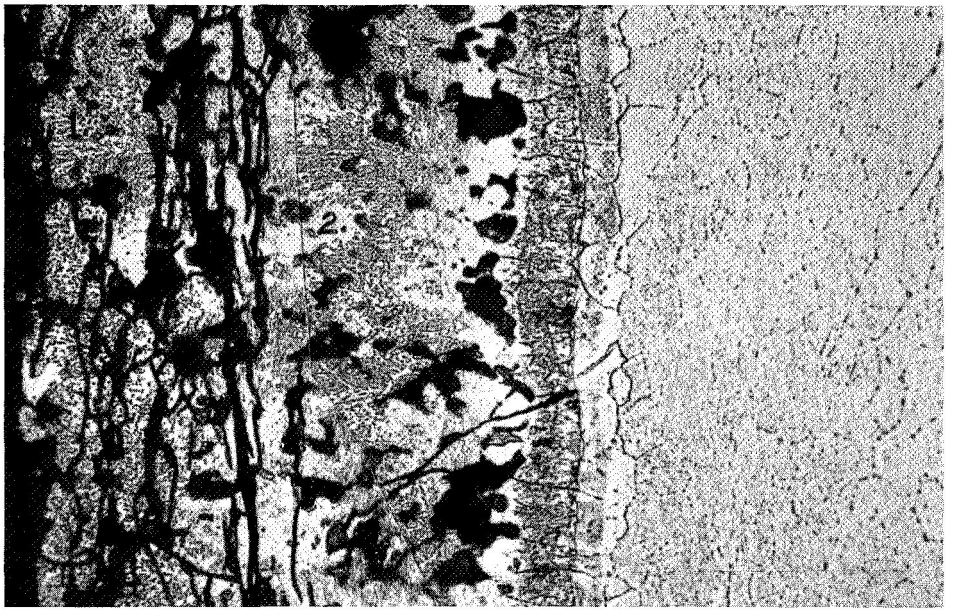

500X

RESULTS

Location	No. of Phases	Ratio of Characteristic X-Radiation $\frac{I\ element}{I\ standard} \times 100$						
		Si	Mo	W	Ti	V	Ta	Hf
1	2 or more	17	0	35	3	7	0	0
2	1	37	9	23	4	9	0	0

FIGURE 53 - Microprobe Analysis of Phases Observed in the Coating at Position A on Creep Sample 38. Refer to Figure 39.

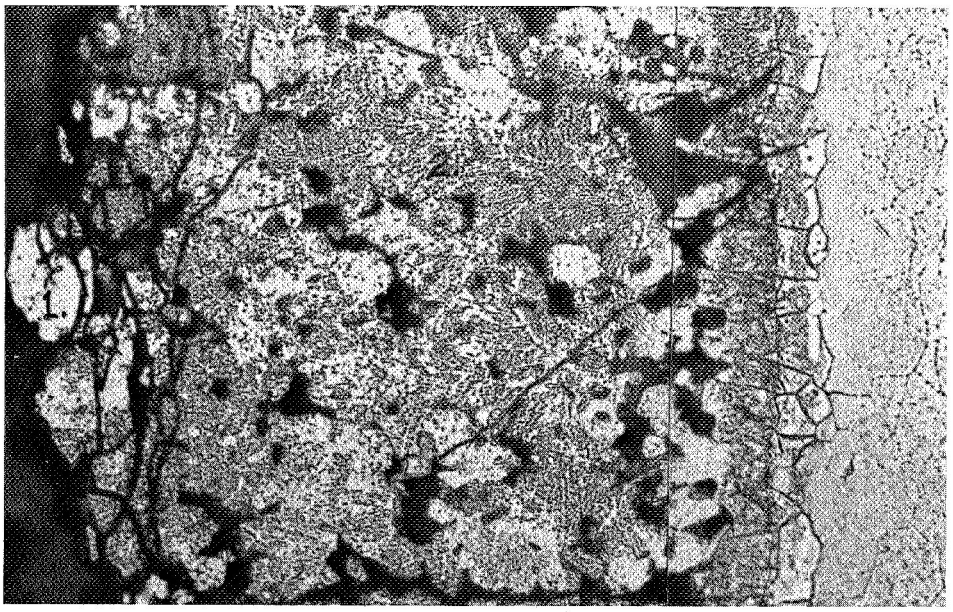

500X

RESULTS

Location	No. of Phases	Ratio of Characteristic X-Radiation $\frac{I\ element}{I\ standard} \times 100$						
		Si	Mo	W	Ti	V	Ta	Hf
1	1	32	15	6	5	7	0	0
2	2 or more	28	5	25	4	6	0	0

FIGURE 54 - Microprobe Analysis of Phases Observed in the Coating at Position B on Creep Sample 38. Refer to Figure 39.

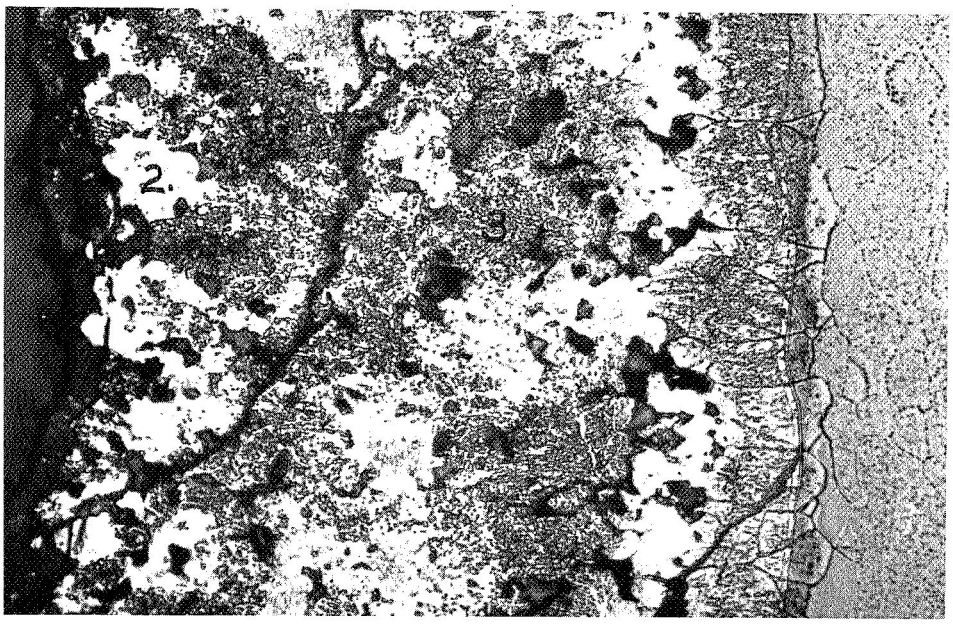

500X

RESULTS

Location	No. of Phases	Ratio of Characteristic X-Radiation $\frac{I\ element}{I\ standard} \times 100$						
		Si	Mo	W	Ti	V	Ta	Hf
1	1	25	0	14	4	5	0	0
2	1	18	10	5	4	8	0	0
3	2 or more	33	5	30	3	9	0	0

FIGURE 55 - Microprobe Analysis of Phases Observed in the Coating at Position C on Creep Sample 38. Refer to Figure 39.

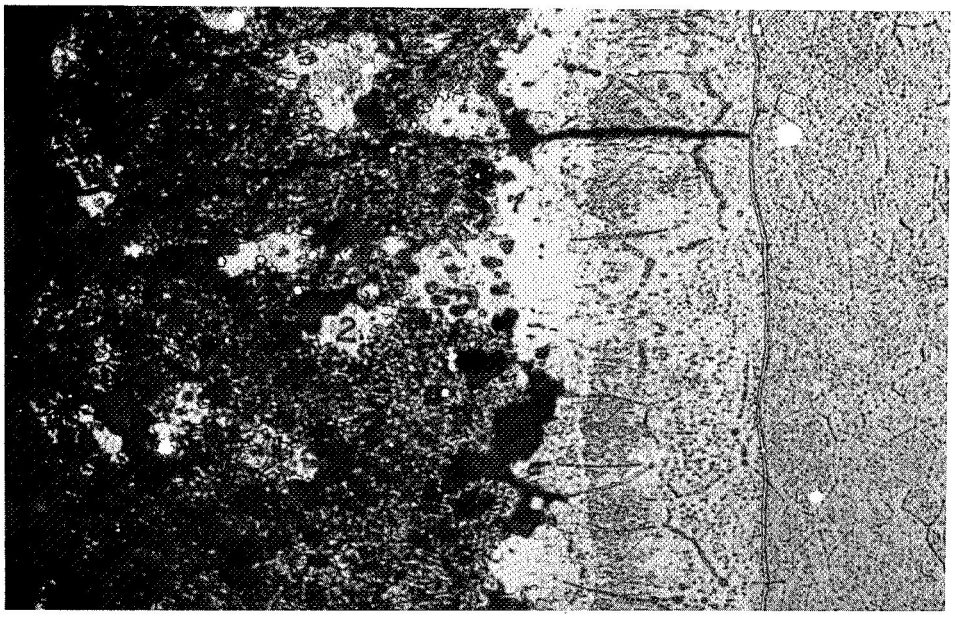

500X

RESULTS

Location	No. of Phases	Ratio of Characteristic X-Radiation $\frac{I\ element}{I\ standard} \times 100$						
		Si	Mo	W	Ti	V	Ta	Hf
1	1	19	0	4	0	0	0	0
2	1	20	12	17	3	12	0	0
3	2 or more	17	9	28	0	3	0	0

FIGURE 56 - Microprobe Analysis of Phases Observed in the Coating at Position E on Creep Sample 38. Refer to Figure 39.

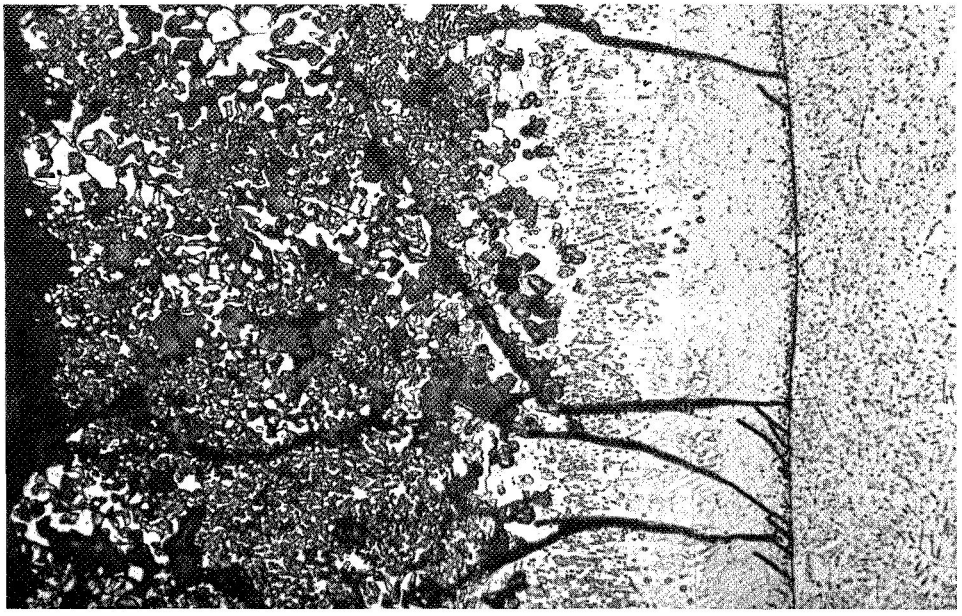

500X

RESULTS

Location	No. of Phases	Ratio of Characteristic X-Radiation $\frac{I\ element}{I\ standard} \times 100$						
		Si	Mo	W	Ti	V	Ta	Hf
1	1	17	0	0	0	0	0	0
2	1	28	26	5	1	9	0	0
3	1	26	0	9	0	1	0	0
4	2 or more	13	5	33	2	5	0	0

FIGURE 57 - Microprobe Analysis of Phases Observed in the Coating at Position F on Creep Sample 38. Refer to Figure 39.

metallic-intermetallic reservoir phases. Some particles similar in appearance to those of the metallic-intermetallic reservoir can be seen in the region of primary barrier analyzed at position C.

Particles of a phase similar in appearance to the primary oxide barrier also formed within the metallic-intermetallic reservoir at positions C, E and F. Microprobe examination of one of these particles confirmed it as primary oxide — location 3, Figure 57. Oxide formation within cracks and voids developed in the metallic-intermetallic reservoir had been previously suggested in discussion of samples air exposed at 2400° F — Figures 23 and 24. This must be a major mechanism minimizing oxygen permeation through the coating.

Microprobe data obtained from individual phases common to the metallic-intermetallic reservoir reflect the overall isomorphous behavior of the coating elements. In this respect, distinction cannot be made between the results from single and multiphase areas.

Microprobe traces for major coating and substrate elements, taken across the coating cross section at positions A, B, C, E, and F, are presented in Figures 58 through 62. With exception of the elements titanium and vanadium at positions A, B and C, detection of coating elements in the T-222 substrate beyond its interface with the metallic diffusion zone, was not obtained. As previously noted, little development of the metallic diffusion zone beyond that formed during the coating process was effected by the exposure conditions at positions A, B and C. As a consequence, presence of titanium and vanadium a short distance into the substrate at these positions probably reflects a condition characteristic of the coating process.

Close examination of the substrate at positions A, B and C, in the vicinity of its interface with the metallic diffusion zone, reveals some structural evidence of reaction in the substrate beyond the boundary. Similar structural evidence of reaction in the substrate near the boundary made with the metallic diffusion zone is also apparent in Figure 35, where microprobe traces are presented for the as-coated condition.

Microprobe evidence of the small amount of coating-substrate interaction in this area was probably lost for this case by error associated with traces-to-structure matching, and translation of the data to reportable form.

The first thermal treatment performed during coating involves sintering the metallic coating constituents at 2800° F for 15 hours — Table 2. A likely result of this is interaction of the lower melting point constituents, titanium and vanadium, with the T-222 substrate. It appears the subsequent step converting the coating to the disilicide does not entirely eliminate the reactive metal-to-substrate reaction zone. Exposure to oxidation conditions where formation of a well developed metallic diffusion zone occurs seems to restrict coating elements to the structurally obvious region of interaction with the substrate— Figures 61 and 62.

Other interesting features revealed by the microprobe traces are the pronounced changes of hafnium content throughout the substrate regions examined, and a general decrease of metallic coating constituent level in the vicinity of the coating surface apparent at the higher temperature positions. The former observation is further confirmation that hafnium rich particles form the bulk of precipitation developed in the T-222 substrate.

Formation of a silica rich primary barrier by oxidation of the coating at the higher temperature positions is indicated by the decrease of metallic constituent concentration near the surface. As previously suggested, the elements tungsten, molybdenum and vanadium must be eliminated from the region by formation of their volatile oxides. Titanium, on the other hand, forms the TiO_2 platelets observed as part of the primary oxide barrier. Particles of TiO_2, known from surface studies to be present in the primary oxide barrier at the higher temperature positions, were not apparent at the cross sections inspected by microprobe traces, accounting for the apparent decrease in concentration of titanium in the vicinity of the coating surface. A particle or two of TiO_2 traversed by the microprobe beam in the primary oxide barrier might not result in a pronounced concentration peak in any case.

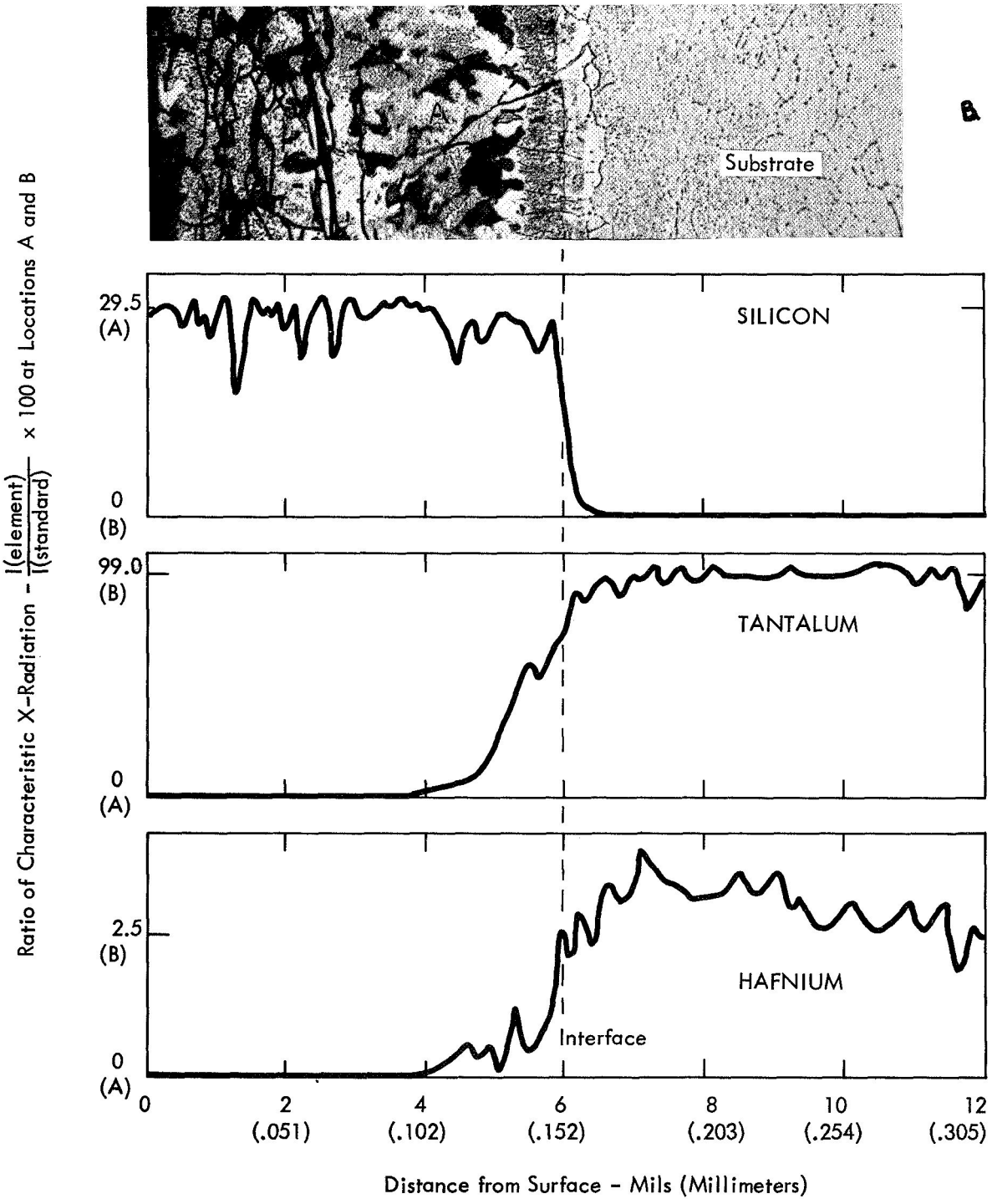

FIGURE 58 - Electron Microprobe Traverses at Position A on Creep Sample 38. Refer to Figure 39.

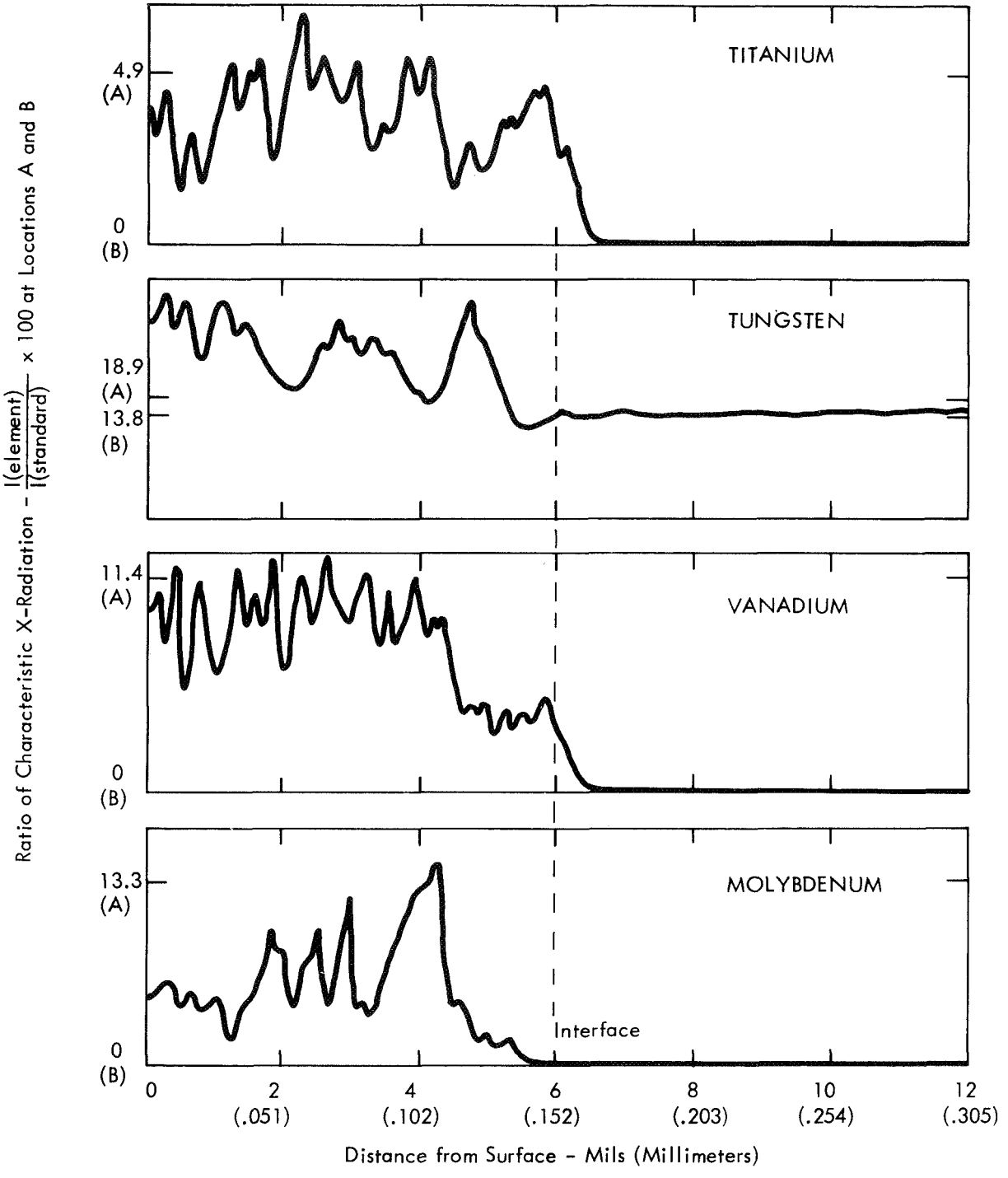

FIGURE 58 (Continued) - Electron Microprobe Traverses at Position A on Creep Sample 38. Refer to Figure 39.

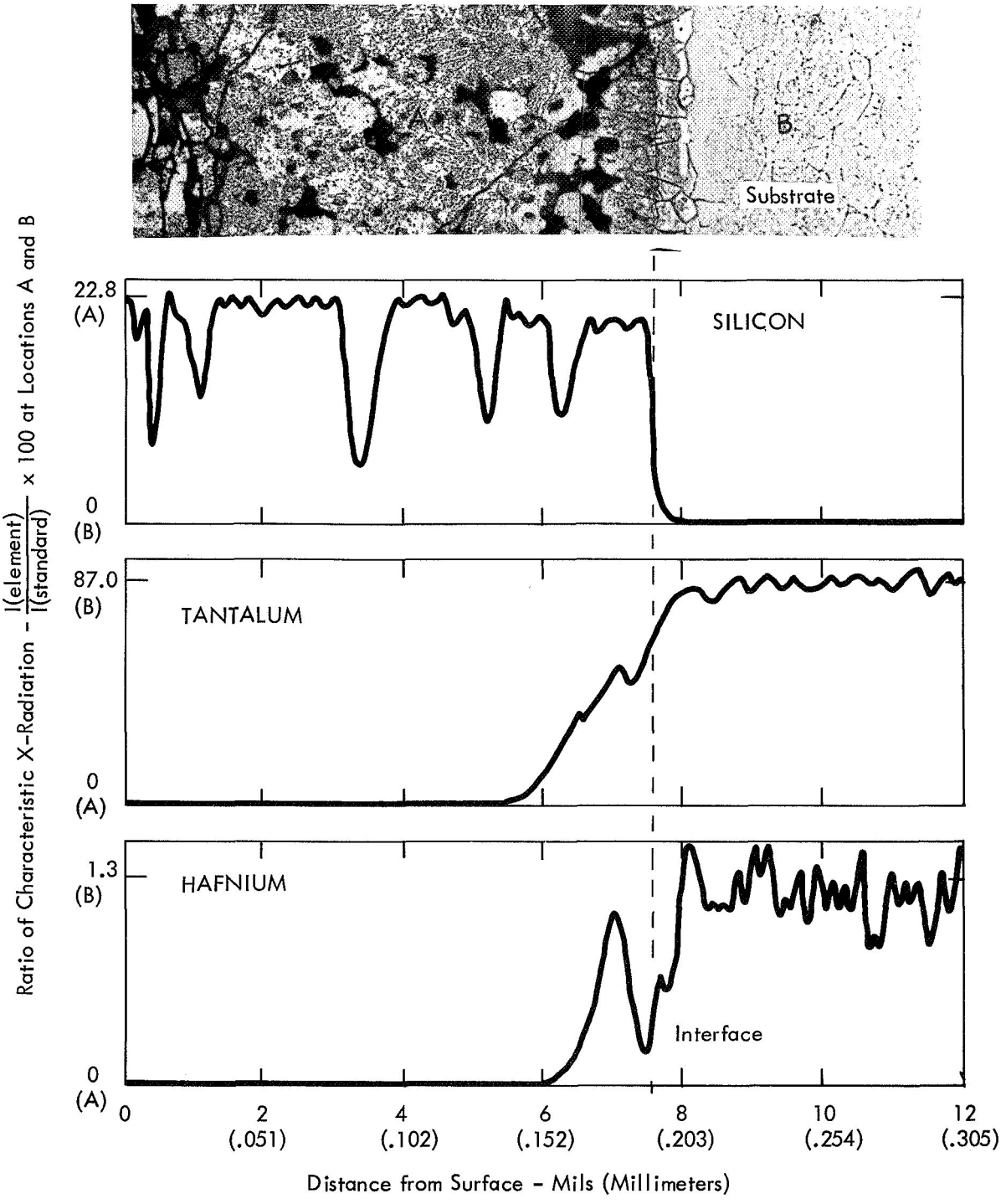

FIGURE 59 - Electron Microprobe Traverses at Position B on Creep Sample 38. Refer to Figure 39.

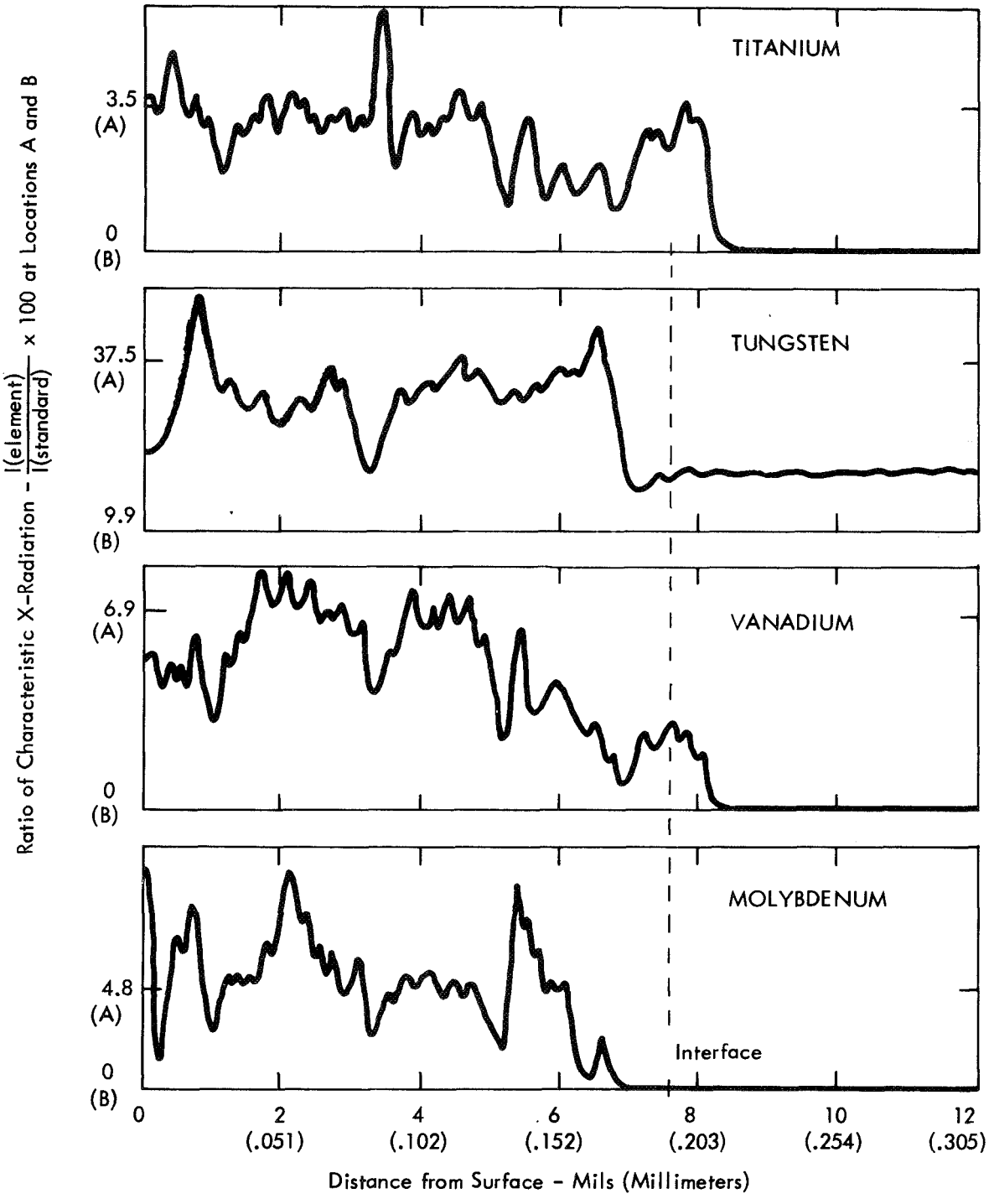

FIGURE 59 (Continued) - Electron Microprobe Traverses at Position B on Creep Sample 38. Refer to Figure 39.

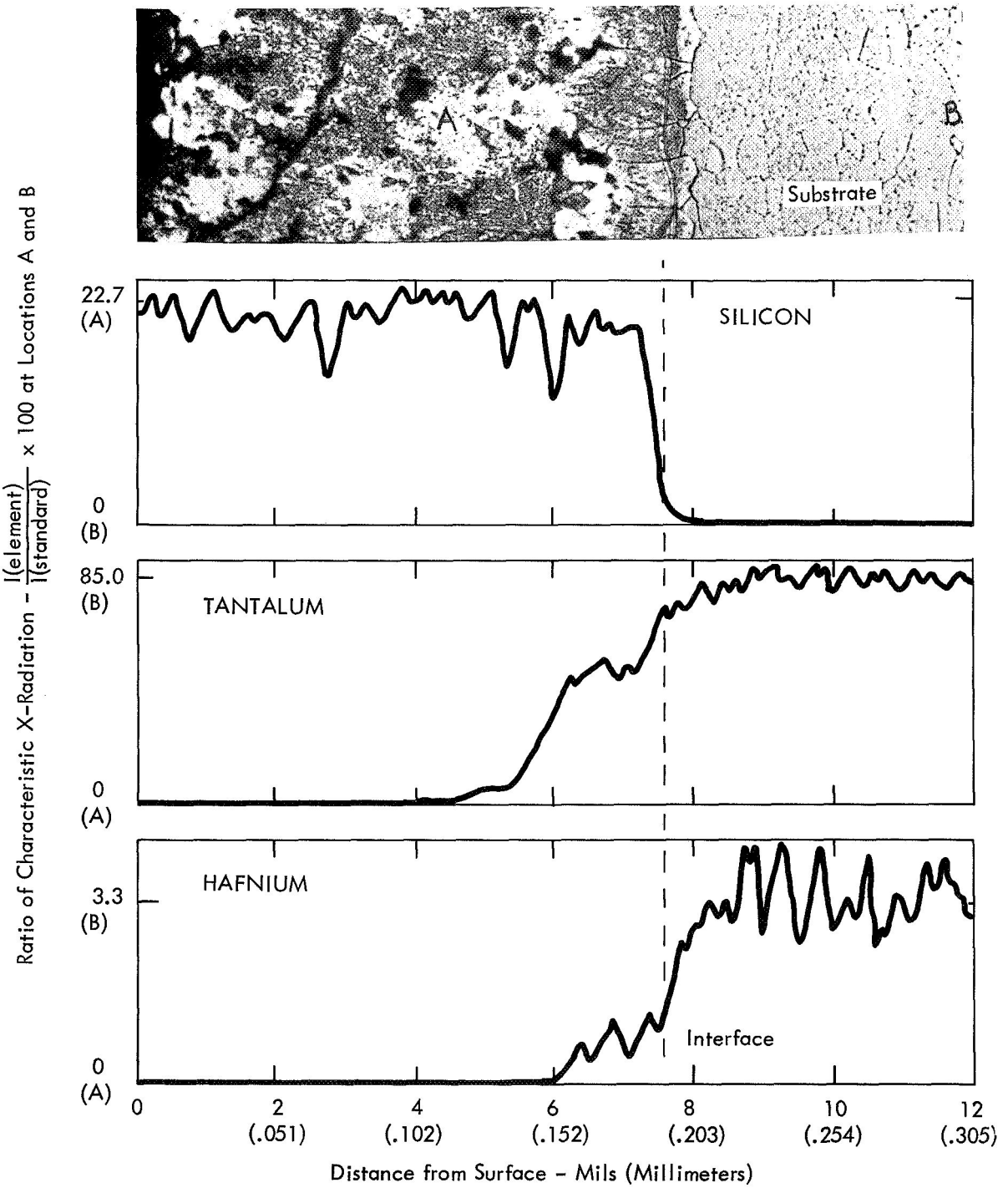

FIGURE 60 - Electron Microprobe Traverses at Position C on Creep Sample 38. Refer to Figure 39.

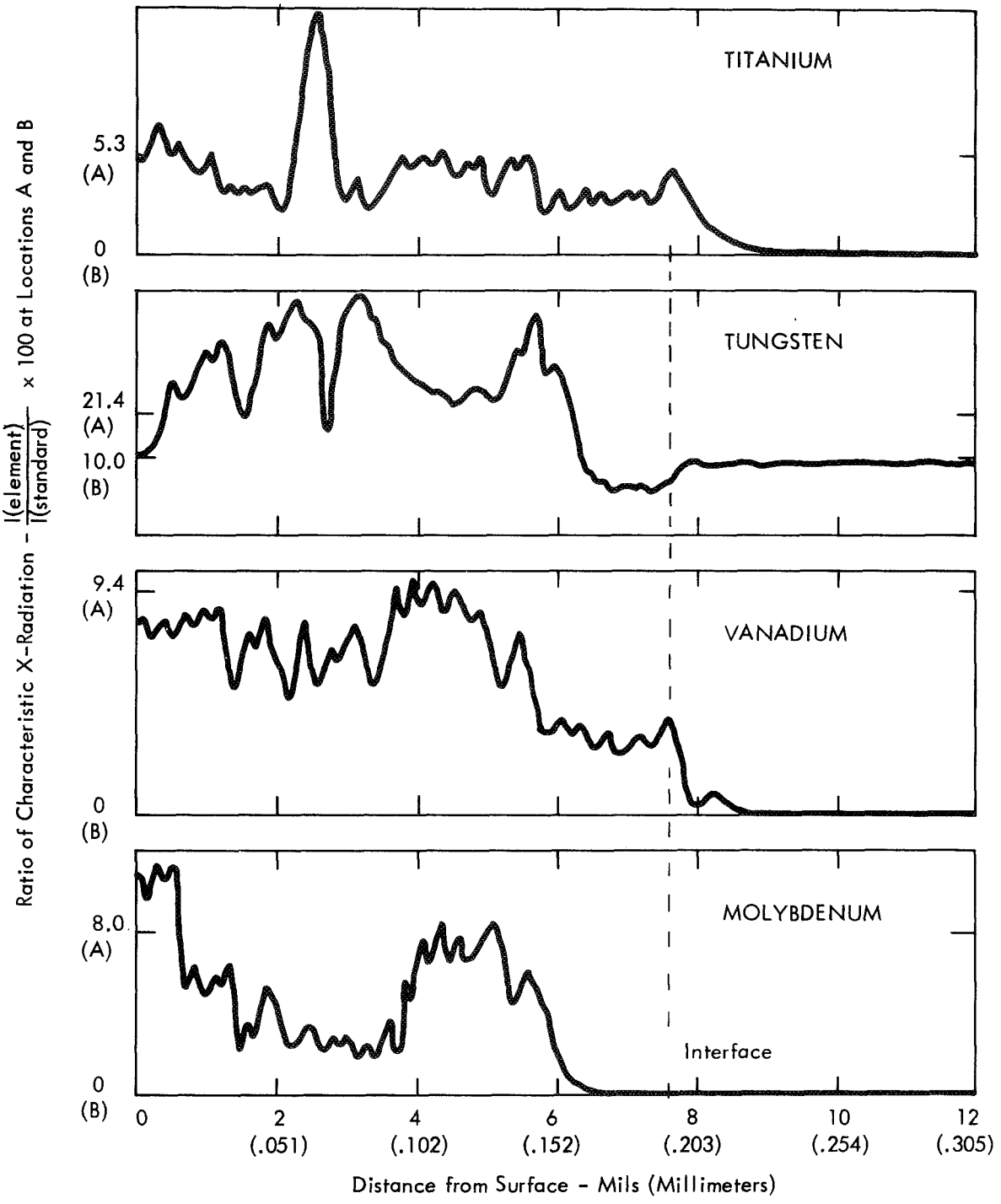

FIGURE 60 (Continued) - Electron Microprobe Traverses at Position C on Creep Sample 38. Refer to Figure 39.

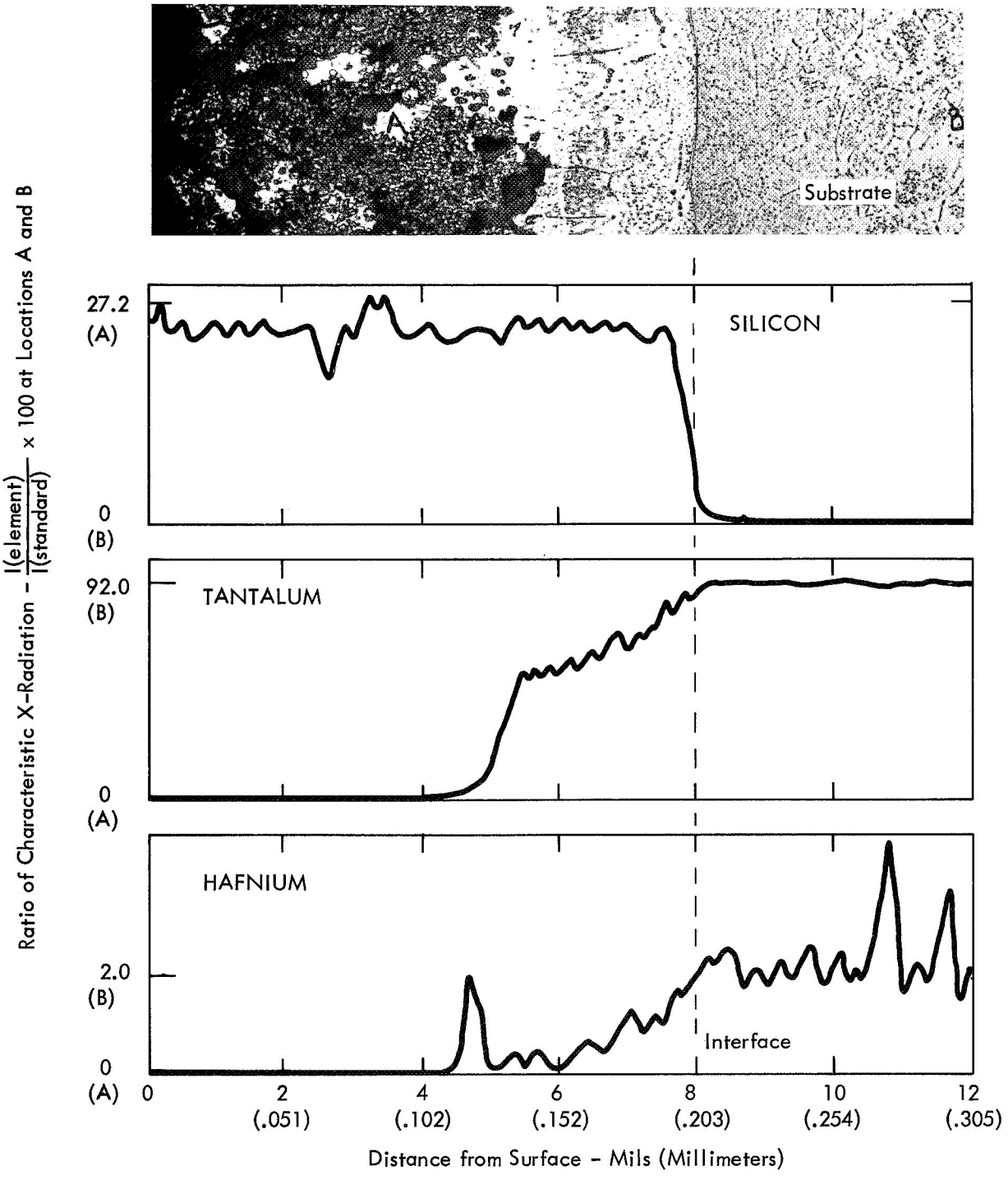

FIGURE 61 - Electron Microprobe Traverses at Position E on Creep Sample 38. Refer to Figure 39.

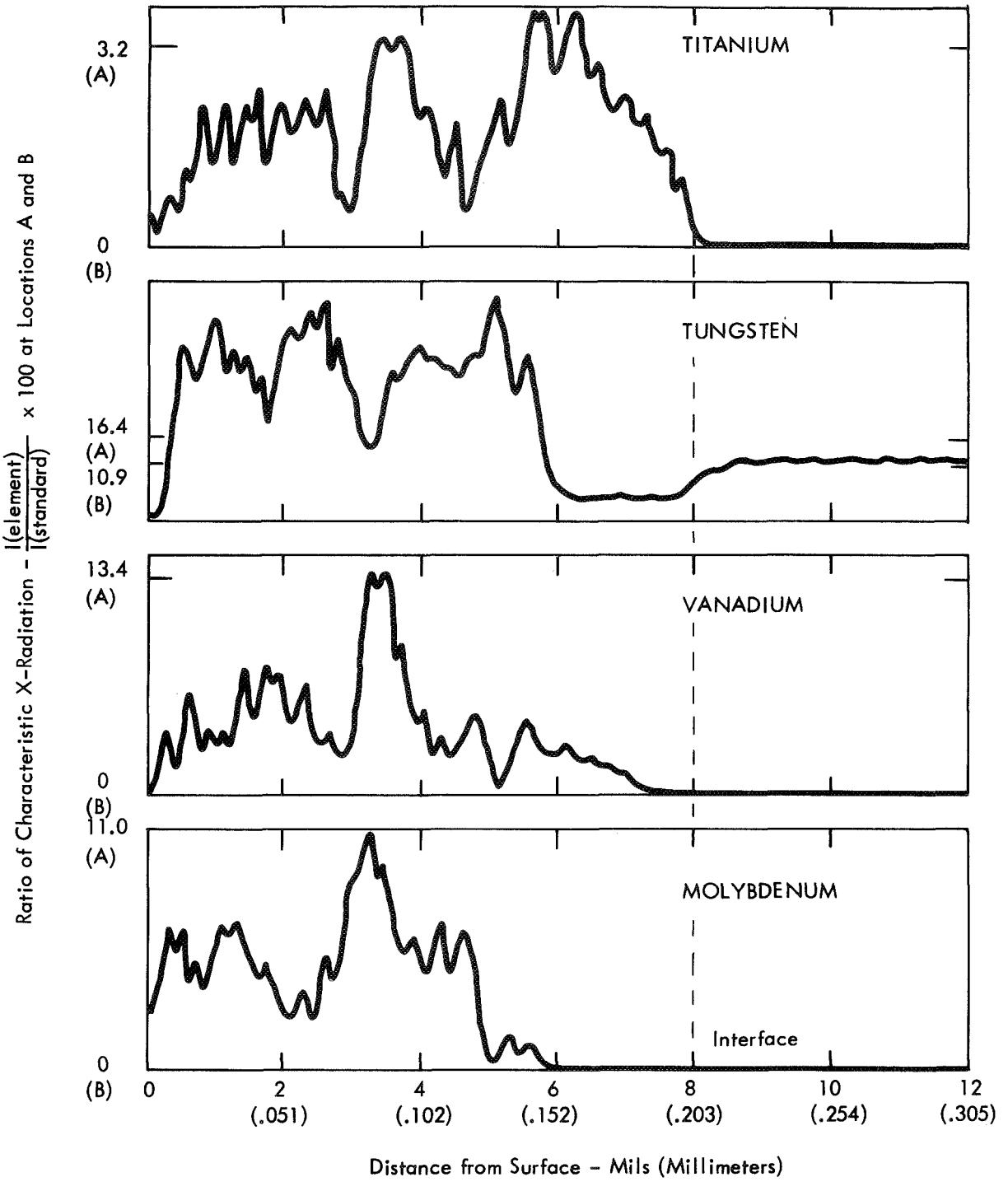

FIGURE 61 (Continued) - Electron Microprobe Traverses at Position E on Creep Sample 38. Refer to Figure 39.

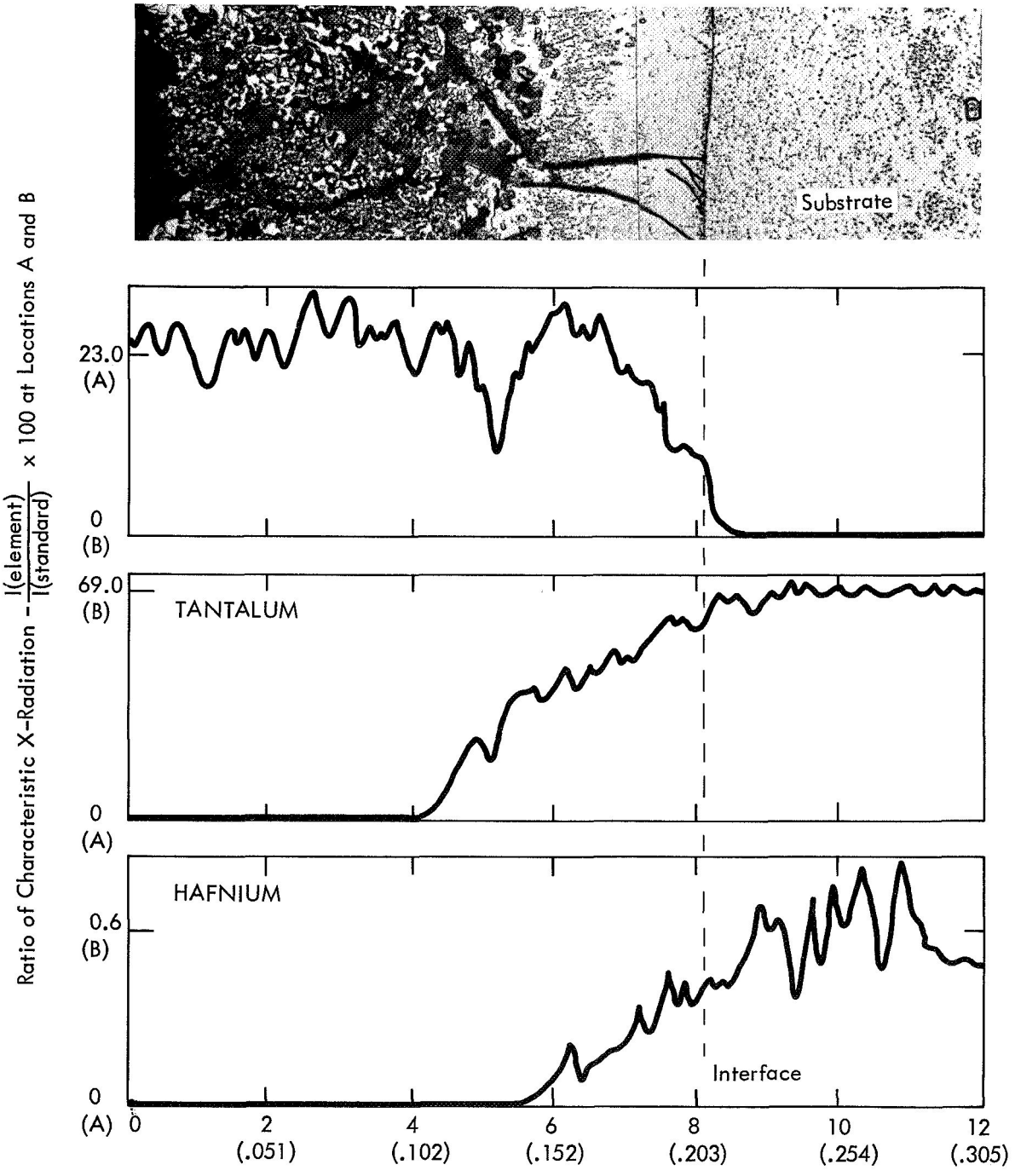

FIGURE 62 - Electron Microprobe Traverses at Position F on Creep Sample 38. Refer to Figure 39.

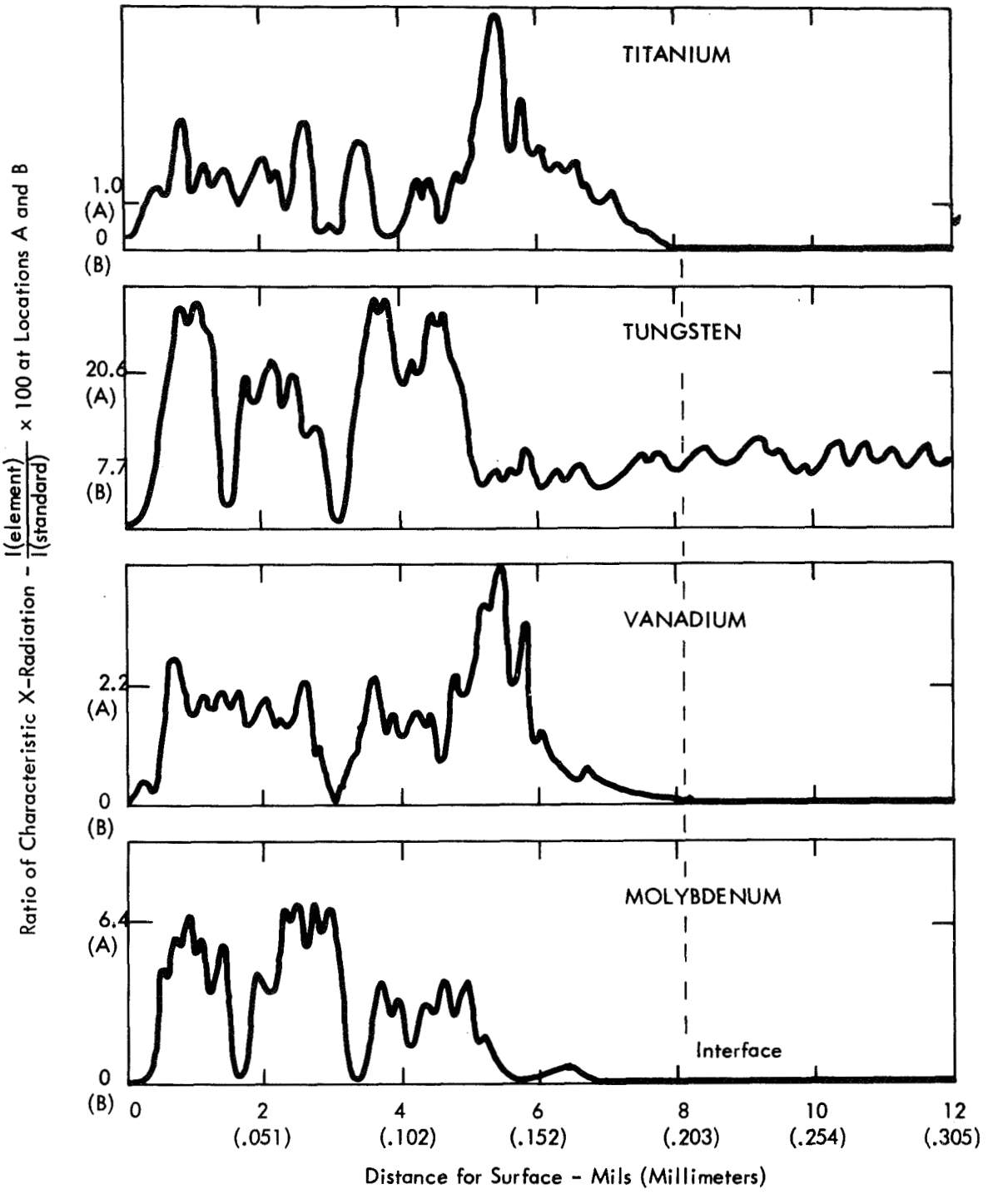

FIGURE 62 (Continued) - Electron Microprobe Traverses at Position F on Creep Sample 38. Refer to Figure 39.

The titanium rich layer found in the vicinity of the coating surface on the sample oxidized at 2400°F for 437 hours (Figures 37 and 38), was not found at any of the positions studied on creep sample 38, which represent lower exposure temperatures.

IV. CONCLUSIONS

Evaluation of a promising slurry applied silicide coating optimized for protecting the tantalum alloy T-222 from oxidation was made in this study. Conclusions established by this work are:

1. The coating can protect 0.030" T-222 sheet from oxidation in air at 2400°F for 500 hours under isothermal exposure and 300 hours when intermittent cycling to room temperature is employed.

2. The coating-substrate combination can sustain, without failure, 9 percent creep strain applied over a period of 400 to 500 hours in air environment at 2400°F.

3. The as-applied coating is susceptible to failure in a few hours when oxidized at 1400°F, but prior higher temperature exposure can extend life at this temperature to beyond 600 hours.

4. Oxygen, nitrogen and carbon contents of the 0.030" thick T-222 sheet increased during the coating process, but subsequent oxidation in air for 600 hours at 1400°F or 300 hours at 2400°F did not significantly change these levels. As coated material and material coated and oxidized for these conditions did not display any significant change in mechanical properties from that inherent to the T-222 alloy.

5. The oxidation rate measured over two hour exposure periods at 2400°F, employing air cooling to room temperature between periods, is much higher than observed on oxidation periods of 16 hours or longer.

6. Oxidation of the study coating promotes formation of a primary barrier structure consisting of TiO_2 particles in a SiO_2 matrix, and the amount of TiO_2 present increases with increased oxidation temperature and time-at-temperature. Oxidation products can form inside microscopic coating fissures and pores in the metallic-intermetallic reservoir at temperatures as low as 1000°F. At 2400°F, the products of oxidation can fill cracks at the coating surface large enough to be obvious to the unaided eye and forestall coating failure for some time.

7. Roughly 0.0002 inch to 0.0004 inch recession of the substrate surface occurs upon coating. An additional 0.0020 inch to 0.0025 inch surface recession will result from 500 hour treatment at 2400°F.

8. Coating and subsequent oxidation promotes development in the T-222 substrate of large individual precipitates located primarily at grain boundary triple points which are not present in contamination free material.

9. Conditions promoting growth of the metallic diffusion zone do not cause coating elements to diffuse into the substrate beyond the structurally obvious reaction boundary.

Conclusions suggested by the results of this work are:

1. Oxidation plugs coating fissures minimizing permeation of atmospheric impurities to the substrate. This mechanism allows the coating-substrate combination to sustain creep strain.

2. The higher oxidation rate measured at 2400°F over short time exposure periods compared to longer time periods, results from oxidation within coating fissures induced by the thermal shock of cooling between periods.

3. Some coating failures experienced during oxidation of tensile specimens were associated with coating preparation.

4. Abrupt failure of the as-applied coating when exposed in air at 1400°F was linked to a "pest" mechanism.

5. The coating elements, tungsten, molybdenum and vanadium, are lost from the coating surface during oxidation by formation of their volatile oxides.

6. The large individual precipitates formed primarily at grain boundary triple points in the substrate of coated and oxidized samples are HfO_2.

7. Conditions which promote formation of a well defined metallic diffusion zone may improve substrate protection against oxidation.

8. Creep behavior determined on coated material in air at 2400°F was not significantly different from that reported for uncoated T-222 tested in vacuum.

V. REFERENCES

1. A. G. Metcalfe, A. R. Stetson, "Interactions in Coated Refractory Metal Systems," Refractory Metal Alloys, Plenum Press 1968, pgs. 121-165.

2. R. T. Wimber, A. R. Stetson, "Silicide Coatings for Tantalum and Columbium Alloys," Contract NAS 3-9412, April 1, 1967 - Oct. 31, 1967.

3. R. T. Wimber, A. R. Stetson, "Development of Coatings for Tantalum Alloy Nozzle Vanes," Contract NAS 3-7276, Final Report, July 1967.

4. R. L. Ammon, R. T. Begley, "Pilot Production and Evaluation of Tantalum Alloy Sheet," Contract N600(19)59762, Summary Phase Report Part II, July 1, 1964.

5. R. L. Ammon, A. M. Filippi, D. L. Harrod, "Pilot Production and Evaluation of Tantalum Alloy Sheet," Contract NOw-64-0394-d, Summary Phase Report Part III, Oct. 30, 1965.

6. A. M. Filippi, "Production and Quality Evaluation of T-222 Tantalum Alloy Sheet," Contract NOw-66-0538-d, Final Report, January 31, 1968.

7. J. B. Berkowilz-Mattuch, P. E. Blackburn, E. J. Felten, "The Intermediate-Temperature Oxidation Behavior of Molybdenum Disilicide, Trans. AIME, Vol. 233, June 1965.

8. R.W. Buckman, Jr., R. C. Goodspeed, "Considerations in the Development of Tantalum Base Alloys," AIME Symposium on Metallurgy and Technology of Refractory Metal Alloys, April 1968.

9. J. C. Sawyer, E. A. Steigerwald, "Generation of Long Time Creep Data of Refractory Alloys at Elevated Temperatures," Contract NAS 3-2545, Final Report, June 6, 1967.

10. R. H. Titran, R. W. Hall, "Ultra High-Vacuum Creep Behavior of Columbium and Tantalum Alloys at 2000 and 2200°F for Times Greater than 1000 Hours," Metallurgical Society AIME Conferences Vol. 41, October 1965.

11. O. D. Sherby, "Factors Affecting the High Temperature Strength of Polycrystalline Solids," Acta Met, 10, 1962.

12. W. V. Green, "High Temperature Creep of Tantalum," Trans. AIME, October 1965.

13. R. T. Begley, D. L. Harrod, R. E. Gold, "High Temperature Creep and Fracture Behavior of the Refractory Metals," AIME Symposium on Metallurgy and Technology of Refractory Metal Alloys, April 1968.

14. J. Weertman, "Theory of Steady-State Creep Based on Dislocation Climb," JAP, Vol. 46, Oct. 1955.

15. R. L. Ammon, R.T. Begley, "Pilot Production and Evaluation of Tantalum Alloy Sheet," Contract NOw-62-0656-d, Summary Phase Report, June 15, 1963.